Universität Potsdam

Institut für Physik und Astronomie

Casimir-Polder interaction in second quantization

Jürgen Schiefele

Betreuer:

PD Dr. Carsten Henkel

Abstract

The Casimir-Polder interaction between a single neutral atom and a nearby surface, arising from the (quantum and thermal) fluctuations of the electromagnetic field, is a cornerstone of cavity quantum electrodynamics (cQED), and theoretically well established. Recently, Bose-Einstein condensates (BECs) of ultracold atoms have been used to test the predictions of cQED. The purpose of the present thesis is to upgrade single-atom cQED with the many-body theory needed to describe trapped atomic BECs. Tools and methods are developed in a second-quantized picture that treats atom and photon fields on the same footing. We formulate a diagrammatic expansion using correlation functions for both the electromagnetic field and the atomic system.

The formalism is applied to investigate, for BECs trapped near surfaces, dispersion interactions of the van der Waals-Casimir-Polder type, and the Bosonic stimulation in spontaneous decay of excited atomic states. We also discuss a phononic Casimir effect, which arises from the quantum fluctuations in an interacting BEC.

Zusammenfassung

Die durch (quantenmechanische und thermische) Fluktuationen des elektromagnetischen Feldes hervorgerufene Casimir-Polder-Wechselwirkung zwischen einem elektrisch neutralen Atom und einer benachbarten Oberfläche stellt einen theoretisch gut untersuchten Aspekt der Resonator-Quantenelektrodynamik (*cavity quantum electrodynamics*, cQED) dar. Seit kurzem werden atomare Bose-Einstein-Kondensate (BECs) verwendet, um die theoretischen Vorhersagen der cQED zu überprüfen. Das Ziel der vorliegenden Arbeit ist es, die bestehende cQED Theorie für einzelne Atome mit den Techniken der Vielteilchenphysik zur Beschreibung von BECs zu verbinden. Es werden Werkzeuge und Methoden entwickelt, um sowohl Photon- als auch Atom-Felder gleichwertig in zweiter Quantisierung zu beschreiben. Wir formulieren eine diagrammatische Störungstheorie, die Korrelationsfunktionen des elektromagnetischen Feldes und des Atomsystems benutzt.

Der Formalismus wird anschließend verwendet, um für in Fallen nahe einer Oberfläche gehaltene BECs Atom-Oberflächen-Wechselwirkungen vom Casimir-Polder-Typ und die bosonische Stimulation des spontanen Zerfalls angeregter Atome zu untersuchen. Außerdem untersuchen wir einen phononischen Casimir-Effekt, der durch die quantenmechanischen Fluktuationen in einem wechselwirkenden BEC entsteht.

Contents

Introduction

The Casimir effect, cavity quantum electrodynamics, and Bose-Einstein condensates

The name of the Dutch physicist Hendrik Casimir is associated with several phenomena where detectable forces between macroscopic bodies or single atoms arise from a –quoting Casimir and Polder (1948)– 'somewhat academic exercise in quantum electrodynamics'.

In its strict sense, the term 'Casimir effect' refers to Casimir's prediction of an attractive force acting between two neutral, electrically conducting plates placed in the vacuum (Casimir, 1948). From the standpoint of classical electromagnetism, there is no interaction between the two neutral plates, but Casimir took into account the vacuum-fluctuations of the electromagnetic (em) field. The plates impose boundary conditions on the em field, and the spectrum of the vacuum energy contained in the resonator volume between the plates changes upon varying their separation L. Casimir found a resulting force which varies as L^{-4}, at a distance of $1\,\mu$m, two plates of area 1 mm^2 attract each other with a force of 10^{-9} N. An early attempt by Sparnaay (1958) to experimentally verify this effect did not yield conclusive results, but a series of precision experiments in the late 1990s, beginning with Lamoreaux (1997), could establish the Casimir force as a direct manifestation of the electromagnetic zero-point energy.[1]

For Casimir's argument, it is, however, not essential that the fluctuating medium is the em field in its vacuum state. Mehra (1967) showed that the effect of thermal fluctuations of the em field on the interaction of the plates actually dominates the quantum Casimir force for large plate separations. At room temperature, this thermal contribution to the Casimir effect changes the distance-dependence of the

---

[1]For a comprehensive review of the Casimir effect, see for example Bordag *et al.* (2001); Lamoreaux (2005); Milton (2001); Mostepanenko and Trunov (1997).

force into a $k_B T/L^3$ power-law for distances larger than $3\,\mu$m, an effect observed in the recent experiment by Sushkov *et al.* (2011).

The so-called critical Casimir effect does not deal with the em field at all, but describes forces that arise in adsorbed films of liquids near a second order phase transition. The fluctuating quantity is the order parameter, the resulting forces are observable in the thickness of the film (see Gambassi *et al.* (2009) and the references therein).

Two other effects involving neutral atoms with electric dipole moments were explained within the framework of quantum electrodynamics by Casimir and Polder in their 1948 seminal paper: The Casimir-Polder-van der Waals (CPvdW) interaction between two atoms, and the Casimir-Polder (CP) interaction between an atom and a macroscopic body. (For simplicity, we will only consider the case of the macroscopic body being a plane, infinitely extended surface.) As in the well-known Lamb shift in atomic hydrogen (Bethe, 1947), the energy level structure of an atom is disturbed by the zero-point fluctuations of the em field. If the presence of an additional atom or a surface alters the spectrum of the zero-point fluctuations, the first atom's energy shift depends on the inter-atomic distance or the atom surface distance, respectively, resulting in an interaction potential.

For two atoms in their internal ground state (separated by a distance r), Casimir and Polder found an attractive CPvdW-potential which behaves as r^{-6} for inter-atomic distances smaller than typical atomic transition wavelengths from the ground state, and as r^{-7} for larger distances. Historically, the r^{-6} potential had already been found in 1930 by Eisenschitz and London[2] in an attempt to quantum-mechanically explain the weak intermolecular forces which were introduced heuristically half a century earlier by van der Waals (see Maxwell, 1874) in his equation of state. While London's calculation is based on the interaction energy of fluctuating dipole moments, Casimir focused on the local action of fields at the position of the atoms. This includes the effect of retardation due to the finite speed of light, which results in the modification of the power-law behavior at large distances. For a comprehensive derivation of the CPvdW-potential, see Craig and Thirunamachandran (1998, chap. 7).

The CP-potential between a single atom and a surface shows the same effect of retardation, the power law changes from d^{-3} to d^{-4} with increasing atom-surface separation d.[3] Again, the non-retarded behavior was already known from an earlier calculation by Lennard-Jones (1932). The retardation effect in the CP-potential has been observed in the experiments of Sukenik *et al.* (1993) and Bender *et al.* (2010).

Since a thorough understanding of the vacuum state is vital for any quantum

---

[2]See Eisenschitz and London (1930); London (1930).

[3]A compilation of the different power law forces mentioned here can be found in (Scheel and Buhmann, 2008, p. 780).

field theory (see Milonni, 1993), the Casimir effect is an interesting topic of theoretical physics in its own right. Precise knowledge of Casimir forces also enables tests on possible extensions of the Standard Model of particle physics, where additional fields or extra-dimensional physics predict long range interactions between massive bodies. Upon measuring the forces between two macroscopic, neutral bodies, these hypothetical interactions would result in deviations from the combined gravitational- and Casimir force. Precision measurements of Casimir forces are used to set upper bounds on the strength of the hypothetical interactions, which are called non-Newtonian gravity in the present context (see Mostepanenko *et al.*, 2008).

Apart from their appeal to theorists, Casimir- and CP-forces play also an important role in several technological applications. In atom chips, ultracold atoms are confined and manipulated by magnetical traps above a microstructured surface (see Reichel and Vuletic (2011) for a recent review). Quantum bits can be stored and processed in superpositions of the internal states of the trapped atoms, but interaction with the em-field fluctuations near the chip surface limits their coherence time. This limits applications in quantum-computing, where several quantum gate operations have to be processed during the lifetime of the superposition states. In microelectromechanical systems (MEMS), the Casimir force between different mechanical components has been identified as one of the main causes for the phenomenon of stiction: movable elements collapse into nearby surfaces, resulting in their permanent adhesion.[4] For micromachined parts with nanometer-scale surface roughness, which are in direct mechanical contact with each other, Casimir forces between the non-contacting portions of the interface are also the main causes for interfacial adhesion and friction (DelRio *et al.*, 2005). A bridge between the language used in such problems of the applied sciences and engineering and Casimir's 'academic exercise' is provided in the book by Parsegian (2005), which presents formulae for calculating Casimir forces in a wide variety of geometries.

Since Casimir's calculation, the study of the perturbation produced by boundaries on the em field and on the radiative properties of atoms coupled to the field has evolved into the discipline of cavity quantum electrodynamics (cQED, see for example Haroche (1992) or Hinds (1994) for an overview). Apart from the effects of CP-forces, the excited atomic state decay can be suppressed or enhanced by placing an atom in a cavity structure or close to a surface, as the process of spontaneous emission also depends on the vacuum fluctuations of the em field.

Experiments in cQED have mostly been focusing on the manipulation of single atoms. Only in the past few years have trapped Bose-Einstein condensates (BECs) of ultracold alkali atoms emerged as a tool to explore cQED effects. A trapped BEC with its well-controlled quantum state, which can be theoretically characterized by only a few parameters (like the atomic mass and s-wave scattering length

---

[4]See Buks and Roukes (2001); Stipe *et al.* (2001).

and the frequencies of the trapping potential) provides a sensitive probe of cQED interactions. In an experimental setup proposed by Antezza *et al.* (2004), a particular trap oscillation mode (the so-called dipole mode) is excited in a BEC trapped a few micrometers above a surface. This oscillation is only very weakly damped, and the shift in the oscillation frequency due to the CP-potential can be measured with high accuracy. The measurement proved sensitive enough to detect the retardation of the CP-potential and also the crossover into the thermal regime in the experiments of Harber *et al.* (2005) and Obrecht *et al.* (2007). Likewise, Dalvit *et al.* (2008) and Moreno *et al.* (2010) calculated the effects of the CP-potential above a corrugated surface on the excitation spectrum of a BEC trapped close to the surface.

The calculations mentioned above use a local CP-potential which then acts by spatially averaging over the density distribution of the trapped atom cloud. As BECs show spatial coherence over a macroscopic range, one might expect that not all effects of the condensate-field interaction can be fully captured by such a local approach. The aim of this thesis is therefore to develop a calculational framework in which the fluctuations of the em-field, which underlie cQED effects, and the many-body field theory describing atomic BECs are treated on the same footing. We build our approach on the quantum field theory for photons and atoms established by Lewenstein *et al.* (1994) and Zhang and Walls (1994) for the case of the em-field in free space.

The present text is organized as follows: chapter 2 gives a brief account of the treatment of trapped atomic BECs within the Bogoliubov approximation, focusing on the low-temperature properties of interacting Bose gases and on the phenomenon of long-range correlation. In chapter 3, we consider a weakly interacting uniform BEC at zero temperature, and discuss how the quantum fluctuations on top of the condensate ground state give rise to Casimir forces, an effect similar to the critical Casimir effect mentioned above. The remaining sections deal with the interaction of atoms and BECs with the em-field: in chapter 4, we lay out our perturbative formalism for the atom-field interaction, and apply it to calculate the self-energy acquired by single atoms through their interaction with the field. We then discuss how the self-energy is modified by the presence of a nearby surface, and thereby reproduce in an economical fashion the results for atomic transition rates and the CP-interaction near a surface. In chapter 5, we derive an expression for the collective CP-interaction of a trapped gas of condensed bosons with a plane surface, and point out the differences to the single atom theory. In chapter 6, we show how the spontaneous emission rate of an excited two-level atom placed in a trapped BEC of ground-state atoms is enhanced by bosonic stimulation. This stimulation provides a probe of the spatial coherence of the Bose gas. The effect can be used to amplify the distance-dependent decay rate of an excited atom near an interface. Finally, chapter 7 briefly describes how processes of higher order in the atom-field interaction can be described with the techniques developed in the

previous chapters.

Weakly interacting, dilute BECs

In the textbook model of an ideal Bose gas consisting of noninteracting particles, a large fraction of particles accumulates in the ground state of the trapping potential for temperatures below a critical value T_c. The presence of such a macroscopically occupied state in dilute vapors of trapped alkali atoms was first observed by Anderson *et al.* (1995) and Davis *et al.* (1995). While in the ideal gas model at zero temperature all particles occupy the ground state, the effect of (repulsive) interparticle interactions is to scatter particles out of the condensate state. Following the approach of Bogoliubov (1947), which we introduce in section 2.1, the particles in the condensate mode can be described as a classical field. We analyze the coherence properties of this matter-wave field in section 2.2. For sufficiently dilute samples of ultracold alkali atoms, the interaction-induced depletion of the condensate will be a small effect, which permits a perturbative expansion in the interparticle interactions.[1] After introducing an effective Hamiltonian for the interparticle-interaction in section 2.3, we follow the treatment of Fetter (1972, 1999) to obtain equations of motion governing the macroscopically occupied state and small fluctuations of non-condensed particles, namely the Gross-Pitaevskii and Bogoliubov-de Gennes equations.[2] We apply the perturbative approach of section 2.4 to treat the case of an uniform interacting BEC in section 2.5 and of a BEC in a harmonic trap in section 2.6.

The main purpose of the sections below is to collect basic results which are applied in the description of BEC in the following chapters. For a systematic overview on the vast amount of theoretical work on Bose-Einstein condensation in

---

[1] In contrast, superfluid helium is a strongly interacting system (see Hohenberg and Martin, 1965).

[2] For an overview on other perturbative methods that also include backaction of the non-condensate fraction on the condensate, see Castin (2001); Proukakis and Jackson (2008).

atomic gases, see for example Pitaevskii and Stringari (2003) or Pethick and Smith (2002).

2.1 Field operators and the Bogoliubov approximation

We describe the system of trapped atoms by second quantized field operators[3] $\hat{\Psi}^\dagger(\mathbf{r})$ and $\hat{\Psi}(\mathbf{r})$ that create (annihilate) an atom at point $\mathbf{r}$. They fulfill the usual bosonic commutation relations

$$[\hat{\Psi}(\mathbf{r}_1), \hat{\Psi}^\dagger(\mathbf{r}_2)] = \delta(\mathbf{r}_1 - \mathbf{r}_2), \quad [\hat{\Psi}(\mathbf{r}_1), \hat{\Psi}(\mathbf{r}_2)] = 0 . \tag{2.1}$$

The one-body correlation function

$$n^{(1)}(\mathbf{r}_1, \mathbf{r}_2) = \langle \hat{\Psi}^\dagger(\mathbf{r}_1)\hat{\Psi}(\mathbf{r}_2) \rangle \tag{2.2}$$

accounts for the spatial coherence between $\mathbf{r}_1$ and $\mathbf{r}_2$. In particular, the density $n(\mathbf{r}) \equiv n^{(1)}(\mathbf{r}, \mathbf{r})$ is the probability of finding a boson at $\mathbf{r}$, and the total number of particles is

$$N = \int d^3r\, n(\mathbf{r}) . \tag{2.3}$$

The eigenvalue equation

$$\int d^3r_2\, n^{(1)}(\mathbf{r}_1, \mathbf{r}_2)\chi_j(\mathbf{r}_2) = n_j\chi_j(\mathbf{r}_1) \tag{2.4}$$

provides a basis of orthonormalized single particle wave functions $\{\chi_i(\mathbf{r})\}$ (see Pitaevskii and Stringari, 2003, chap. 1). These functions can be used to expand the field operator in the form

$$\hat{\Psi}(x) = \sum_j \chi_j(\mathbf{x})\, \hat{a}_j , \tag{2.5}$$

where $\hat{a}_j^\dagger$ and $\hat{a}_j$ are the creation and annihilation operators of a particle in the state $|\chi_j\rangle$. They obey the commutation relations

$$[\hat{a}_i, \hat{a}_j^\dagger] = \delta_{ij}, \quad [\hat{a}_i, \hat{a}_j] = 0 . \tag{2.6}$$

The eigenvalues n_j of eqn. (2.4) are the occupation numbers of the single particle states $|\chi_j\rangle$. Bose-Einstein condensation occurs when one of these states (labeled by $j = 0$) is occupied in a macroscopic way, that is, when the eigenvalue n_0

---

[3]In chapter 4, we also consider the internal electronic state of the condensate atoms and introduce operators $\hat{\Psi}_g$ and $\hat{\Psi}_e$ that annihilate a ground state or an excited state atom, respectively. In the present context, the (indistinguishable) atoms are all supposed to be in the same electronic state, and we therefore skip the label.

assumes a value N_0 which is of the order of the total particle number N, while the other single particle states have an occupation of order 1 (see Penrose and Onsager, 1956). As the so-called condensate wave function relative to the macroscopic eigenvalue N_0 plays a crucial role in the theory of BEC, it is useful to separate the condensate term from the other components in the field operator:

$$\hat{\Psi}(\mathbf{r}) = \chi_0(\mathbf{r})\,\hat{a}_0 + \sum_{j \neq 0} \chi_j(\mathbf{r})\,\hat{a}_j \;. \tag{2.7}$$

We now apply the Bogoliubov approximation (see Bogoliubov, 1947): it consists of replacing the operators $\hat{a}_0$ and $\hat{a}_0^\dagger$ by the c-number $\sqrt{N_0}$. We thus ignore the noncommutativity of $\hat{a}_0$ and $\hat{a}_0^\dagger$ and treat the component $\chi_0 \hat{a}_0$ of the field operator as a classical field. This is a good approximation for describing the macroscopic phenomena associated with BEC, where $\langle \hat{a}_0^\dagger \hat{a}_0 \rangle = N_0 \gg 1$, while the commutator between the two operators is equal to 1. The resulting field operator in the Bogoliubov approximation reads

$$\hat{\Psi}(\mathbf{r}) \approx \Phi(\mathbf{r}) + \hat{\phi}(\mathbf{r}) \;, \tag{2.8}$$

where we defined $\Phi = \sqrt{N_0}\chi_0$ and $\hat{\phi} = \sum_{j \neq 0} \chi_j(\mathbf{r})\hat{a}_j$, and the number density is given by

$$n(\mathbf{r}) = |\Phi(\mathbf{r})|^2 + \langle \hat{\phi}^\dagger(\mathbf{r})\hat{\phi}(\mathbf{r}) \rangle \equiv n_0(\mathbf{r}) + n'(\mathbf{r}) \;. \tag{2.9}$$

2.2 Critical temperature and long-range order in an ideal Bose gas

For a system of non-interacting atoms, the total Hamiltonian consists of a sum of single particle Hamiltonians $H^{(1)}$, and the single particle states χ_i are obtained by solving the Schrödinger equation

$$H^{(1)}\chi_i(\mathbf{r}) = \epsilon_i\,\chi_i(\mathbf{r}) \;.$$

For this simple case, the grand canonical partition function can be evaluated analytically (see Pitaevskii and Stringari, 2003, sec. 3.1), and the total particle number N is expressed in terms of the average occupation numbers $\overline{n}_i$ of the ith single particle state via

$$N = \sum_i \frac{1}{e^{\beta(\epsilon_i - \mu)} - 1} = \sum_i \overline{n}_i \;. \tag{2.10}$$

For all occupation numbers to be non-negative, this provides the constraint $\mu < \epsilon_0$ for the chemical potential of the ideal Bose gas, where ϵ_0 is the lowest eigenvalue of the Hamiltonian $H^{(1)}$. We can split the total particle number into particles in the condensate and particles out of the condensate (also called the thermal component):

$$N = N_0 + N' \;, \tag{2.11}$$

9
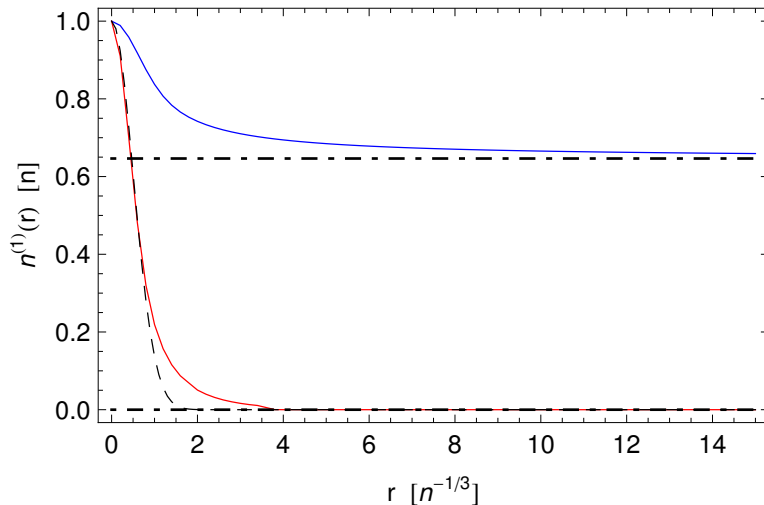
Figure 2.1: One-body density function $n^{(1)}(\mathbf{r}_1, \mathbf{r}_2) = n^{(1)}(|\mathbf{r}_1 - \mathbf{r}_2|) \equiv n^{(1)}(r)$ (see eqn. (2.16)) for an ideal Bose gas of density n confined to a box, at temperatures above and below the critical temperature T_c (2.14). *Blue (red) curve:* $T = 0.5\,T_c$ and $T = 1.2\,T_c$, respectively. *Horizontal dashed-dotted line:* the condensate fraction N_0/N (2.15) for $T = 0.5\,T_c$. *Dashed curve:* the asymptotic expression (2.17) at $T = 1.2\,T_c$.

where $N_0 \equiv \overline{n}_0$ and

$$N'(T, \mu) = \sum_{i \neq 0} \overline{n}_i(T, \mu) \ .$$

For a fixed temperature, the function $N'(\mu)$ reaches its maximum at $\mu = \epsilon_0$ (see Pitaevskii and Stringari, 2003, sec. 3.1), and we can define a critical temperature T_c by the relation

$$N'(T_c, \mu = \epsilon_0) = N \ . \tag{2.12}$$

If $N'(T, \mu = \epsilon_0)$ is smaller than the total particle number (or, equivalently, $T < T_c$), then μ will approach ϵ_0 in the thermodynamic limit in order to fulfill the condition (2.11), and N_0 becomes increasingly large (see eqn. (2.10)). Thus T_c defines the temperature below which Bose-Einstein condensation, that is, the macroscopic occupation of a single particle state, takes place.

For the simple model of an ideal Bose gas confined to a box of volume V at a density $n = N/V$ (with periodic boundary conditions imposed on the plane wave functions χ_i), the number of particles out of the condensate takes the value (see Pitaevskii and Stringari, 2003, sec. 3.2)

$$N' = \frac{V}{\lambda_T^3} g_{3/2}(z) \ , \tag{2.13}$$

where $g_n(z)$ denotes the polylogarithm, $z = e^{\beta\mu}$ is the fugacity and λ_T the thermal wavelength

$$\lambda_T = \sqrt{\frac{2\pi\hbar^2}{Mk_BT}} \, .$$

Relation (2.12) yields

$$k_BT_c = \frac{2\pi\hbar^2}{M}\left(\frac{n}{g_{3/2}(1)}\right)^{2/3} \tag{2.14}$$

(with $g_{3/2}(1) = \zeta_{3/2} \approx 2.61$), the critical temperature is fully determined by the density n and the atomic mass M. By setting $\mu = \epsilon_0 = 0$ in eqn. (2.13), we obtain the value of the condensate fraction for $T < T_c$:

$$\frac{N_0}{N} = 1 - \left(\frac{T}{T_c}\right)^{3/2} \, . \tag{2.15}$$

The one-body correlation function (2.2) evaluates to (see Cohen-Tannoudji and Robilliard, 2001, sec. 2.3)

$$n^{(1)}(r) = \frac{N_0}{V} + \frac{1}{\lambda_T^3}\sum_{l=1}^{\infty}\frac{z^l}{l^{3/2}}\exp\left[\frac{-\pi r^2}{l\lambda_T^2}\right] \, , \tag{2.16}$$

where $r \equiv |\mathbf{r}_1 - \mathbf{r}_2|$. For $T \gg T_c$, we have $z \ll 1$ and N_0 is negligibly small. From eqn. (2.13), we then get $n = z/\lambda_T^3 + \mathcal{O}(z^2)$. Setting $z = n\lambda_T^3$ in eqn. (2.16) and again neglecting N_0 and terms of $\mathcal{O}(z^2)$, we have

$$n^{(1)}(r) \approx n\,e^{-\pi r^2/\lambda_T^2}, \quad T \gg T_c \, , \tag{2.17}$$

which recovers the coherence length $\lambda_T/\sqrt{\pi}$ of a classical Maxwell-Boltzmann gas. If, on the other hand, $T < T_c$, we have $z = 1$ and the distance-independent term N_0/V in eqn. (2.16) assumes a finite value. This prevents $n^{(1)}(r)$ from going to zero at large distances, corresponding to an infinite correlation length. The macroscopic population of the condensate state thus goes along with a long range spatial order, which is in reality of course limited by the spatial extent of the system. In fig. 2.1, $n^{(1)}(r)$ is shown for two different temperatures above and below the critical value (red (blue) curve, respectively), compare to fig. 2.2 for a spatially inhomogeneous system. The phenomenon of long-range spatial coherence can be observed in the formation of interference patterns, see for example Andrews *et al.* (1997); Bloch *et al.* (2000).

2.3 Effective Hamiltonian for interacting atomic BECs

As the ground state of most interacting atomic systems corresponds to a solid, the gas phase in the quantum degenerate regime represents a metastable configuration, where thermalization is ensured by two-body collisions. Eventually, three-body collisions will drive the system into the solid configuration, but the experimental realization of the quantum gas phase with several atomic species has shown that the metastable state survives long enough to allow for systematic measurements. To arrive at a simple description of the BE-condensed gas phase, we neglect effects due to collisions involving more than two atoms. This is supposed to be a good approximation if the atomic gas is sufficiently dilute, that is, if the range of the interatomic potential is much smaller than the average distance between the particles. In terms of the field operators defined above, a generic Hamiltonian then reads

$$H = \int d^3r \left\{ \hat{\Psi}^\dagger (T + V_t)\hat{\Psi} \right\} + H_{AA} \,, \tag{2.18}$$

with the kinetic energy operator

$$T = -\frac{\hbar^2 \vec{\nabla}^2}{2M} \,, \tag{2.19}$$

a trapping potential $V_t(\mathbf{r})$, and H_{AA} describing the interaction between pairs of atoms via an interatomic potential $V(\mathbf{r}_1 - \mathbf{r}_2)$:

$$H_{AA} = \frac{1}{2} \int d^3r_1 \int d^3r_2 \, \Psi^\dagger(\mathbf{r}_2)\Psi^\dagger(\mathbf{r}_1) \, V(\mathbf{r}_1 - \mathbf{r}_2) \, \Psi(\mathbf{r}_2)\Psi(\mathbf{r}_1) \,. \tag{2.20}$$

The interatomic potential for alkali atoms has a repulsive hard core, but as it also contains bound states corresponding to molecular states of two atoms, it is not feasible to retain the true potential $V(\mathbf{r}_1 - \mathbf{r}_2)$ in the Hamiltonian (2.18).[4] With the binary interactions in a Bose condensed gas taking place only at low energies (the collision energy $\hbar k^2/M$ is on the order of $k_B T$ in the thermal gas), their effect on the macroscopic properties of the gas is not sensitive to the details of the scattering potential, but only to the s-wave scattering amplitude. We can therefore replace the exact interaction potential by a model potential that reproduces the same scattering properties at low energy, that is, that has the same scattering length. Using the singular contact potential[5]

$$V(\mathbf{r}_1 - \mathbf{r}_2) = g \, \delta(\mathbf{r}_1 - \mathbf{r}_2) \,, \tag{2.21}$$

---

[4]See Castin (2001, chap. 3) for a detailed account.

[5]We will only consider the case $g > 0$, although condensates with attractive interaction (for example ^{7}Li (Bradley *et al.*, 1997, 1995)) can also be held in a metastable state in traps as long as the particle number does not exceed a critical value.

the Born approximation for the s-wave scattering length a_s and its first correction yield in the low energy limit (see Fetter, 1999, chap. 1)

$$\frac{4\pi\hbar^2 a_s}{M} = g - \frac{Mg^2}{\hbar^2} \int \frac{d^3p}{(2\pi)^3} \frac{1}{p^2} \ . \tag{2.22}$$

To relate the potential-strength g to the measurable s-wave scattering length, we can set

$$g = \frac{4\pi\hbar^2 a_s}{M} \tag{2.23}$$

in calculations involving interactions between condensate atoms only. We will see below that the divergent $\mathcal{O}(g^2)$ term in eqn. (2.22) is needed as a counterterm to cancel divergences when scattering between condensate and non-condensate atoms is considered. The condition of diluteness formulated at the beginning of the section can now be expressed as $\bar{n}|a_s|^3 \ll 1$, where $\bar{n}$ is the mean density.

Using the pseudopotential (2.21) in the interaction term H_{AA}, our effective many-body Hamiltonian for a dilute, weakly interacting Bose gas finally reads

$$H = \int d^3r \left\{ \hat{\Psi}^\dagger (T + V_t)\hat{\Psi} + \frac{1}{2}g\hat{\Psi}^\dagger \hat{\Psi}^\dagger \hat{\Psi}\hat{\Psi} \right\} \ . \tag{2.24}$$

After the Bogoliubov approximation eqn. (2.8) is made, the above Hamiltonian no longer conserves the number of particles. We therefore introduce a chemical potential μ and work in the following with the expression

$$K = H - \mu \int d^3r \, \hat{\Psi}^\dagger \hat{\Psi} \ , \tag{2.25}$$

rather than with H itself. The expectation value of K is the thermodynamical potential in the grand canonical ensemble at temperature T and chemical potential μ.

2.4 Perturbative treatment of weak interactions

By inserting the field operator in the Bogoliubov approximation into the general expression (2.25) for K and sorting the terms in orders of the fluctuation operator $\hat{\phi}$, we can obtain equations governing the condensate wavefunction and the fluctuation operator.

Including only the condensate wavefunction in all field operators in K, we obtain the condensate part K_0 of the modified Hamiltonian, which is assumed to dominate the physics at low temperatures:

$$K_0 = \int d^3r \left\{ \Phi^*(T + V_t - \mu)\Phi + \frac{1}{2}g\Phi^*\Phi^*\Phi\Phi \right\} \ . \tag{2.26}$$

In the presence of a macroscopic condensate, K_0 is approximately the thermodynamic potential $\langle K \rangle$. In thermodynamic equilibrium at zero temperature, $\langle K \rangle$ takes its minimal value, so the value of the integral K_0 must be stationary under variations $\Phi^* \to \Phi^* + \delta\Phi^*$ (see Fetter, 1972). Introducing the Hartree potential $V_H(\mathbf{r})$ as the interaction potential of a particle at $\mathbf{r}$ with all the other condensed particles

$$V_H(\mathbf{r}) \approx \int d^3 r'\, V(\mathbf{r} - \mathbf{r}') n_0(\mathbf{r}') \approx g n_0(\mathbf{r}) = g|\Phi(\mathbf{r})|^2 \, , \qquad (2.27)$$

the Euler-Lagrange equation for K_0 reads

$$\big[T + V_t + V_H - \mu \big] \Phi = 0 \, . \qquad (2.28)$$

It is known as the Gross-Pitaevskii equation (GPE), found independently by Gross (1961) and Pitaevskii (1961) in the study of vortex lines in weakly interacting Bose gases.

To account for the particles scattered out of the condensate wave function, we have to retain those terms in K that are quadratic in the fluctuation operator $\hat{\phi}$ after the substitution (2.8) is applied. (The linear contribution to K vanishes if Φ is a solution of the GPE.) We can diagonalize the fluctuation part K' with the linear transformation

$$\hat{\phi}(\mathbf{r}, t) = \sum_j{}' \big\{ u_j(\mathbf{r}) \alpha_j(t) - v_j^*(\mathbf{r}) \alpha_j^\dagger(t) \big\} \qquad (2.29)$$

(where the primed sum runs over all excited states), which introduces the quasiparticle operators α_j with the time dependence $\alpha_j(t) = \alpha_j \exp[-iE_j t/\hbar]$. The normalization

$$\int d^3 r \, \big\{ |u_j|^2 - |v_j|^2 \big\} = 1 \qquad (2.30)$$

for the set of self-consistent normal modes $\{u_j\}$ and $\{v_j\}$ ensures that the quasiparticle operators obey bosonic commutation relations at equal times. The Heisenberg equations of motion for $\hat{\phi}$ and $\hat{\phi}^\dagger$ then lead to the coupled Bogoliubov-de Gennes (BdG) equations

$$\big(T + V_t - \mu + 2g|\Phi|^2 \big) u_j - g\Phi^2 v_j = E_j u_j \, , \qquad (2.31a)$$

$$\big(T + V_t - \mu + 2g|\Phi|^2 \big) v_j - g(\Phi^*)^2 u_j = -E_j v_j \, , \qquad (2.31b)$$

which determine the wave functions $u_j(\mathbf{r})$ and $v_j(\mathbf{r})$ and the energy eigenvalues E_j.[6] For the number of particles out of the condensate, the expansion (2.29) yields

$$N' = \sum_j{}' \int d^3 r \, |v_j|^2 \equiv \sum_j{}' N_j' \qquad (2.32)$$

---

[6]Alternatively, the BdG equations can also be derived as the linear response of the GP equation to a weak perturbation of the condensate wavefunction (see Pitaevskii and Stringari, 2003, sec. 5.6).

with $N_j{}'$ the occupation of the j-th eigenstate, and the diagonalized fluctuation part of the Hamiltonian reads

$$K' = -\sum_j{}' E_j N_j' + \sum_j{}' E_j \alpha_j^\dagger \alpha_j \ . \tag{2.33}$$

Together with the c-number term K_0 of eqn. (2.26), the Hamiltonian

$$K = K_0 + K' \tag{2.34}$$

describes the original system of interacting particles in terms of independent quasi-particles with energy E_j. For a particular choice of the condensate wavefunction, the lowest state vector $|\mathbf{0}\rangle$ of K satisfies the condition

$$\alpha_j |\mathbf{0}\rangle = 0, \quad j \neq 0 \ ,$$

it corresponds to the vacuum of quasiparticles. The excited states are obtained by applying the creation operators $\alpha_j^\dagger$ to $|\mathbf{0}\rangle$.

For a treatment of the ideal Bose gas, we do not actually need to apply the diagonalization procedure developed above: With the interaction strength g set to zero in the Hamiltonian (2.24), the single particle wave functions $\{\chi_j\}$ are simply the eigenfunctions of the operator $T + V_t$, the BdG-equations eqns. (2.31) are solved by $u_j = \chi_j, v_j = 0$, and with these the transformation (2.29) yields quasiparticle operators that are identical with the original particle operators. As the Hamiltonian without the interaction term is quadratic in the field operators, the expansion up to second order in the fluctuations is actually exact. Thus the one-body correlation function (2.2) for the ideal gas can also be calculated at temperatures near and above T_c, in a regime where condensate depletion is large.

2.5 The interacting uniform system

The effect of repulsive interaction on a BEC in a spatially uniform trapping potential (for the sake of simplicity, we can set $V_t = 0$) is to scatter particles from the non-interacting ground state $\mathbf{k} = 0$ to pairs of higher momentum states with $\pm\mathbf{k} \neq 0$. This simple structure allows for a complete explicit solution for the spectrum of quasiparticle excitations.

In leading order, that is, neglecting contributions from the fluctuation operator $\hat{\phi}$, the constant condensate wavefunction that minimizes the thermodynamic potential (2.26) is

$$\Phi = \sqrt{\mu g} \ . \tag{2.35}$$

The free energy density at this order is obtained by evaluating K_0 at the minimum,

$$\mathcal{F}_0(\mu) = -\frac{\mu^2}{2g} \ , \tag{2.36}$$

and inverting the relation $n = -\partial \mathcal{F}/\partial \mu$ yields the mean-field result for the chemical potential:

$$\mu_0(n) = gn \ . \tag{2.37}$$

The modes $u_{\mathbf{k}}(\mathbf{r})$ and $v_{\mathbf{k}}(\mathbf{r})$ in eqn. (2.29) are plane waves ($u_{\mathbf{k}}(\mathbf{r}) = u_{\mathbf{k}} \exp[i\mathbf{kr}]$ and $v_{\mathbf{k}}(\mathbf{r}) = v_{\mathbf{k}} \exp[i\mathbf{kr}]$), and using these and the above expressions for μ_0 and Φ in the Bogoliubov-de Gennes eqns. (2.31) yields the dispersion relation

$$E_k = \sqrt{\epsilon_k^0(\epsilon_k^0 + 2\mu_0)} \ , \tag{2.38}$$

where $\epsilon_k^0 = \hbar^2 k^2/(2M)$.

The fluctuation part of the free energy density is obtained by evaluating the expectation value of K' (eqn. (2.33)) in the Bogoliubov vacuum, with the values of E_k and v_k obtained from the BdG equations; this yields

$$\mathcal{F}_1(\mu) = \frac{1}{2} \int \frac{d^3k}{(2\pi)^3} \left\{ E_k - \epsilon_k^0 - \mu_0 \right\} + \Delta \mathcal{F}_1(\mu) \tag{2.39}$$

and

$$v_k^2 = u_k^2 - 1 = \frac{1}{2} \left(\frac{\epsilon_k^0 + \mu_0}{E_k} - 1 \right) \ . \tag{2.40}$$

The first term of the free energy (2.39) shows a linear divergence for large k, the counterterm $\Delta \mathcal{F}_1$ which is necessary to render the expression finite arises from a renormalization of the interacting strength g. Setting $g \to g + \Delta g$ in $\mathcal{F}_0(\mu)$ and expanding to first order in Δg yields

$$\Delta \mathcal{F}_1(\mu) = \frac{\mu^2}{2g^2} \Delta g \ , \tag{2.41}$$

and the value $\Delta g = M g^2 (2\pi)^{-3} \int d^3k \, (\hbar k)^{-2}$ can be read from eqn. (2.22). With this, we arrive at the explicit form

$$\mathcal{F}(\mu) = \mathcal{F}_0(\mu) + \mathcal{F}_1(\mu) \tag{2.42}$$

$$= \frac{\mu^2}{2g} + \frac{1}{2} \int \frac{d^3k}{(2\pi)^3} \left\{ E_k - \epsilon_k^0 - \mu_0 + \frac{M\mu^2}{\hbar^2 k^2} \right\} \tag{2.43}$$

$$= -\frac{\mu^2}{2g} \left(1 - \frac{4\sqrt{2\mu g^2}}{15\pi^2} \right) \tag{2.44}$$

for the free energy density. The ground state energy can be obtained by using the relation

$$\mathcal{E}(n) = \mathcal{F}(\mu) + n\mu \ , \tag{2.45}$$

in terms of the physical parameter a_s, this yields

$$\frac{E_g}{N} = \frac{2\pi\hbar^2 a_s n}{M}\left[1 + \frac{128}{15}\left(\frac{na_s^3}{\pi}\right)^{1/2}\right] \tag{2.46}$$

for the ground-state energy per particle. The result (2.46) was first obtained by Lee *et al.* (1957). There, instead of our contact potential (2.21), the pseudo potential $V(\mathbf{x}) = g\,\delta(\mathbf{x})(\partial/\partial x)x/2$ was used, which avoids the appearance of ultraviolet divergences. The above result represents an expansion in the diluteness parameter $n|a_s^3|$, which agrees with our initial assumptions in section 2.3 that this parameter is small.

The dispersion law for quasiparticles

In order to analyze how the repulsive interaction alters the excitation spectrum with respect to the ideal gas, it is convenient to define a characteristic length scale ζ, the so called healing length[7]

$$\zeta = \hbar/(2\sqrt{Mng}) \;, \tag{2.47}$$

and a velocity of sound

$$c = \hbar/(2M\zeta) = \sqrt{gn/M} \;. \tag{2.48}$$

The quasiparticle dispersion (2.38) then takes the form

$$E_k = \hbar c\sqrt{k^2(1 + k^2\zeta^2)} \;. \tag{2.49}$$

The quasiparticle operators α_k introduced in eqn. (2.29) are linear superpositions of the original particle operators a_k and $a_k^\dagger$, with u_k and v_k as the weight factors. For small momenta, these coefficients are both large, and the long-wavelength quasiparticle operators represent a nearly equal superposition of a particle and a hole. The dispersion relation in this regime takes the form

$$E(k) \approx c\,\hbar k \quad \text{for} \quad k\zeta \ll 1 \;, \tag{2.50}$$

the Bogoliubov theory predicts that the long wavelength excitations of an interacting Bose gas are sound waves. If the Bogoliubov approximation (2.8) is understood as an operation that breaks the gauge symmetry of the theory, these excitations can be identified with the Goldstone modes associated with BE-condensation (see Leggett and Sols, 1991). In the opposite limit of large momenta, the behavior of the coefficients changes to $u_k^2 \approx 1$, $v_k^2 \ll 1$, so that the short-wavelength

---

[7]For a condensate confined by an infinitely high box potential, the condensate density goes to zero at the walls of the box. ζ is the length scale over which the density profile 'heals' back to its homogeneous value (see Pitaevskii and Stringari, 2003, sec. 11.2).

quasiparticle creation operator is effectively a pure particle creation operator. Correspondingly, the dispersion approaches the free particle law

$$E(k) \approx \epsilon_k^0 + gn \quad \text{for} \quad k\zeta \gg 1 , \tag{2.51}$$

shifted by a constant potential gn, the Hartree interaction with the remaining particles.

2.6 Trapped gases

In the following, we will consider Bose gases confined by a harmonic trapping potential. This is a good approximation to the experimentally obtainable magneto-optical trapping potentials and offers the additional advantage of simple analytic results for the ideal Bose gas. For an overview on the experimental realization of trapping potentials for cold atoms, see for example Pethick and Smith (2002, chap. 3-4).

Harmonic traps

Usually, the trap constitutes an axisymmetric harmonic potential of the form

$$V_t(\mathbf{r}) = V_t(r_\perp, z) = \frac{1}{2} M (\omega_\perp^2 r_\perp^2 + \omega_z^2 z^2) , \tag{2.52}$$

where M denotes the atomic mass. It is common to introduce the anisotropy parameter λ as the ratio of axial to radial angular frequencies

$$\lambda \equiv \omega_z / \omega_\perp . \tag{2.53}$$

For an ideal Bose gas, the single particle states χ_j in the potential (2.52) are the well known eigenfunctions of the harmonic oscillator. The one body correlation function (2.2) can be constructed from the mode expansion of $\hat{\Psi}$, a useful form that combines the summations over the multiple index j of eqn. (2.7) into a single sum is given in eqn. (B.1) (see the plot in fig. 2.2). The lowest state, playing the role of the condensate wavefunction, is a Gaussian (the dashed curve in fig. 2.3)

$$\chi_0(\mathbf{r}) = \left(\frac{M\overline{\omega}}{\pi\hbar} \right)^{3/4} e^{-\frac{1}{2}(r_\perp^2/a_\perp^2 + z^2/a_z^2)} , \tag{2.54}$$

where $\overline{\omega} \equiv (\omega_\perp^2 \omega_z)^{1/3}$. The radial and axial widths in eqn. (2.54) are given by the oscillator lengths

$$a_\perp = \sqrt{\frac{\hbar}{M\omega_\perp}} , \tag{2.55a}$$

$$a_z = a_\perp / \sqrt{\lambda} , \tag{2.55b}$$

the size of the condensate is, in the absence of interparticle interaction, solely determined by the trapping potential and independent of the particle number. For an ideal Bose gas, $(a_z/a_\perp)^2 = \lambda^{-1}$ yields the anisotropy in the density profile, allowing for oblate- and cigar-shaped condensate clouds by keeping $\lambda \gg 1$ or $\lambda \ll 1$, respectively. We will see below that the size of the condensate is significantly increased by repulsive interactions and can be several times larger than the oscillator lengths (2.55). The critical temperature T_c for the onset of quantum degeneracy in three spatial dimensions[8] is

$$k_B T_c = \hbar\overline{\omega}\left(\frac{N}{\zeta_3}\right)^{1/3} \tag{2.56}$$

(see Bagnato *et al.*, 1987), where $\zeta_3 \approx 1.20$ denotes the Riemann Zeta-function. Note the different N-dependence compared to expression (2.14) for the uniform system. In typical experiments with Rubidium atoms in magnetic traps (see Baym and Pethick, 1996), mean trap frequencies are around $\overline{\omega}/(2\pi) \approx 100$ Hz, resulting in oscillator lengths around 2 μm. At the onset of BE condensation the system is very dilute, and the corrections to eqn. (2.56) due to two-body interactions are small (see Pitaevskii and Stringari, 2003, chap. 13). With typical samples containing around 10^6 particles, T_c is in the range of 0.5 μK.

Dipole modes

There are three collective modes (one for each Cartesian direction $\alpha = x, y, z$) in the excitation spectrum of harmonically confined Bose gases which correspond to the harmonic oscillation of the center of mass of the condensate cloud. If the interacting condensate is displaced without deformation, as described by the generalized Kohn theorem (see Dobson, 1994; Kohn, 1961), the frequency E_α of the oscillation due to the restoring force is identical to the frequency of the trapping potential ω_α, independent of the strength of interparticle interactions. For any condensate wavefunction $\Phi(\mathbf{r})$ fulfilling the GPE, the excited state corresponding to the dipole mode in direction α is given by the solution

$$u_\alpha(\mathbf{r}) = a_\alpha^\dagger \Phi(\mathbf{r}) \,,$$
$$v_\alpha(\mathbf{r}) = a_\alpha \Phi^*(\mathbf{r}) \,,$$

to the BdG-equations (2.31) (see Fetter and Rokhsar, 1998), where the operators a_α and $a_\alpha^\dagger$ are the familiar raising and lowering operators for the harmonic oscillator.

---

[8] Quasi two (one) dimensional systems can be constructed using a trapping potential which is very steep in one (two) directions, such that the excited trap modes cannot be occupied in these directions (see Posazhennikova, 2006).
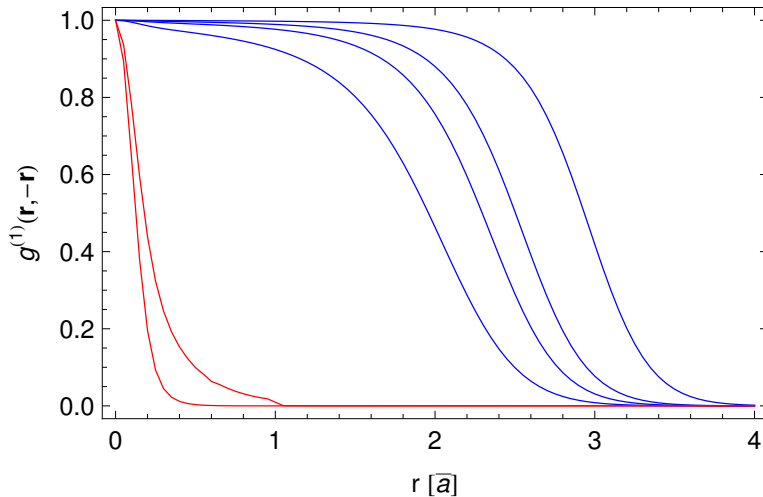
Figure 2.2: The normalized one-body correlation function $g^{(1)}(\mathbf{r}_1, \mathbf{r}_2) = n^{(1)}(\mathbf{r}_1, \mathbf{r}_2)/\sqrt{n^{(1)}(\mathbf{r}_1, \mathbf{r}_1)n^{(1)}(\mathbf{r}_2, \mathbf{r}_2)}$ for an ideal Bose gas in an isotropic harmonic trap. *Blue:* different temperatures below T_c ($T = 0.2, 0.5, 0.7, 0.9\,T_c$, from right to left). *Red:* temperatures above T_c ($T = 1.1, 1.2\,T_c$). Between coordinates close to the trap center ($r < \overline{a}$), the temperature dependence of spatial correlations behaves similar as for the uniform system in fig. 2.1. For distances $r \gg \overline{a}$, the correlation function goes to zero at any temperature, reflecting the finite spatial extent of the system.

The appearance of the trap frequencies in the spectrum of excitation energies provides a valuable cross-check for numerical calculations. Dipole modes can be excited by periodic variations of the trap potential (see Japha and Band, 2002). As they are not damped by interparticle interactions, the oscillations are very long-lived, which made them an ideal probe for the Casimir-Polder measurements of Harber *et al.* (2005) and Obrecht *et al.* (2007).

Thomas-Fermi approximation

The effect of repulsive interactions on the condensate fraction of a trapped BEC is to broaden the density profile, thus decreasing the density in the center of the trap. More quantitatively, rewriting the GPE in dimensionless variables (with the abbreviations $\overline{\omega} = (\omega_{\perp}^2 \omega_z^2)^{1/3}$, $\overline{a} = \sqrt{\hbar/(M\overline{\omega})}$ and the rescaled coordinates $\overline{r} = r/\overline{a}$, $\overline{\mu} = \mu/(\hbar\omega_0)$, $\overline{\Phi} = \Phi\,\overline{a}^{3/2}/N^{1/2}$) yields

$$\left[-\overline{\nabla}^2 + \overline{\mathbf{r}}^2 + 8\pi\left(\frac{Na_s}{\overline{a}}\right)|\overline{\Phi}(\overline{\mathbf{r}})|^2 - 2\overline{\mu}\right]\overline{\Phi}(\overline{\mathbf{r}}) = 0 \;. \tag{2.57}$$

From this equation, it is evident that the importance of the interatomic interactions on the condensate wavefunction is completely fixed by the value of $Na_s/\overline{a}$, which
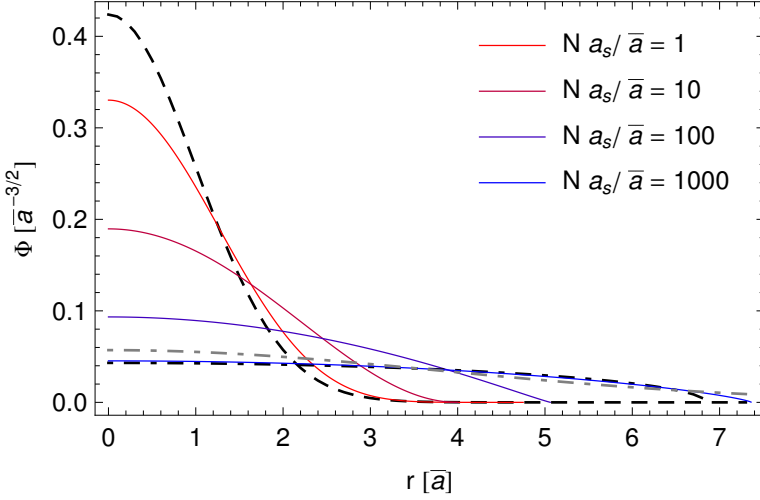
Figure 2.3: Condensate wavefunctions in an isotropic harmonic trap for different values of the Thomas-Fermi parameter $Na_s/\overline{a}$, illustrating the effect of repulsive interparticle interactions on the density profile of the condensate. *Dashed curve:* Gaussian ground-state wavefunction eqn. (2.54) for a noninteracting Bose-gas, corresponding to $a_s = 0$. *Solid curves:* the variational wavefunction eqn. (2.61) for $Na_s/\overline{a} = 1, 10, 100, 1000$. *Black (gray) dot-dashed curve:* the Thomas-Fermi wavefunction eqn. (2.58) and the variational-Gaussian wavefunction of (Pérez-García *et al.*, 1997), both for $Na_s/\overline{a} = 1000$.

is called the Thomas-Fermi (TF) parameter. As the increase in width goes along with a smoothening of the density profile, for large values of the TF parameter it is a good approximation to neglect the kinetic energy term in the GPE. We then obtain the analytical solution (see Baym and Pethick, 1996; Huse and Siggia, 1982)

$$|\Phi_{TF}(\mathbf{r})|^2 = \frac{\mu}{g}\left(1 - \frac{r_\perp^2}{R_\perp^2} - \frac{r_z^2}{R_z^2}\right)\Theta\left[1 - \frac{r_\perp^2}{R_\perp^2} - \frac{r_z^2}{R_z^2}\right] \qquad (2.58)$$

where Θ denotes the unit step function and radial and axial extent of the condensate cloud is given by the TF radii

$$R_{\perp,z}^2 = \frac{2\mu}{M\omega_{\perp,z}^2} \;. \qquad (2.59)$$

As a result of the repulsive interaction, the anisotropy of the condensate is now given by $R_z^2/R_\perp^2 = \lambda^{-2}$ instead of λ^{-1} for the non-interacting gas. Fixing the value of the chemical potential by normalizing Φ (and neglecting the small condensate depletion) determines the radii

$$R_{\perp,z} = \overline{a}\left(\frac{15Na_s}{\overline{a}}\right)^{1/5}\frac{\overline{\omega}}{\omega_{\perp,z}} \;, \qquad (2.60)$$

which shows that the spatial extent of the condensate cloud grows with the number of trapped particles as $N^{1/5}$, in contrast to the ideal gas, where it is fully determined by the trapping potential. For large values of the TF-parameter, the momentum distribution of the atomic cloud, which is the Fourier transform of $\Phi_{TF}(\mathbf{r})$, approaches a δ-function, a typical feature of uniform Bose-Einstein condensed systems (see Pitaevskii and Stringari, 2003, sec. 11.3).

By inserting Φ_{TF} in the BdG equations, it is possible to derive solutions for the fluctuation operator $\hat{\phi}(\mathbf{r})$ in terms of Jacobi polynomials and spherical harmonics (see Öhberg *et al.*, 1997). As the final expressions are rather involved, we do not show them here.

Variational solutions for the condensate wave function

Another possibility for obtaining approximate solutions for the condensate wavefunction is to take a trial function for Φ which depends on variational parameters. For a given value of the Thomas-Fermi parameter, the variational parameters are then determined such that the energy of the condensate is minimized.

An ansatz for a trialfunction with a single parameter is a Gaussian with a variational width depending on the TF parameter, which has to incorporate the broadening of the condensate cloud due to interactions. For large values of the TF parameter (and an isotopic trap), the width of the Gaussian (2.54) is then replaced by $\sigma(N) = \overline{a}(\sqrt{2/\pi}Na_s/\overline{a})^{1/5}$ (see Pérez-García *et al.*, 1997). The resulting wavefunction is shown as the gray dot-dashed curve in fig. 2.3. Because of its simple functional form, we will use it in chapter 5.

A more sophisticated ansatz which we will use in chapter 6 can be used to interpolate smoothly between small and large values of the TF-parameter and involves two variational parameters (see Fetter, 1997):

$$\Phi(\mathbf{r}) = \frac{c_0(\lambda, R)}{N_0}\left(1 - \frac{r_\perp^2}{d_\perp^2} - \frac{r_z^2}{d_z^2}\right)^{(1+\lambda)/2}\Theta\left(1 - \frac{r_\perp^2}{d_\perp^2} - \frac{r_z^2}{d_z^2}\right), \qquad (2.61)$$

where c_0 is a normalization constant and $d_\perp$, d_z and λ can be chosen such that they minimize the energy of the trapped gas. For large values of the TF-parameter, this procedure yields $\lambda \ll 1$, and eqn. (2.61) reproduces the shape of the Thomas-Fermi condensate wave function, while in the opposite limit, the shape approaches that of the Gaussian ground-state wave function of the ideal gas (see fig. 2.3). In a similar manner as for the TF-condensate wavefunction, the field operator describing fluctuations around the variational solution eqn. (2.61) can be explicitly constructed by solving the BdG equations (see Hu *et al.*, 2004).

CHAPTER 3

Phononic Casimir effect

The material presented in this chapter is based on the paper 'Casimir energy of a BEC: from moderate interactions to the ideal gas' *by* J. Schiefele and C. Henkel, *Journal of Physics A* **42**, 045401 (2009).

The Casimir effect is a consequence of the distorted vacuum fluctuation spectrum of quantized fields in bounded domains or spaces with non-trivial topologies. In Casimir's original calculation, the system under consideration is the electromagnetic vacuum (Casimir, 1948). Imposing Dirichlet boundary conditions along one spatial direction by confining the system between two (idealized) parallel plates causes a change in the (infinite) vacuum energy-density. The variation of the vacuum energy-density with respect to the plate separation is called Casimir pressure, and, after renormalization, yields a finite expression for an attractive interaction energy per unit area between the plates. The electromagnetic Casimir force, caused by quantum fluctuations of the electromagnetic vacuum, varies as $\hbar c/L^4$, with L the plate separation and c the speed of light. It has been measured in a number of experiments using various experimental settings (see Bordag *et al.*, 2001, sec. 6). The comparison between quantum vacuum experiments like these and the predictions of different theoretical models provides the possibility of testing fundamental physics (like higher dimensions or additional interactions), in much the same way as accelerator experiments in high-energy physics do at the other end of the energy scale (see Decca *et al.*, 2003; Gies, 2008).

We consider here, instead of the electromagnetic vacuum, a weakly interacting uniform BEC at zero temperature, and expect, in a similar manner, the quantum fluctuations on top of the ground state of the BEC to give rise to observable Casimir forces: As we have see in section 2.5, within the Bogoliubov approximation, the excited states of a BEC can be treated as quasiparticles characterized by the dispersion relation

$$E(k) = \hbar c \sqrt{k^2(1 + k^2\zeta^2)} \, , \tag{3.1}$$

that behaves linearly for small momenta, with the 'sound velocity' $c = \hbar/(2M\zeta)$ being inverse to the healing length ζ. In eqn. (3.1), the wave-number $1/\zeta$ characterizes the transition between the linear (phonon) and the quadratic (free-particle) regimes. ζ is also related to the s-wave scattering length a_s of the atoms and to the BEC density n via $\zeta = 1/(4\sqrt{\pi n a_s})$. For small momenta, the quasiparticles (phonons) propagate in the same way as the massless electromagnetic field, except for the propagation velocity being different. Hence, the zero temperature quantum fluctuations in a spatially confined BEC can be expected to result in an observable Casimir force.

Different scenarios for Casimir forces in BECs have been analyzed by previous work: for the parallel plate geometry, an asymptotic expansion of the Casimir force has been calculated by Edery (2006a), the small expansion parameter being the ratio between healing length and plate separation. In the leading order, it reproduces exactly the same $\hbar c/L^4$ behavior as in the electromagnetic vacuum. The next order corrections scale with the ratio ζ/L. Replacing the perfectly reflecting plates by impurities embedded in a quantum liquid, Casimir forces between these impurities have been calculated by Recati *et al.* (2005) and Klein and Fleischhauer (2005) as a function of the impurity-liquid coupling. Scattering of Bogoliubov excitations by a single impurity potential has been studied by Gaul and Müller (2008). If the impurities are realized by atoms which, in a certain internal state, interact with the atoms of the quantum liquid through s-wave scattering, the Casimir interaction should be detectable as a shift of spectral lines that depends on the distance between the impurities. In the limit of an infinitely strong impurity-liquid coupling, the result for the (one-dimensional) parallel plate scenario was recovered (Recati *et al.*, 2005); for a weak coupling, however, the interaction between the impurities vanishes exponentially with the impurity separation on a scale set by the healing length. For the ideal Bose gas, it was found that there is no Casimir force at all between impurities of arbitrary interaction strength, including the idealized parallel plate scenario (see Recati *et al.*, 2005, appendix C). This is consistent with the quite general method of Bachmann and Kempf (2008), which is mapping (polynomial) dispersion relations to Casimir forces in the parallel plate geometry: this method shows that media with quadratic dispersion relations, and hence the ideal Bose gas, do not give rise to any zero-temperature Casimir forces. A non-vanishing Casimir force in the ideal Bose gas can arise due to *thermal* fluctuations, as calculated by Biswas (2007) and Martin and Zagrebnov (2006). All these forces are small but finite observable quantities, which—if experimentally confirmed—would provide direct evidence of the quantum fluctuations in weakly interacting BECs.

The system under consideration in the present chapter is a homogeneous, weakly-interacting dilute BEC at zero temperature, confined to a parallel plate geometry with periodic boundary conditions in one of the three spatial dimensions. For this system, we will give a renormalized expression for the Casimir energy-density per

unit area. Our expression has the form of an integral over a 'density of modes' $\rho(x)$ times the Bose distribution function:

$$\mathcal{E}_C = \int_0^\infty \frac{dx\,\rho(x)}{e^{2\pi x} - 1} \,, \tag{3.2}$$

where $\rho(x)$ has a simple analytic form (see eqn. (3.20)), and correctly describes the vanishing of the Casimir force in the limit of the interaction strength going to zero. The possibility to express the zero temperature Casimir energy in the above form, resembling the density of states of a bosonic system at finite temperature, is connected to a topological analogy between our parallel plate scenario and finite temperature field theory: In the parallel plate geometry, one spatial coordinate of the field is subject to periodic boundary conditions, while in finite temperature field theory, the imaginary time coordinate is subject to a similar periodicity condition. This analogy has been pointed out some time ago by Toms (1980); it does not carry over, however, to Casimir calculations for non-linear dispersion relations. The periodic boundary conditions for the BEC have mainly been chosen because they make the relation to the finite temperature case particularly evident. In experiments, periodic boundary conditions can be realized in toroidal traps, but they also appear in optical lattices. If the boundaries are taken as real physical plates, the perfect mirror scenario (i.e. Dirichlet boundary conditions as discussed by Bachmann and Kempf (2008); Biswas (2007); Edery (2006b)) is closer to an experimentally realizable situation. When Dirichlet boundary conditions are imposed on the fluctuations on top of the BEC ground state, the expansion of $\mathcal{E}_C$ for moderate interaction shows in the leading term again the same behavior as a massless scalar field propagating at the speed of sound c, but with a different numerical prefactor (see Schiefele and Henkel, 2009, appendix A).

3.1 Free energy in a weakly interacting, dilute BEC at $T = 0$

As we have seen in section 2.5, the free energy density of a weakly interacting uniform BEC at $T = 0$ (in three spatial dimensions) is approximated by the perturbative expansion

$$\mathcal{F} = \mathcal{F}_0 + \mathcal{F}_1 \,, \tag{3.3}$$

where $\mathcal{F}_1$ contains the counterterm $\Delta_1 \mathcal{F}$ that renders the expression (3.3) finite. The concrete form of the counterterm depends on the renormalization scheme; in this chapter we will follow the approach of Andersen (2004, see sec. III.B-C for more details), which yields

$$\mathcal{F}_0 \;\; = \;\; -\frac{\mu^2}{2g} \tag{3.4}$$

$$\mathcal{F}_1 \;\; = \;\; \frac{1}{2} \int \frac{d^3k}{(2\pi)^3} \; \sqrt{k^2(k^2 + 2\mu)} + \Delta_1 \mathcal{F} \,. \tag{3.5}$$

25

(Here and for the rest of this chapter, we work in units where $2M = \hbar = k_B = 1$.) In the above expression, μ is the chemical potential (which, in section 3.3, will be connected to the speed of sound in the medium), and $g = 8\pi a_s$ is the effective coupling constant eqn. (2.23). The term $\Delta_1 \mathcal{F}$ can be set to zero if, as in (Andersen, 2004), dimensional regularization is used to calculate the integral eqn. (3.5). If instead a momentum cut-off M in the ultraviolet is used for the regularization of $\mathcal{F}_1$, the linear, cubic and quintic divergences can be absorbed by renormalizing g, μ and the vacuum energy respectively, and the counterterm reads

$$\Delta_1 \mathcal{F} = \frac{1}{2} \int^M \frac{d^3 k}{(2\pi)^3} \left\{ \frac{\mu^2}{2k^2} - \mu - k^2 \right\} , \qquad (3.6)$$

which recovers the expressions of eqn. (2.39) and eqn. (2.41). $\mathcal{F}$ is then finite in the limit $M \to \infty$, and using

$$\mathcal{E}(n) = \mathcal{F}(\mu) + n\mu , \qquad (3.7)$$

one recovers the ground state energy (2.46). The chemical potential μ can be obtained from eqn. (3.3) by inverting

$$n(\mu) = -\frac{\partial \mathcal{F}}{\partial \mu} , \qquad (3.8)$$

which yields

$$\mu(n) = gn \left\{ 1 + \mathcal{O}\left(\sqrt{n a_s^3} \right) \right\} , \qquad (3.9)$$

as we already obtained in eqn. (2.37).

3.2 The Casimir energy as an integral over a mode density

Now, in order to describe a BEC between a pair of parallel plates separated by a finite distance L (with periodic boundary conditions), we have to quantize the momentum component perpendicular to the plates:

$$k^2 \to k^2 + \omega_n^2, \quad \omega_n = \frac{2\pi}{L} n, \quad n \in \mathbb{Z} \qquad (3.10)$$

Correspondingly, the momentum integration perpendicular to the plates is replaced by a discrete sum:

$$\int \frac{d^3 k}{(2\pi)^3} \to \sum_{n=-\infty}^{\infty} \int \frac{d^2 k}{(2\pi)^2} \qquad (3.11)$$

The area of the plates is taken to be $L_1 L_2$ with $L_1, L_2 \gg L$, so the system now inhabits the volume $\overline{V} = L_1 L_2 L$. The mean field contribution $\mathcal{F}_0$ (see eqn. (3.4)) depends only trivially on the new boundary conditions, with the volume $\overline{V}$ entering through μ in eqn. (3.9).

The Casimir energy $\mathcal{E}_C$ of the BEC is related to the free energy calculated in second-order perturbation theory. We are interested in its change per unit area that is due to the introduction of the boundary conditions:

$$\overline{\mathcal{F}}_1 = L\mathcal{F}_1\big|_{V=\overline{V}} + \mathcal{E}_C \,, \tag{3.12}$$

where the first term gives the the free energy in a homogeneous system. After applying the substitutions (3.10) and (3.11) to eqn. (3.5), we are left with the following expression for $\overline{\mathcal{F}}_1$, now describing the leading quantum corrections to the free energy of a BEC confined between parallel plates:

$$\overline{\mathcal{F}}_1 = \frac{1}{2\,\overline{L}^2} \sum_{n=-\infty}^{\infty} \int \frac{d^2k}{(2\pi)^2} \sqrt{\left[(\overline{L}\,k)^2 + n^2\right]\left[M(k)^2 + n^2\right]} \,, \tag{3.13}$$

where we have used the abbreviations

$$M(k,L,\zeta) = \overline{L}\,\sqrt{k^2 + 1/\zeta^2} \,, \tag{3.14}$$

with $\overline{L} = L/(2\pi)$ and $\zeta = 1/\sqrt{2\mu}$. The summation over n can be converted into two integrals by using the Abel-Plana formula in the form

$$\sum_{n=0}^{\infty} f(n) = \int_0^{\infty} dx\, f(x) + \frac{1}{2}\,f(0) + i \int_0^{\infty} dx\, \frac{f(ix) - f(-ix)}{e^{2\pi x} - 1} \tag{3.15}$$

(see Saharian, 2008). Application of eqn. (3.15) splits eqn. (3.13) into the two terms written in eqn. (3.12), as the $f(0)$–term cancels out. The first term, $L\mathcal{F}_1\big|_{V=\overline{V}}$, is divergent, but of the same form as the free-space expression eqn. (3.5) itself. Hence, it can be renormalized as described above.

The term $\mathcal{E}_C$ in eqn. (3.12), an energy per area, describes the effects induced by restricting the periodicity in one spatial dimension to be much smaller than the remaining ones, that is, confining the system to a volume $\overline{V}$ with one 'short' side L. $\mathcal{E}_C$ is convergent for any finite L, strictly negative, and goes to zero for $L \to \infty$:

$$\mathcal{E}_C = -\frac{2}{\overline{L}^2} \int \frac{d^2k}{(2\pi)^2} \int_{\overline{L}k}^{M(k)} dx\, \frac{\left[x^2 - (\overline{L}\,k)^2\right]^{1/2}\left[M(k)^2 - x^2\right]^{1/2}}{e^{2\pi x} - 1} \,. \tag{3.16}$$

The integration domain is sketched in fig. 3.1(a) (the shaded regions).

This domain as well as the form of the integrand are due to the branch-points of the integrand in eqn. (3.13): In order to stay clear of the branch-cuts, we have evaluated the last term in the Abel-Plana formula eqn. (3.15) along an integration contour slightly to the right of the imaginary axis. Inserting the function f given by eqn. (3.13),

$$f(x) = \sqrt{(x^2 + \overline{L}^2\,k^2)(x^2 + M^2)} \,, \tag{3.17}$$
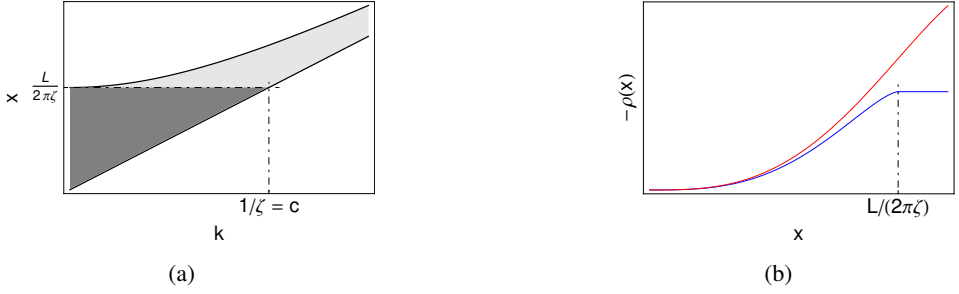
27

Figure 3.1: (a) The upper curve shows the function $M(k, L, \zeta)$ from eqn. (3.14), the lower one is $\overline{L}k \equiv Lk/(2\pi)$. The two shaded regions make up the total area of integration in eqn. (3.16). **(b)** The exact 'density of states' function $\rho(x)$ from eqn. (3.20) *(blue)* and its small-argument expansion eqn. (3.21) *(red)*.

the numerator in the last term of eqn. (3.15) evaluates to

$$i\left(f(ix+0)-f(-ix+0)\right) = -2\sqrt{(x^2 - \overline{L}^2 k^2)(M^2 - x^2)}\,, \qquad \overline{L}k < x < M\,,$$
(3.18)

being zero everywhere else along the contour of integration (see Mostepanenko and Trunov, 1997, sec. 2.2). By changing the order of integration in eqn. (3.16), the k-integral can be performed, and we find the expression (3.2) for the Casimir energy:

$$\mathcal{E}_C = \int_0^\infty \frac{dx\,\rho(x,\overline{L})}{e^{2\pi x} - 1}$$
(3.19)

In the form of eqn. (3.19), $\mathcal{E}_C$ is expressed as an integral over a 'density of states' (DOS) for a bosonic system, as setting the integration variable $x = \beta\omega/(2\pi)$ will reproduce the Boltzmann factor in the denominator.

The 'mode density' $\rho(x)$ is obtained by integrating separately over the lower triangular region in fig. 3.1(a) (dark gray) and the 'hyperbolic tail' (light gray). In terms of the dimensionless variable $\eta = (\zeta/\overline{L})\,x$, we have

$$\rho(x,\overline{L}) = \begin{cases} -\frac{1}{8\pi\zeta^4}\left\{\arcsin(\eta) - \eta\left(1 - 2\,\eta^2\right)\sqrt{1 - \eta^2}\right\} & , \quad 0 \le x < \overline{L}/\zeta\,, \\ -\frac{1}{16\,\zeta^4} & , \quad x \ge \overline{L}/\zeta\,. \end{cases}$$
(3.20)

Above $x = \overline{L}/\zeta$, the function $\rho(x)$ changes into a constant independent of x (see the blue line in fig. 3.1(b)). The Casimir energy $\mathcal{E}_C$ as a function of the normalized distance $\overline{L}/\zeta$ is shown in fig. 3.2, obtained by numerically integrating eqn. (3.19).

To provide a cross-check for the above results, we will show in the following section that the function $\rho(x)$ reproduces the asymptotic expansion for the Casimir energy given by Edery (2006a) and Roberts and Pomeau (2005), which is valid for small values of the parameter ζ/L. In section 3.5 we then show that the formula
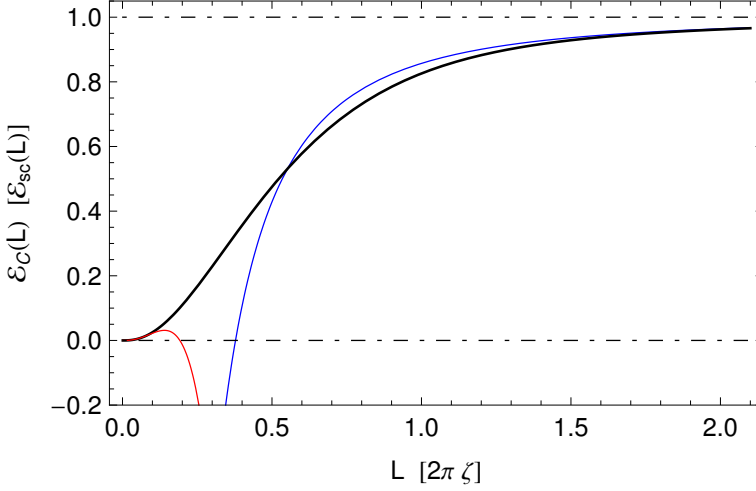
Figure 3.2: Casimir energy per unit area as a function of the plate separation L, normalized to the healing length ζ. Recall that $\zeta = \frac{\hbar}{2}\sqrt{1/(gnm)}$ with g the effective interaction constant and n the BEC density. The Casimir energy has been normalized to its value $\mathcal{E}_{sc}(L) = -(\pi^2/90)\hbar c/L^3$ for a massless scalar field propagating with a velocity $c = \hbar/(2m\zeta)$; this limit is approached at large distance. *Blue:* the asymptotic expansion for $L/\zeta \gg 1$ eqn. (3.23). *Red:* the opposite limit $L/\zeta \to 0$ (non-interacting Bose gas), of eqn. eqn. (3.33). *Solid black curve:* numerical evaluation of the integral in eqn. (3.19) with the mode density $\rho(x)$ of eqn. (3.20). It smoothly describes the dependence of $\mathcal{E}_C$ on the interaction strength in the regime where both of the asymptotic expansions diverge.

for $\rho(x)$ in eqn. (3.20) also yields correct results in the opposite limit of the ideal BEC, i.e. $\zeta \to \infty$.

3.3 Expansion at large distance and moderate interactions

In this section, we will assume the plate separation to be much greater than the healing length of the BEC, i.e., the ratio $\zeta/L \ll 1$ can be treated as a small parameter. Note that this limit cannot describe a strongly interacting Bose gas in the proper sense, since this would lead to a break-down of the perturbative expansion at the basis of our approach.

As can be seen in fig. 3.1(b), the kink in the function $\rho(x)$ happens at the large value $x = \overline{L}/\zeta \gg 1$ in our limit. In evaluating the Casimir energy with eqn. (3.19), large values of x, and hence the behavior of $\rho(x)$ after the kink, get exponentially suppressed by the denominator. Thus we can approximate the function $\rho(x)$ by

expanding its small-x part as a power-series around $x = 0$:

$$\rho(x) = -\frac{1}{L^4}\left\{\frac{1}{\pi}\frac{x^3}{3}\left(\frac{\zeta}{\overline{\overline{L}}}\right)^{-1} - \frac{1}{\pi}\frac{x^5}{10}\frac{\zeta}{\overline{\overline{L}}} + \mathcal{O}((\zeta/L)^3)\right\} \tag{3.21}$$

The integrals in expression (3.19) for the Casimir energy can be performed explicitly with the identities

$$\int_0^\infty dt\,\frac{t^{2r-1}}{e^{2\pi t}-1} = \frac{\Gamma(2r)\,\zeta(2r)}{(2\pi)^{2r}} \tag{3.22}$$

in terms of Gamma- and Zeta-functions. Upon setting $c \equiv 1/\zeta$ (the speed of sound in the medium), we recover the result derived by Edery (2006a):

$$\mathcal{E}_C = -\frac{\pi^2}{90}\frac{c}{L^3} + \frac{2\pi^4}{315}\frac{c\,\zeta^2}{L^5} + \mathcal{O}(\zeta^3/L^7)\,. \tag{3.23}$$

The leading term $\mathcal{E}_{sc} = -\pi^2 c/(90L^3)$ is, as noted in (Edery, 2006a,b), equal to the Casimir energy (per unit area) of a massless scalar field with propagation velocity c confined between two parallel plates with periodic boundary conditions (see Svaiter and Svaiter, 1991). Its presence can be understood as a manifestation of the Goldstone-theorem, the long wavelength part of the Bogoliubov spectrum representing the gap-less Goldstone modes (Hugenholtz and Pines, 1959). The next-to-leading term in eqn. (3.23) is referred to as the *Bogoliubov correction* (see Edery, 2006a) due to the non-linearity of the dispersion. Indeed, if we express the Bogoliubov dispersion relation (3.1) as a power series around $k = 0$ and put the first few terms into the expression for the Casimir force derived by Bachmann and Kempf (2008, eqn. (16)), the leading term in the same manner reproduces the result for the scalar field (in one dimension), followed by terms that are smaller in magnitude and of opposite sign. As can be seen in fig. 3.2, the contribution of these corrections gets smaller as the ratio between plate separation and healing length increases, leaving only the dominant scalar term $\mathcal{E}_{sc}$ depicted by the horizontal dashed line in fig. 3.2.

When finally calculating the Casimir pressure from eqn. (3.23), one has to consider that, for a constant average particle number, the derivative of the speed of sound with respect to L is not zero, as discussed in (Edery, 2006a).

3.4 A formal analogy to finite temperature systems

As already mentioned, our expression (3.19) for $\mathcal{E}_C$ at $T = 0$ formally resembles the DOS for a bosonic system at finite temperature. This can be understood by recalling that a finite temperature system can be described in imaginary time, combined with periodic boundary conditions with period β. The same topology is realized in the parallel plate system at $T = 0$, when one spatial dimension is

subject to periodic boundary conditions with period L (see Hawking, 1977; Toms, 1980).

Let us briefly re-phrase the argument of Toms (1980) within our notation. The canonical partition function $\mathcal{Z}$ for a system at temperature $T = 1/\beta$ in D spatial dimensions can be expressed as the path integral

$$\mathcal{Z} \approx \oint d[\Phi] \exp\left[\int_0^\beta d\tau \int d^D x \, \mathcal{L}(\Phi)\right] , \qquad (3.24)$$

where $\mathcal{L}$ is the Lagrangian (a scalar functional of the field Φ), and the field is constrained in such a way that $\Phi(\mathbf{x}, 0) = \Phi(\mathbf{x}, \beta)$. If we take $\mathcal{L} = (c^2/2) \, \partial_\mu \Phi \, \partial^\mu \Phi$, the path-integral in eqn. (3.24) can, after Fourier expansion of the field, be evaluated to yield (see Bernard, 1974; Kapusta and Gale, 2006)

$$\ln[\mathcal{Z}] = -V \frac{1}{2} \sum_n \int \frac{d^D k}{(2\pi)^D} \, \ln\left[\omega_n^2 + \omega(k)^2\right] , \quad \omega_n = \frac{2\pi}{\beta} n , \quad \omega(k) = c \, |\vec{k}| . \tag{3.25}$$

Here, ω_n with $n = 0, \pm 1, \pm 2, \ldots$ are the Matsubara-frequencies due to the periodicity condition in eqn. (3.24), and ω_k with the continuous parameter k is the dispersion relation of the massless scalar field. Note the similarity to eqn. (3.10), where we had periodic boundary conditions not in imaginary time but in one spatial dimension.

The sum over n in eqn. (3.25) is usually evaluated by multiplying with a factor $\frac{1}{2}\beta \cot(\frac{1}{2}\beta\omega)$, which has poles of residue 1 at $\omega = 2\pi n/\beta$, and then integrating over a contour in the complex ω-plane which includes all the poles (see Kapusta and Gale, 2006, sec. 3.4). This technique is actually the same that is used by Saharian (2008) to prove the Abel-Plana formula eqn. (3.15). The well-known result is

$$\ln[\mathcal{Z}] = \ln[\mathcal{Z}]\Big|_{\beta \to \infty} - V \int \frac{d^D k}{(2\pi)^D} \, \ln\left[1 - e^{-\beta \omega(k)}\right] , \qquad (3.26)$$

where we have already subtracted the zero-point fluctuations. After integrating by parts and employing eqn. (3.22) we obtain (Ω_D denotes the volume of the unit sphere in D dimensions)

$$\ln[\mathcal{Z}] = -V\beta c \, \frac{\Omega_D/D}{(2\pi)^D} \int_0^\infty \frac{dk \, k^D}{e^{\beta \, ck} - 1} . \qquad (3.27)$$

Note that, upon setting $k = (2\pi/\beta c) \, x$, the above expression has the same form as $\mathcal{E}_C$ in eqn. (3.19), with $\rho(x)$ being proportional to x^D. Now, let the system inhabit a volume $\overline{V} = L_1 L_2 L$. With $D = 3$ we get for the free energy per unit area

$$\frac{F}{L_1 L_2} = -\frac{\pi^2}{90} \frac{L}{\beta \, (\beta c)^3} . \qquad (3.28)$$

Tentatively exchanging βc with L in eqn. (3.28) will reproduce the Casimir energy for a massless scalar field, i.e. the first term in eqn. (3.23) (see Toms, 1980):

$$\frac{F}{L_1 L_2} \xrightarrow{\beta c \leftrightarrow L} -\frac{\pi^2}{90}\frac{c}{L^3} = \mathcal{E}_{sc} \tag{3.29}$$

So, we have seen that the zero temperature Casimir energy of a massless scalar field confined between two parallel plates can be obtained by a simple change of variables, once we know the thermal contribution to the free energy density of that field. Unfortunately, this simple mapping does not carry over to fields characterized by nonlinear dispersion relations: The temperature dependent part of the free energy for a BEC is (in the Bogoliubov approximation) still given by eqn. (3.26) with the dispersion now being $\omega(k) = ck\,(k^2 + 1/\zeta^2)^{1/2}$. But a simple interchange of βc with L in eqn. (3.26) will no longer yield $\mathcal{E}_C$, because the discretized Matsubara frequencies ω_n (that become a discretized momentum) always enter in eqn. (3.25) in the same way as a spatial momentum component enters in a *linear* dispersion relation. It thus seems very difficult to mimic the fully nonlinear behavior of the dispersion relation.

3.5 The non-interacting limit

The transition from the weakly interacting BEC to the ideal BEC should be accomplished by sending the effective coupling $g = 8\pi a_s$ to zero, corresponding to $\zeta \to \infty$. The Casimir energy is expected to vanish in this limit, as shown in (Bachmann and Kempf, 2008; Recati *et al.*, 2005).

The series expansion eqn. (3.21) was constructed for $\zeta/L \ll 1$, which is a physically reasonable assumption for finite L and a weak but finite interaction. But with the effective coupling strength $g \to 0$, the chemical potential μ in eqn. (3.9) will vanish, too, and the healing length ζ will diverge. As L is kept finite, the non-interacting BEC is hence described by the limit $L/\zeta \to 0$, which is the opposite to the case considered in section 3.3. The asymptotic form of eqn. (3.21) for the mode density $\rho(x)$—as well as the Casimir energy in eqn. (3.23)—diverges in the limit of zero interaction strength. Our calculation of the exact mode density $\rho(x)$ suggests that this divergence is due to a branch point in the complex x-plane that moves towards $x = 0$ and makes the power series expansion behind eqn. (3.23) break down. We show here that the exact mode density eqn. (3.20) leads to a Casimir energy that smoothly vanishes with the interaction strength (see fig. 3.2).

To examine the asymptotic behavior of $\mathcal{E}_C$ for $\overline{L}/\zeta \ll 1$, we again start from eqn. (3.19) and eqn. (3.20), separately treating the behavior of $\rho(x)$ to the left and

the right of the kink at $\overline{L}/\zeta$:

$$\mathcal{E}_C = \int_0^{\overline{L}/\zeta} \frac{dx \, \rho(x)}{e^{2\pi x} - 1} - \frac{1}{16\zeta^4} \int_{\overline{L}/\zeta}^\infty \frac{dx}{e^{2\pi x} - 1} \tag{3.30}$$

$$= \mathcal{E}_1 + \mathcal{E}_2 \tag{3.31}$$

As the upper limit of the integration in $\mathcal{E}_1$ is going to zero, we can replace $\rho(x)$ by the first term in the expansion of eqn. (3.21), and Taylor-expand the denominator about $x = 0$. After integrating over this expansion, $\mathcal{E}_1$ will yield terms of $\mathcal{O}\big((\overline{L}/\zeta)^4\big)$. Integrating $\mathcal{E}_2$, from the lower border of the integral we get a contribution

$$\mathcal{E}_2 = \frac{\pi^3}{2L^4} \left(\frac{\overline{L}}{\zeta}\right)^4 \ln\big[e^{2\pi (\overline{L}/\zeta)} - 1\big] \,. \tag{3.32}$$

Altogether, we find for the behavior of $\mathcal{E}_C$ in the non-interacting limit

$$\mathcal{E}_C = -\frac{1}{L^4} \left(\frac{\overline{L}}{\zeta}\right)^4 \left\{\frac{4\pi^2}{3} - \frac{\pi^3}{2} \ln\big[e^{2\pi (\overline{L}/\zeta)} - 1\big]\right\} + \mathcal{O}\big((\overline{L}/\zeta)^5\big) \,. \tag{3.33}$$

Note that the leading order for $\zeta \to \infty$ at fixed L goes like $\zeta^{-4} \ln \zeta$. Conversely, at fixed ζ, a logarithmic divergence remains for $L \to 0$. The logarithmic term changes sign for $L/\zeta > \ln[2] \approx 0.7$ and, for large values of $\overline{L}/\zeta$, the above expression diverges, just as the expansion eqn. (3.23) does for small values of $\overline{L}/\zeta$ (see fig. 3.2). Hence, eqn. (3.33) and eqn. (3.23) provide two asymptotic expansions to $\mathcal{E}_C$ for opposite limits, while the exact formula is given by eqn. (3.19).

3.6 Summary

Starting from the free energy in a weakly interacting dilute BEC, we derived a renormalized expression for the 'phononic' Casimir energy of the BEC confined at zero temperature to a parallel plate geometry with periodic boundary conditions. Our formula for the Casimir energy (per unit plate area), eqn. (3.19), has the form of an integral over a mode density ρ times the Bose distribution. The function ρ is given by a rather simple analytic expression in eqn. (3.20). In section 3.3, we provided a cross-check for our result by showing that a series expansion of ρ in the parameter $L/\zeta \gg 1$ reproduces the asymptotic series for the Casimir energy derived in (Edery, 2006a). There, the Euler-MacLaurin formula was used to extract the long wavelength behavior out of the UV-divergent sum over all Bogoliubov modes satisfying the boundary conditions. This approach fails to reproduce the non-interacting limit.

As pointed out by Edery (2006a,b), the Casimir energy of the weakly interacting BEC is, due to the linear dispersion of its low lying excitations, in the leading order determined by a term analogous to the Casimir energy of a massless scalar

field propagating with vacuum velocity $c = 1/\zeta$. Our result displays this behavior in the regime of the weakly interacting BEC where the plate separation is much larger than the healing length, as can be seen in fig. 3.2. In addition, for $\zeta \to \infty$ with L kept finite (the non-interacting limit), our result (3.20) correctly describes the Casimir energy going to zero and displays the Casimir energy as a smoothly varying function of the interaction strength in the intermediate range. The subtleties of the asymptotic expansions illustrate the rich physical content behind the nonlinear dispersion relation of the Bogoliubov vacuum.

Quantum field theory of the Casimir-Polder interaction

The interaction potential between a neutral, polarizable atom or molecule and a macroscopic surface originates in the coupling between the atom and the (thermal- or quantum-) fluctuations of the electromagnetic (em) field. The surface contains sources that radiate a field, and it imposes boundary conditions on both the intrinsic field fluctuations and the field radiated by the atom. In this section we present in some detail a rather general formalism developed in (Schiefele and Henkel, 2010) for the treatment of Casimir-Polder (CP) interactions between dilute atomic gases and macroscopic surfaces. The theory has to deal with a confined atomic system in a trap (including inter-atomic interactions), and the interaction with the electromagnetic field is the relevant perturbation. In section 4.1, we briefly describe our procedure for perturbation theory, which offers a pictorial representation in terms of Feynman diagrams and permits us to compute the electromagnetic self-energy of the atomic system, expanded in a Dyson series.

Traditionally, the techniques employed in the calculation of CP forces are lent from non-relativistic QED: a mode expansion of the electromagnetic field and a first quantized theory for the remaining (atomic) part of the system.[1] In contrast, our approach is formulated in terms of second-quantized atom field operators, as they are commonly used in the theory concerning BEC. We here build on the quantum field theory of atom-photon interaction as formulated by Lewenstein *et al.* (1994) and Zhang and Walls (1994), and introduce, in section 4.2, atom field operators which also consider the internal electronic degree of freedom.

Concerning the electromagnetic field, we will not work with explicit mode expansions adapted to boundary conditions, but instead use another approach which

---

[1]See, for example, Barton and Fawcett (1988) or Craig and Thirunamachandran (1998).

makes use of the fluctuation-dissipation theorem (see Wylie and Sipe, 1984, 1985): the level shift is cast in a form involving generalized susceptibilities from linear response theory, the (retarded) Green functions. The influence of the surface is then encoded in the appropriate scattering amplitudes of the body, that is, reflection coefficients for a planar interface. This makes the approach applicable to very general descriptions of the surface material, including absorption and dispersion. Another advantage of the formalism lies in the fact that renormalization gets simplified, as the (divergent) free-space part of the Lamb shift is easily isolated from the surface-dependent contributions, the latter being finite. The relevant correlation functions of $\mathbf{E}$ near the surface will be dealt with in section 4.4.

To illustrate our formalism and to provide a cross-check with existing results, we calculate the electromagnetic self-energy of a single two-level atom in second order perturbation theory in section 4.3 and use these results to derive the CP interaction of the atom with a plane surface in section 4.5. Our approach provides a consistent modular concept to describe effects associated with different atomic systems near interfaces, as field and atomic system are separately described by their respective correlation functions. The techniques described below will be put to use in chapter 5 and chapter 6 to describe effects involving Bose-Einstein condensates near interfaces.

4.1 Perturbative framework

The total Hamiltonian of our system can be split as follows:

$$H = H_A + H_{AF} + H_F \ . \tag{4.1}$$

Here, H_F describes the free em-field (without any perturbation by the atoms, but in the presence of the surface), H_{AF} contains the atom-field interaction, and the Hamiltonian H_A describes the trapped atoms.

To investigate the CP interaction between the atomic system and the surface, we employ perturbation theory in the atom-field coupling H_{AF}. Technically, we use the Dyson series[2] to approximate the S-matrix

$$S = 1 + \sum_{n=1}^{\infty} \frac{(-i)^n}{n!} \int dt_1 \dots dt_n \, T\{H_{AF}(t_1) \dots H_{AF}(t_n)\} \ , \tag{4.2}$$

which yields an asymptotic expansion in the coupling constant appearing in H_{AF}. The symbol $T\{\dots\}$ in eqn. (4.2) denotes time ordering, and the operators $H_{AF}(t_i)$ are taken in the interaction picture, with a time dependence governed by the unperturbed Hamiltonian $H_A + H_F$. The T-matrix is defined by separating the trivial

---

[2] See Dyson (1949b) or Weinberg (2005, chap. 3).

part of the S-matrix (which describes a transition from an initial state $|i\rangle$ into an identical final state $|f\rangle$ with no interaction taking place)

$$S_{if} = \delta(i - f) - 2\pi i \, \delta(E_i - E_f) \, T_{if} \ , \qquad (4.3)$$

where E_i and E_f denote the energies of the initial and final state, respectively. The energy-shift $\mathrm{Re}\,[\Delta E]$ acquired by an eigenstate of $H_A + H_F$ through interaction with the em-field can be computed from

$$S_{fi} = e^{-2\pi i \delta(E_i - E_f)\Delta E}$$

(see Rodberg, 1958). By retaining only the first few terms of the series (4.2), we can calculate this energy-shift up to the desired order in the atom field interaction, once a specific form of the interaction Hamiltonian H_{AF} is established.

4.2 Atom-field coupling

Our description of the atom-field coupling basically follows the treatment of Lewenstein *et al.* (1994). We consider alkali atoms which can be modeled as consisting of heavy nuclei of effective positive charge with a much lighter valence electron of negative charge. Electron and core interact via a screened Coulomb potential. The interaction between atoms and the em-field can be incorporated by the standard minimal coupling (or $\mathbf{p}.\mathbf{A}$ coupling) procedure which consists of replacing the canonical momenta of cores and electrons by $\mathbf{p}_j \rightarrow \mathbf{p}_j - e/c\,\mathbf{A}(\mathbf{r}_j)$, with $\mathbf{A}(\mathbf{r})$ the transverse electromagnetic potential in the Coulomb gauge. For our purposes, it is more practical to use the Hamiltonian in the $\boldsymbol{\mu}.\mathbf{E}$ gauge (where $\boldsymbol{\mu}$ denotes a transition matrix element of the electric dipole operator), as it does neither contain $\mathbf{A}^2$ terms nor static dipole-dipole interactions between atoms. The $\boldsymbol{\mu}.\mathbf{E}$ Hamiltonian is obtained by applying a unitary transformation to the minimal coupling Hamiltonian.[3] For our purposes, two approximations that will greatly simplify the Hamiltonian seem appropriate: the dipole- and two-level approximation for the atoms.

In the dipole approximation, one uses the fact that electrons are bound tightly to the core, with typical distances of the order of a few Bohr radii, while the typical interatomic distances in dilute ultracold atomic gases are of the order of several s-wave scattering lengths.[4] Also, the wavelength of photons involved in atom-field interactions is much larger than the Bohr-radius, which means that atoms keep their bosonic or fermionic identity in the course of the dynamics. Hence, with the distance between electrons and core being much smaller than any other relevant

---

[3] See Power and Zienau (1959) or Craig and Thirunamachandran (1998); Healy (1982).

[4] For ^{87}Rb, $a_s = 5.77$ nm $\approx 110\,a_{Bohr}$, $\lambda = 780$ nm $\approx 15 \times 10^3\,a_{Bohr}$ for the D_2 line (see Boesten *et al.*, 1997).

length scale, we can safely replace the electromagnetic potential at the position of the electron for that at the position of the corresponding core.

Furthermore, in many quantum-optical systems we can limit the description of the atomic energy-level structure to a few relevant levels, for example to those atomic dipole transitions with the largest oscillator strengths. In this work we restrict our Hamiltonian to a manifold of electronic 'ground' and 'excited' states, labeled $|g\rangle$ and $|e\rangle$, which are eigenstates of the Hamiltonian for free, noninteracting atoms.[5] The energy difference between the two levels is denoted by $\hbar\omega_{eg} = \hbar(\omega_e - \omega_g)$. Keeping in mind that this two-level approximation will fail to describe situations in which transitions from an excited state of a multilevel atom to higher lying states play a role, it can be used to calculate the energy-shift of the ground state $|g\rangle$ or the decay rate of the excited state $|e\rangle$. The expressions thus obtained can be generalized to realistic atoms in a straightforward way by summing over the relevant transitions (see Hinds and Sandoghdar, 1991).

The quantum-statistical properties of the atoms could be described by restricting the Hamiltonian to the space of symmetric (or antisymmetric) wave functions of the coordinates that represent the position of the cores for bosons (or fermions). Instead, we apply the second-quantization procedure (see Fetter and Walecka, 2003; Ziman, 1969), introducing the (bosonic or fermionic) fields $\Psi_g(\mathbf{r})$ and $\Psi_e(\mathbf{r})$ which describe the annihilation of an atom in the ground or excited electronic state at the location $\mathbf{r}$. Within the dipole- and two level approximations, the second quantized Hamiltonian for the atom-field interaction in the $\boldsymbol{\mu}.\mathbf{E}$-gauge finally reads

$$H_{AF} = -\int d^3r \sum_\alpha \left\{ E_\alpha(x) \left[\mu_\alpha^{ge} \Psi_g^\dagger(x)\, \Psi_e(x) + \mu_\alpha^{eg} \Psi_e^\dagger(x)\, \Psi_g(x) \right] \right\}, \quad (4.4)$$

where $\alpha = x, y, z$ (see Lewenstein *et al.*, 1994). We do not make the rotating wave (or resonance) approximation here because otherwise relevant processes in the intermediate states would be missed.

The dipole moment $\boldsymbol{\mu}$ plays the role of the coupling constant in the above Hamiltonian. We will see below and in chapter 7 that the small dimensionless parameter appearing in the perturbation series, analogous to the fine structure constant α_{fs} in QED of elementary particles, is $(\boldsymbol{\mu}\omega_{eg})^2/(\hbar c^3) \approx \alpha_{fs}^3 \approx 10^{-7}$.

4.3 Single atom self energies

In order to illustrate the formalism laid out above, we now calculate the self-energy of the most simple atomic system, namely a single two level atom (see for example Scheel and Buhmann, 2008, sec. 5.2).

---

[5]A generalization to states with an additional index for the spin state is straightforward (see Lewenstein *et al.*, 1994).

We assume that both internal states of the atom experience a trapping potential which localizes the atoms in space, and define the single-particle eigenfunctions as $\Phi_{\mathbf{n}}^g(\mathbf{r}) = \langle \mathbf{r}|g_{\mathbf{n}}\rangle$ and $\Phi_{\mathbf{m}}^e(\mathbf{r}) = \langle \mathbf{r}|e_{\mathbf{m}}\rangle$, where the collective indices $\mathbf{n}, \mathbf{m}$ label the different modes of the trapping potentials (see appendix C for details). Their eigenenergies $\omega_{\mathbf{n}}^g$ and $\omega_{\mathbf{m}}^e$ are typically several orders of magnitude smaller than the optical transition frequency ω_{eg}. To calculate the energy shift of an atom in the internal state $|g\rangle$ or $|e\rangle$, we have to consider S-matrix elements between the unperturbed states $|\{N_k\}, g_{\mathbf{n}}\rangle$ and $|\{N_k\}, e_{\mathbf{m}}\rangle$. Here, the notation $|\{N_k\}\rangle$ denotes an eigenstate of H_F, with the field in equilibrium at a temperature T_F, such that

$$N_k = \langle \hat{N}_k \rangle = \frac{1}{e^{\hbar\omega_k/(k_B T_F)} - 1} \tag{4.5}$$

(with $\omega_k = ck$) is the mean thermal occupation number of the photon mode k. The leading contribution to the self-energy is of second order in H_{AF}:

$$\text{(diagram)} \quad = T_{g,\mathbf{n}}^{(2)} \times [-2\pi i \delta(E_f - E_i)] \tag{4.6a}$$

$$= \frac{(-i)^2}{2!} \int dt_1 \int dt_2 \, \langle g_{\mathbf{n}}, \{N_k\}| T\{H_{AF}(x_1) H_{AF}(x_2)\} |\{N_k\}, g_{\mathbf{n}}\rangle$$

$$\text{(diagram)} \quad = T_{e,\mathbf{m}}^{(2)} \times [-2\pi i \delta(E_f - E_i)] \tag{4.6b}$$

In the diagrams above, we used solid lines for the propagation of ground state atoms, dashed lines for excited atoms, and a wiggled line for the Feynman propagator of the electric field,

$$D_{\alpha\beta}^F(x_1; x_2) = \text{(wiggle)} \quad = \langle \{N_k\}| T\{E_\alpha(x_1) E_\beta(x_2)\} |\{N_k\}\rangle \tag{4.7}$$

$$= \int \frac{d\omega}{2\pi} e^{i\omega(t_1 - t_2)} D_{\alpha\beta}^F(\mathbf{r}_1, \mathbf{r}_2; \omega) . \tag{4.8}$$

The time-ordered product $T\{\dots\}$ in eqns. (4.6) can, via Wick's theorem, be decomposed into contractions of field operators, see eqns. (C.4). Performing the time integrations in the first line of eqn. (4.6a) yields the expression

$$T_{g,\mathbf{n}}^{(2)} = \mu_\alpha^{eg} \mu_\beta^{ge} \int d^3 r_1 \int d^3 r_2 \, \Phi_{\mathbf{n}}^{g\,*}(\mathbf{r}_2) \Phi_{\mathbf{n}}^g(\mathbf{r}_1)$$

$$\times \sum_{\mathbf{m}} \langle \mathbf{r}_2|e_{\mathbf{m}}\rangle \langle e_{\mathbf{m}}|\mathbf{r}_1\rangle \int \frac{d\omega}{2\pi} \frac{D_{\alpha\beta}^F(\mathbf{r}_1, \mathbf{r}_2, \omega)}{\omega - \omega_{eg} - \omega_{\mathbf{m}}^e + \omega_{\mathbf{n}}^g + i\epsilon} . \tag{4.9}$$

When evaluated in free space, the above expression depends on the Franck-Condon factors $\Phi_{\mathbf{n}}^g(\mathbf{r})\Phi_{\mathbf{m}}^{e\,*}(\mathbf{r})e^{i\mathbf{kr}}$ (see Lewenstein *et al.*, 1994, sec. VIII). The optical transition frequency in the denominator of eqn. (4.9) is slightly shifted by the

eigenenergies ω_n^g and ω_m^e, we will in the following neglect this shift by assuming that the field correlation function is varying slowly on the scale of the trap-frequencies.[6] After shifting the integration variable $\omega \to \omega + \omega_m^e - \omega_n^g$ and setting $D_{\alpha\beta}^F(\omega + \omega_m^e - \omega_n^g) \approx D_{\alpha\beta}^F(\omega)$, eqn. (4.9) simplifies considerably: with $\sum_m \langle \mathbf{x}_2 | e_m \rangle \langle e_m | \mathbf{x}_1 \rangle = \delta(\mathbf{r}_1 - \mathbf{r}_2)$, the initial state wavefunction enters the result only through the probability density $|\Phi_n^g(\mathbf{r})|^2$. The argument proceeds completely analogously for $T_{e,m}^{(2)}$, and after performing the time and space integrations in eqns. (4.6), we arrive at

$$T_{a,j}^{(2)} = \int d^3r \, |\Phi_j^a(\mathbf{r})|^2 \, T_a^{(2)}(\mathbf{r}) \, , \qquad (4.10)$$

where $j = \mathbf{n}, \mathbf{m}$,

$$T_a^{(2)}(\mathbf{r}) = \mu_\alpha \mu_\beta \int \frac{d\omega}{2\pi} \frac{D_{\alpha\beta}^F(\mathbf{r}, \mathbf{r}, \omega)}{\omega \mp \omega_{eg} + i\epsilon} \, , \qquad (4.11)$$

and the upper/lower sign in the denominator corresponds to $a = g, e$, respectively. This result can also be obtained immediately from the diagrams in eqns. (4.6) by applying the Feynman rules given in appendix C.

As the extent of the region in which the atom is localized should be small compared to the atom-surface separation, the atoms are usually described as completely localized pointlike objects. We adopt this approach in the rest of this section by setting $|\Phi_j^a(\mathbf{r})|^2 = \delta(\mathbf{r} - \mathbf{r}_A)$ in eqn. (4.10) (with $\mathbf{r}_A$ the location of the atom), which substitutes $T_a^{(2)}(\mathbf{r}_A)$ for $T_{a,j}^{(2)}$. The atomic wavefunctions will play a role in the following chapters, where we use the same technique for treating condensed Bose gases and the macroscopic extent of the condensate wavefunction plays a prominent role.

The energy shift of an atom due to its interaction with the field is usually not expressed in terms of the Feynman-propagator (4.7), but with the retarded field correlation function

$$G_{\alpha\beta}(x_1, x_2) = i \langle \{N_k\} | [E_\alpha(x_1), E_\beta(x_2)] | \{N_k\} \rangle \Theta(t_2 - t_2) \qquad (4.12)$$

and a polarizability $\alpha_{\alpha\beta}^a$ of the atomic state $|a\rangle$, which is likewise expressed as a retarded correlation function of the polarization operator (see appendix A for more calculational details). By rearranging the time ordered product in eqn. (4.7) and using the fluctuation-dissipation theorem (see Wylie and Sipe, 1985, appendix B),

---

[6]In chapter 5, we explicitly evaluate this shift of the optical transition frequency for an interacting trapped Bose gas, and show that the resulting correction for the self-energy is proportional to the (small) ratio between trap- and atomic frequency.

we can express the Fourier transform (4.8) of the Feynman propagator as

$$i\, D_{\alpha\beta}^{F}(\mathbf{r}_1, \mathbf{r}_2, \omega) = \text{Re}\left[G_{\alpha\beta}(\mathbf{r}_1, \mathbf{r}_2, \omega)\right] + i\,\text{Im}\left[G_{\alpha\beta}(\mathbf{r}_1, \mathbf{r}_2, \omega)\right]$$

$$\times \coth\left[\frac{\omega}{2k_B T_F}\right] \tag{4.13}$$

(see Fetter and Walecka, 2003, sec. 31). Here we assume the field and its sources in thermal equilibrium at the temperature T_F,[7] while the atomic part of the system may have a temperature $T_A \neq T_F$ and is even allowed to be in a non-thermal state, as is the case for the excited two-level atom in eqn. (4.6b). Using the fact that $G(\omega)$ has poles only in the lower half of the imaginary ω-plane, the frequency-integral in eqn. (4.11) can be evaluated with the help of identity (A.7). Assuming for simplicity that the dipole moments μ_α^{ge} are real, eqn. (4.11) reads

$$T_g^{(2)} = \langle N_{eg}\rangle \mu_\alpha\mu_\beta G_{\alpha\beta}(\mathbf{r}_A, \mathbf{r}_A, -\omega_{eg}) - k_B T_F \sum_{n=0}^{\infty}{}' G_{\alpha\beta}(\mathbf{r}_A, \mathbf{r}_A, i\xi_n)\alpha_{\alpha\beta}^{g}(i\xi_n) ,$$

$$\tag{4.14a}$$

$$T_e^{(2)} = -(\langle N_{eg}\rangle + 1)\mu_\alpha\mu_\beta G_{\alpha\beta}(\mathbf{r}_A, \mathbf{r}_A, \omega_{eg}) - k_B T_F \sum_{n=0}^{\infty}{}' G_{\alpha\beta}(\mathbf{r}_A, \mathbf{r}_A, i\xi_n)$$

$$\times \alpha_{\alpha\beta}^{e}(i\xi_n) , \tag{4.14b}$$

where the primed sum denotes that the $n = 0$ term is multiplied with a factor $\frac{1}{2}$, the Matsubara frequencies are defined as $\xi_n = 2\pi n T_F$, and the polarizability $\alpha_{\alpha\beta}^{a}(\omega)$ reads

$$\alpha_{\alpha\beta}^{a}(\omega) = \frac{\pm 2\omega_{eg}\mu_\alpha\mu_\beta}{\omega_{eg}^2 - (\omega + i\epsilon)^2} , \tag{4.15}$$

the upper/lower sign corresponding to $a = g, e$, respectively. The last terms of eqns. (4.14) now assume a form familiar from linear response theory, with the answer of the atom to a perturbation being proportional to a retarded response function multiplied with the atomic polarizability. The real part of $T_a^{(2)}$ yields the energy shift of the atomic state $|a\rangle$, while the rate for the transition between states $|a\rangle$ and $|a'\rangle$ is given by

$$\gamma_{aa'} = -2\text{Im}\left[T_a^{(2)}\right] . \tag{4.16}$$

The Matsubara sums in eqns. (4.14) are purely real, as the retarded field correlation function $G_{\alpha\beta}$ and the polarizability are evaluated at imaginary frequencies. The imaginary parts of the first terms of eqns. (4.14) are proportional to the lifetime of the atomic states $|g\rangle$ and $|e\rangle$, respectively. At $T_F = 0$, only $T_e^{(2)}$ keeps an imaginary part describing spontaneous emission. The transition rate is given by

$$\gamma_{eg} = 2\mu_\alpha\mu_\beta\text{Im}\left[G_{\alpha\beta}(\mathbf{r}_A, \mathbf{r}_A, \omega_{eg})\right] . \tag{4.17}$$

---

[7] More general cases like a heated substrate are treated in (Obrecht *et al.*, 2007) or (Henkel *et al.*, 2002), for example.

For finite field temperatures, $\gamma_{ge} = -2\text{Im}\,[T_g^{(2)}] \neq 0$ describes the rate for absorption of a thermal photon by a $|g\rangle$-state atom. We will come back to the topic of single-atom emission processes in chapter 6.

The generalization of eqns. (4.14) to atoms with several energy levels is straightforward by introducing summations over lower and higher lying states as in Gorza and Ducloy (2006, eqn. (2.11)).

4.4 Correlation functions of the electric field in the presence of an interface

For the electromagnetic field in free space, the time-ordered propagator eqn. (4.7) can be worked out explicitly from a mode expansion of the **E**-field. The Matsubara sums in eqns. (4.14) then give rise to a formally divergent self energy of the atom due to its interaction with the field. The corresponding effect in atomic hydrogen is well known as the Lamb-shift which, starting with Bethe's seminal paper (Bethe, 1947), gave rise to the systematic development of renormalization techniques in QED.

The mode function approach works in the presence of a non-dispersive surface, too, but is rather cumbersome because the boundary conditions at the surface require more complicated mode functions (see Carnaglia and Mandel, 1971; Eberlein and Robaschik, 2006). Instead, we want to follow here the method described by Wylie and Sipe (1985):[8] From linear response theory (see Fetter and Walecka, 2003, sec. 32) and the linearity of the Maxwell equations, the response function $G_{\alpha\beta}(\mathbf{r}_1, \mathbf{r}_2, \omega)$ can be identified with the classical Green function, that is, the electric field at $\mathbf{r}_1$ generated by a classical dipole, oscillating at frequency ω, which is located at $\mathbf{r}_2$. The explicit form of the Green function in the presence of an interface is well known (see Sipe, 1981) and can be split into a free-space and a reflected part:

$$G_{\alpha\beta} = G_{\alpha\beta}^0 + G_{\alpha\beta}^R ,$$

where $G_{\alpha\beta}^0$ is the retarded Green function in free space. As long as we are only interested in that part of the energy shift caused by the presence of the surface, we do not have to consider $G_{\alpha\beta}^0$ at all. The decomposition above thus permits us in a simple manner to subtract the divergent terms of eqns. (4.14) (involving divergent photon loops in the intermediate states), which arise from $G_{\alpha\beta}^0$. To get the distance-dependent part of the energy shift, we will simply substitute $G_{\alpha\beta}$ by $G_{\alpha\beta}^R$ in eqns. (4.14). The expressions containing $G_{\alpha\beta}^R$ are then finite without any further renormalization.

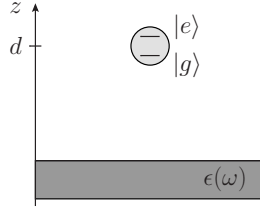[8] See also Agarwal (1975) and Wylie and Sipe (1984).

Figure 4.1: A single two level atom above a surface. The dielectric function $\epsilon(\omega)$ appears in the reflection coefficients eqns. (A.16).

The surface contribution $G^R_{\alpha\beta}$ at imaginary frequencies has the form

$$G^R_{\alpha\beta}(\mathbf{r}_1, \mathbf{r}_2, i\xi) = -\frac{\mu_0 \xi^2}{2\pi} \int \frac{d^2k}{\kappa} R_{\alpha\beta}(\xi, \mathbf{k}) e^{-\kappa(z_1+z_2)} e^{i\mathbf{k}\cdot(\mathbf{x}_1-\mathbf{x}_2)} \ , \qquad (4.18)$$

(see appendix A for more details) where $\mu_0 = (\varepsilon_0 c^2)^{-1}$ is the vacuum permeability and $\kappa = \sqrt{\xi^2/c^2 + k^2}$. The two-dimensional vectors $\mathbf{x}_{1,2}$ and $\mathbf{k}$ denote position and momentum parallel to the surface, respectively. The tensor elements $R_{\alpha\beta}$ contain the reflection coefficients appropriate for the specific surface material. Note that from the viewpoint of perturbation theory, the surface response functions $R_{\alpha\beta}$ depend on the quantum state of matter in the surface; they are calculated, of course, in the absence of the atomic system outside it.

4.5 Attractive atom-surface potential

With the explicit form (4.18) for G^R, we are now in the position to calculate the interaction potential between the two-level atom and a plane surface. For simplicity, we concentrate on the case of a pointlike atom in the internal state $|g\rangle$, located at $\mathbf{r}_A = (0, 0, d)$, where d is the (positive) distance between atom and surface and the surface lies in the x, y-plane (see fig. 4.1). From eqn. (4.14a), we obtain for the position dependent part of the energy-shift

$$\Delta E_g(d) = \langle \hat{N}_{eg} \rangle \, \mu_\alpha \mu_\beta \mathrm{Re} \left[G^R_{\alpha\beta}(\mathbf{r}_A, \mathbf{r}_A, \omega_{eg}) \right] - k_B T_F \sum_{n=0}^{\infty}{}' G^R_{\alpha\beta}(\mathbf{r}_A, \mathbf{r}_A, i\xi_n)$$

$$\times \, \alpha^g_{\alpha\beta}(i\xi_n) \ . \qquad (4.19)$$

As the optical transition frequencies of the atom are under typical conditions much higher than the thermal energy, the first term is small compared to the Matsubara-sum, and we will neglect it in the following. For a given optical transition frequency and dipole moment, eqn. (4.19) can be evaluated numerically as a function of the atom-surface separation d for a wide range of surface materials.[9] As an

---

[9]For calculations of the atom-surface potential involving different models for the surface material, see Gorza and Ducloy (2006); Sipe (1981); Wylie and Sipe (1984, 1985). Experimentally,
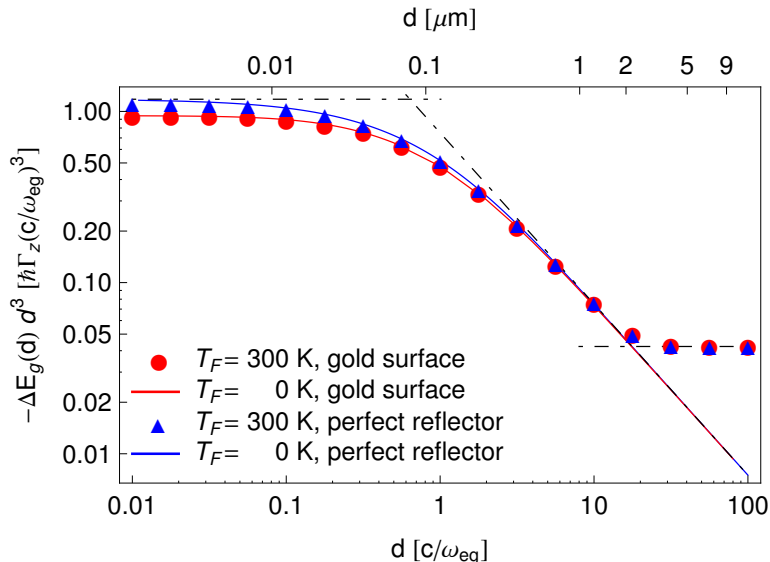
Figure 4.2: Atom-surface interaction eqn. (4.19) between a rubidium atom (resonance frequency $\omega_{eg}/2\pi = 3.85 \times 10^{14}$ Hz) with its dipole moment oriented in the z-direction and a perfectly reflecting surface or a gold surface, respectively. Parameters of the Drude dielectric function for gold, eqn. (A.17): $\omega_p = 5.74\,\omega_{eg}$ and $\omega_p\tau = 5 \times 10^3$. Solid curves show the results for the em-field at zero temperature, the triangle and circle symbols for a field temperature of 300 K. The atom-surface distance $d = xc/\omega_{eg}$ is scaled in units of the resonance wavelength, the interaction energy is multiplied by $-x^3$ and scaled by the free-space decay rate $\hbar\Gamma_z = |\boldsymbol{\mu}^z|^2\omega_{eg}^3/(3\pi\varepsilon_0 c^3)$ for a dipole oriented in the z-direction. The dot-dashed lines show, from left to right, the van der Waals potential (4.23), the Casimir-Polder potential (4.22), and the thermal potential (4.21). The length scales separating the different asymptotic potentials take the values $\lambda_{opt} = 0.12\,\mu$m and $\lambda_{T_F}(300K) = 7.64\,\mu$m.

example, fig. 4.2 shows the atom-surface potential for a gold surface with the field at zero temperature and at 300 K (solid red curve and red circles, respectively), and for a perfectly reflecting surface (blue curve and triangles). The values differ mainly in the short-distance regime, where the high-frequency part of the field fluctuations is important. Arbitrarily high frequencies are not reflected by a realistic surface, hence the slightly weaker atom-surface interaction.

In the following section, we will concentrate on the idealized case of the perfectly reflecting surface, which allows for simple asymptotic solutions of eqn. (4.19) in various distance regimes.

---

a potential of the form (4.19) has been observed by Bender *et al.* (2010); Landragin *et al.* (1996); Sukenik *et al.* (1993).

Asymptotic expressions

The characteristic length scales appearing in the potential (4.19) are the thermal wavelength $\lambda_{T_F} = \frac{\hbar c}{k_B T_F}$ and the wavelength related to the optical transition, $\lambda_{opt} = c/\omega_{eg}$. At finite field temperature T_F with $\lambda_{T_F} > \lambda_{opt}$, $\Delta E_g(d)$ shows three distinct regimes.

As the function $G_{\alpha\beta}^R(\mathbf{r}_A, \mathbf{r}_A, i\xi_n)$ in the Matsubara sum of eqn. (4.19) decays as $\exp[-nd/\lambda_{T_F}]$, for distances $d \gg \lambda_{T_F}$ we can approximate the potential by retaining only the $n = 0$ term of the sum. This yields the thermal potential $V_{T_F}(d)$ in eqn. (4.21) below, which is proportional to T_F/d^3.

At distances smaller than the thermal wavelength, all of the terms in the Matsubara sum have to be taken into account. With $d\zeta = \zeta_{n+1} - \zeta_n = 2\pi\omega_{T_F}$, the sum can be approximated by an integral if T_F is sufficiently low such that ω_{T_F} is small compared to the frequency scale ω_{eg} on which the functions $\alpha(i\xi)$ and $G(i\xi)$ vary. Eqn. (4.19) then reads

$$\Delta E_g(d) = -\frac{1}{2\pi} \int_0^\infty d\xi\, G_{\alpha\beta}^R(\mathbf{r}_A, \mathbf{r}_A, i\xi)\, \alpha_{\alpha\beta}^g(i\xi) \,. \tag{4.20}$$

After inserting the explicit expression for G^R (for a perfectly reflecting mirror) into eqn. (4.20), two simple, recognizable interaction potentials emerge as limiting cases (see for example Hinds and Sandoghdar, 1991). These are the well known Casimir-Polder and van der Waals-London potentials (below in eqn. (4.22) and eqn. (4.23)), proportional to d^{-4} and d^{-3}, respectively.[10]

To consider different orientations of the atom's dipole moment with respect to the surface, we introduce $\mu_\rho = \sqrt{\mu_x^2 + \mu_y^2}$, and finally obtain the following asymptotic expressions for the atom-surface potential:

$$V_{T_F}(d) = -\frac{1}{d^3} \frac{\lambda_{opt}}{\lambda_{T_F}} \frac{|\mu_z|^2 + |\mu_\rho|^2}{2}, \quad \text{for} \quad d \gg \lambda_{T_F} \,, \tag{4.21}$$

$$V_{CP}(d) = -\frac{\lambda_{opt}}{d^4} \frac{|\mu_z|^2 + |\mu_\rho|^2}{4\pi}, \quad \text{for} \quad \lambda_{opt} < d < \lambda_{T_F} \,, \tag{4.22}$$

$$V_{vdW}(d) = -\frac{1}{d^3} \left(\frac{|\mu_z|^2}{8} + \frac{|\mu_\rho|^2}{16} \right), \quad \text{for} \quad d \ll \lambda_{opt} \,. \tag{4.23}$$

The van der Waals-London potential (4.23), valid when the atom is close to the mirror, can be understood as the instantaneous interaction of the atom's fluctuating electric dipole with its own electric image in the mirror (see Scheel and Buhmann,

---

[10]In chapter 1, we used the term Casimir-Polder potential for atom-surface interactions, and reserved the name van der Waals interaction for the dispersion interaction between two atoms. In the literature, the names of van der Waals and London are often used to denote any non-retarded potential, and we apply this convention here to distinguish between the two asymptotic expressions for the atom-surface potential.

2008, sec. 5.5.2). Historically, it was derived in this way by Lennard-Jones (1932), preceded by work of Eisenschitz and London (1930) and London (1930) on the interaction between two neutral molecules via their fluctuating electrical dipole moments, which in turn gave a quantum mechanical explanation of the van der Waals forces introduced in a phenomenological way half a century earlier (see Maxwell, 1874).

On the basis of the mirror image picture customarily used for visualizing van der Waals forces, an influence of retardation on the interaction (due to the finite speed of light) is to be expected as soon as the distance between atom and mirror becomes comparable to the wavelength corresponding to the atomic frequencies. Conceptually, the important step in Casimir's derivation of eqn. (4.23) (see Casimir and Polder, 1948) is to take into account the fluctuations of the em-field. In this spirit, the CP potential is most naturally understood as a change in the Bethe contribution to the Lamb shift, caused by the modification of the vacuum field distribution due to the surface.

As, for distances larger than the thermal wavelength, the atom-surface potential is dominated by the thermal fluctuations of the field, resulting in the T_F/d^3 potential of eqn. (4.21), the possibility to observe the crossover between the instantaneous d^{-3} van der Waals and the retarded d^{-4} Casimir-Polder potential depends on the field temperature. For a pronounced d^{-4}-dependence, T_F has to be sufficiently low to guarantee $\lambda_{T_F} \gg \lambda_{opt}$.

Casimir-Polder force on a Bose-Einstein condensate

In the following, we want to extend the approach of the last section to describe the interaction potential between a Bose-condensed atom cloud and a plane surface at second order in the atom-light interaction. As long as interatomic interactions (via effective contact potentials, as described in section 2.3) are neglected, the generalization of the calculation in section 4.5 is straightforward. We will, however, see in section 5.2 that the macroscopic extent of the condensate wavefunction, which we neglected for the single atom calculations altogether, significantly modifies the effective Casimir-Polder potential. We turn to the case of an interacting BEC in section 5.3, and investigate how atom-atom interactions lead to corrections to the single atom theory. In this analysis, we also take account of the propagation of the excited atom in the virtual state, and quantify the (under typical conditions small) shift of the effective resonance frequency associated with it.

5.1 Second-order energy shift

The total Hamiltonian of the system is again split as in eqn. (4.1),

$$H = H_A + H_{AF} + H_F ,$$

with the atom-field interaction H_{AF} introduced in eqn. (4.4). The atomic Hamiltonian H_A now describes N identical two-level atoms in a trap above a flat surface. As in section 4.5, the surface is taken to lie in the xy-plane, the center of the trap

is located a distance d from the surface in the half-space $z > 0$ (see fig. 4.1). We use the notation $\mathbf{r} = (\mathbf{x}, z)$ for spatial vectors, where the two-dimensional vector $\mathbf{x}$ lies in the plane perpendicular to the surface. Spatial integrations $\int d^3r$ run only over the $z > 0$ half-space. Spacetime points are denoted by $x = (\mathbf{r}, t)$. Our units are such that $\hbar = k_B = 1$, the speed of light c and the atomic mass M are kept for the ease of reading.

The leading contribution to the self-energy can then be expressed as

$$\langle T^{(2)} \rangle = \frac{1}{-2\pi i \delta(0)} \times \underset{N \qquad N-1 \qquad N}{\text{———\figure———}} \tag{5.1}$$

$$= -\mu_\alpha^{eg} \mu_\beta^{ge} \int d^4x_1 \, d^4x_2 \, \langle \Psi_g^\dagger(x_2) \Psi_e(x_2) \Psi_e^\dagger(x_1) \Psi_g(x_1) \rangle$$

$$\times \Theta(t_2 - t_1) D_{\alpha\beta}^F(x_2, x_1) \, . \tag{5.2}$$

The brackets $\langle \ldots \rangle$ in eqn. (5.2) denote an expectation value in a stationary state of the atomic Hamiltonian H_A. In contrast to eqn. (4.6a), the in- and outgoing lines in the above diagram represent N atoms in the internal state $|g\rangle$ that make up the unperturbed atomic state. The intermediate state (inner line) consists of an atom in the state $|e\rangle$ (dashed line) propagating in the presence of a background field (solid line) made up of the remaining $N - 1$ ground state atoms (still a large number).

For an ideal gas, the atomic correlation function in eqn. (5.2) reduces to the form that is usually obtained from applying Wick's theorem to a time-ordered product of four interaction picture operators (see appendix C). We treat this case in section 5.2 below. In section 5.3, we address the case of an interacting BEC with interatomic contact interactions which are described by H_A rather than H_{AF}. Contractions between atomic operators then do not reduce to c-numbers; the Feynman rules describing the inner lines in diagram (5.1) must take into account the simultaneous presence of other atoms.

5.2 Ideal Bose gas in a surface trap

For simplicity, we assume an isotropic harmonic trapping potential

$$V_{trap}^g(\mathbf{r}) = \frac{M}{2} \nu^2 \left(\mathbf{x}^2 + (z - d)^2 \right) , \tag{5.3}$$

the single-particle eigenfunctions $\Phi_{\mathbf{n}}^g$ and eigenvalues $\omega_{\mathbf{n}}^g$ that solve eqn. (C.1a) are the well-known solutions of a three-dimensional harmonic oscillator. We set the ground state energy of the trap equal to the zero of energy, and the critical temperature T_c assumes the value (2.56). For a given mean particle number N and atom temperature T_A, the (negative valued) chemical potential $\mu(N, T_A)$ has to be determined from the relation

$$N(\mu, T_A) = \int d^3r \, \langle \Psi_g^\dagger(\mathbf{r}) \Psi_g(\mathbf{r}) \rangle , \tag{5.4}$$

where the brackets $\langle \ldots \rangle$ denote a state of the atomic system at temperature T_A. The correlation function $\langle \Psi_g^\dagger(\mathbf{r})\Psi_g(\mathbf{r})\rangle$ that enters in eqn. (5.4) is the one-particle density matrix $n^{(1)}(\mathbf{r}^{(d)}, \mathbf{r}^{(d)})$ of eqn. (B.1), where the vector $\mathbf{r}^{(d)} \equiv (\mathbf{x}, z - d)$ accounts for the distance d between the surface and the center of the trap.

Surface-induced energy shift - effects of delocalization

Using the same approximations as in eqn. (4.9), the first non-vanishing contribution to the self-energy yields

$$\langle N|T^{(2)}|N\rangle = \frac{1}{-2\pi i\delta(0)} \times \underset{N,\mu,T_A \qquad\qquad N,\mu,T_A}{\underline{\hspace{3cm}}}$$

$$= \mu_\alpha^{ge}\mu_\beta^{eg} \int d^3r \, \langle \Psi_g^\dagger(\mathbf{r})\Psi_g(\mathbf{r})\rangle \int \frac{d\omega}{2\pi} \frac{D_{\alpha\beta}^F(\mathbf{r},\mathbf{r},\omega)}{\omega - \omega_{eg} + i\epsilon} \ .$$

Compared with eqn. (4.10), the above expression consists of a sum of single-atom self energies, where the individual atoms occupy different modes of the trapping potential. Had we kept the single particle energies $\omega_\mathbf{n}^g$ and $\omega_\mathbf{m}^e$, they would appear, as in eqn. (4.9), as a small shift of ω_{eg} in the denominator. (For a trapping frequency $\nu/2\pi = 1$ kHz and a mean number of $N = 10^4$ trapped particles, the mean thermal energy that sets the scale for the relevant $\omega_\mathbf{n}^g$ evaluates to $T_A = (T_A/T_c)\, 2\pi\, 20.3$ kHz, which is still much smaller than ω_{eg} for temperatures of the order of T_c.) . Setting the field temperature $T_F = 0$ for simplicity (and thereby neglecting contributions from thermal photons) we obtain, after employing relation (A.9), the atom-surface potential

$$\Delta E(x) = -\frac{1}{2\pi} \frac{\mu_\alpha^{ge}\mu_\beta^{eg}\omega_{eg}^3}{\varepsilon_0 c^3} \sum_{j=1}^{\infty} \frac{e^{j\mu/T_A}}{\left((1 - e^{-2j\nu/T_A})\tanh[\frac{1}{2}j\nu/T_A]\right)^{3/2}}$$

$$\times \int_0^\infty d\bar{\xi} \int_0^\infty \frac{\bar{k}\, d\bar{k}}{\bar{\kappa}} \, I(\bar{\kappa}, x, \eta_j) \, M_{\alpha\beta}(\bar{k}, \bar{\xi}, R^p, R^s) \frac{1}{1 + \bar{\xi}^2} \ . \qquad (5.5)$$

Here, we introduced the scaled distance $x = \omega_{eg}d/c$, rescaled the integration variables $\bar{\xi} = \xi/\omega_{eg}$, $\bar{k} = ck/\omega_{eg}$, $\bar{\kappa} = c\kappa/\omega_{eg} = c/\omega_{eg}\sqrt{k^2 + \xi^2}$, and defined the quantity $I(\bar{\kappa}, x, \eta_j)$ as

$$I(\bar{\kappa}, x, \eta_j) \equiv \frac{1}{2} \exp[-2\bar{\kappa}x + \bar{\kappa}^2\eta_j^2] \left(1 + \text{erf}[\frac{x}{\eta_j} - \bar{\kappa}\eta_j]\right) , \qquad (5.6)$$

where erf denotes the error function. The energy scale in eqn. (5.5) is set by the natural linewidth $\gamma_{eg} = |\boldsymbol{\mu}^{ge}|^2\omega_{eg}^3/3\pi\varepsilon_0 c^3$. The diagonal matrix $M_{\alpha\beta}$ originates from the scattering tensor $R_{\alpha\beta}$ (A.15) and has elements

$$M_{xx} = M_{yy} = R^p k^2 + (R^p - R^s)(\xi/c)^2 , \qquad (5.7a)$$

$$M_{zz} = 2R^p k^2 , \qquad (5.7b)$$

and $R^{s,p}(k, \xi)$ are the reflection amplitudes from the surface (see eqns. (A.16)).

A subtlety arises because the single-particle wave functions $\Phi_\mathbf{n}^g$ are normalized only in the limit $d \gg a_0 = \sqrt{\hbar/(M\nu)}$ if spatial integrations are restricted over the half-space $z > 0$. We shall always assume this limit, as our approach is clearly not valid for atoms touching the surface. The wave function Φ_0^g is of the order $\mathcal{O}(\exp[-(d/a_0)^2])$ at the surface, and exponentially small terms of this order will be systematically discarded in numerical evaluations of energy shifts. These approximations are dealt with in detail in appendix B, they likewise apply to the numerical calculations in section 5.3.

The Lamb-Dicke parameter $\eta_j = a_j \omega_{eg}/c$ in eqn. (5.5) involves the temperature dependent width

$$a_j = a_0 \left(\coth[\tfrac{1}{2} j\nu/T_A]\right)^{1/2} \geq a_0 \ . \tag{5.8}$$

To compare eqn. (5.5) with the results for the single atom, we note that the constraint (5.4) leads to

$$\sum_{j=1}^{\infty} \frac{e^{j\mu/T_A}}{\left((1 - e^{-2j\nu/T_A}) \tanh[\tfrac{1}{2} j\nu/T_A]\right)^{3/2}} = N \tag{5.9}$$

and consider an interaction energy per atom, $\Delta E/N$. The terms with large j in the sum involve a width a_j equal to the zero-temperature value a_0. These terms describe the condensate atoms in the trap ground state. The terms with small j have larger values of a_j and contribute to the energy shift as a broader trap would do. Indeed, for $j = 1$ and $\nu/T_A \ll 1$, one gets the spatial width of a classical, thermal density distribution.

The deviation from a simple Gaussian density is perceptible in the numerical evaluation of eqn. (5.5) in fig. 5.1. The atom-surface interaction per atom at $T_A = 0.2\, T_c$ (top curve) is larger than at $T_A = 0$ (at the same trap frequency $\nu/2\pi = 1$ kHz), which is due to the larger spatial size of the thermally excited trap levels.

At an atom-surface distance of $d > 2\,\mu$m, the interaction potential for the perfectly localized atom (calculated from eqn. (4.20)) is already deep in the retarded x^{-4} regime. For an atom delocalized in the trap, the interaction potential becomes larger in magnitude because of the curvature of the Casimir-Polder interaction. Averaging a power law $1/z^4$ over a narrow Gaussian distribution of width $\sigma \ll d$ centered at $z = d$, we get to leading order the enhancement factor

$$\langle \frac{1}{z^4} \rangle \approx \frac{1}{d^4} \left[1 + 5(\sigma/d)^2 + \dots\right] \ . \tag{5.10}$$

The dashed black curve in fig. 5.1 shows the asymptotic expression for the Casimir-Polder potential eqn. (4.22) multiplied with the above enhancement factor for a trapping frequency of $\nu/2\pi = 1$ kHz. The estimate (5.10) is seen to be in good agreement with our result from eqn. (5.5) (the red curve in fig. 5.1).
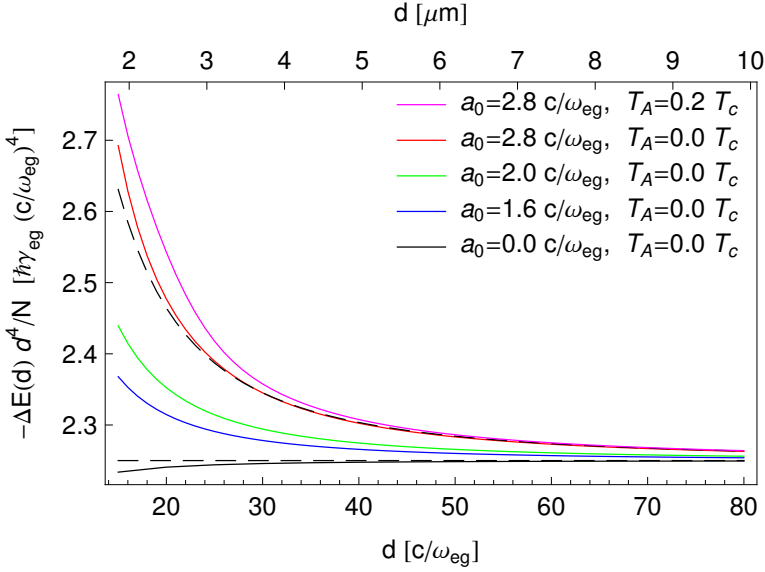
Figure 5.1: Atom-surface interaction per atom between a trapped, ideal BEC of rubidium atoms (resonance wavelength $2\pi c/\omega_{eg} = 780$ nm) and a perfectly reflecting surface (field at zero temperature). Distance d in units of the resonance wavelength, energy multiplied by $-d^4$ and scaled by the natural linewidth $\hbar\gamma_{eg} = |\boldsymbol{\mu}^{eg}|^2\omega_{eg}^3/(3\pi\varepsilon_0 c^3)$. The atoms are supposed to have isotropic dipole matrix elements. The full curves correspond to a single, perfectly localized atom (black) and atom clouds trapped with different trapping frequencies ($\nu/2\pi = 3, 2, 1$ kHz from bottom to top). *Top curve:* interaction energy per atom for a trapped ideal Bose gas at $T = 0.2\, T_c$ and $\nu/2\pi = 1$ kHz [see eqn. (5.5)]. The legend gives the corresponding oscillator widths $a_0 = \sqrt{\hbar/(M\nu)}$ and temperatures in units of the critical temperature T_c [see eqn. (2.56)]. *Horizontal dashed line:* Casimir-Polder asymptote V_{CP}, eqn. (4.22). *Dashed curve:* V_{CP} multiplied with the enhancement factor (5.10) for $\nu/2\pi = 1$ kHz.

5.3 Energy shift of an interacting Bose gas trapped near a surface

Dilute interacting BEC in the single mode approximation

In order to evaluate the self-energy diagram (5.1) for interacting atoms, we further restrict ourselves to the deeply degenerate case, where we can consider a large number N_0 of atoms in a single condensate mode $\Phi_0^g(\mathbf{r})$. The atomic Hamiltonian H_A describes two-level atoms with a contact interaction between excited and ground state atoms:

$$H_A = E(\hat{N}_0) + \sum_{\mathbf{m}} \left(\omega_{eg} + \omega_{\mathbf{m}}^e + b_{ge}\hat{N}_0\right)e_{\mathbf{m}}^\dagger e_{\mathbf{m}} \,, \tag{5.11}$$

where $\hat{N}_0 = g_0^\dagger g_0$ denotes the number operator for condensate atoms. The constant b_{ge} characterizes the interaction between ground- and excited state atoms. We do not take into account any interactions between excited state atoms. This is legitimate since our unperturbed state consists of a large number of ground state atoms. Excited state atoms will then only occur in intermediate states, and their number will be small. The (repulsive) interaction amongst the ground state atoms and the effects of the trapping-potential are contained in the energy $E(\hat{N}_0)$, which depends on the number of condensate atoms. The condensate wavefunction has to be calculated self-consistently by solving the Gross-Pitaevskii-equation[1] (GPE)

$$\left[-\frac{\overrightarrow{\nabla}^2}{2M} + V_{trap}^g(\mathbf{r}) + g\,(N_0 - 1)\,|\Phi_0^g(r)|^2\right] \Phi_0^g(\mathbf{r}) = \mu(N_0)\,\Phi_0^g(\mathbf{r}) . \quad (5.12)$$

Here, $\mu(N) = \partial E(N)/\partial N$ denotes the chemical potential, the constant g (see eqn. (2.23)) characterizes the self-interaction of ground-state atoms, V_{trap}^g denotes the trapping potential felt by the ground-state atoms, and the condensate wavefunction is normalized to $\int d^3r\,|\Phi_0^g(\mathbf{r})|^2 = 1$.

With the particular choice (5.11) for H_A, the time dependence of the field operators Ψ_g and Ψ_e assumes the form

$$\Psi_g(x) = \Phi_0^g(\mathbf{r})\,\exp[-it\,(E_g(\hat{N}_0 + 1) - E_g(\hat{N}_0) + b_{ge}\hat{N}_e)]\,\hat{g}_0 , \quad (5.13a)$$

$$\Psi_e(x) = \sum_{\mathbf{m}} \Phi_{\mathbf{m}}^e(\mathbf{r})\,\exp[-it(\omega_{eg} + \omega_{\mathbf{m}}^e + b_{ge}\,\hat{N}_0)]\,\hat{e}_{\mathbf{m}} , \quad (5.13b)$$

and the correlation function in eqn. (5.2) evaluates to

$$\langle N_0|\Psi_g^\dagger(x_2)\Psi_e(x_2)\Psi_e^\dagger(x_1)\Psi_g(x_1)|N_0\rangle = \quad (5.14)$$
$$N_0\,\Phi_0^g(\mathbf{r}_1)\Phi_0^{g*}(\mathbf{r}_2)\sum_{\mathbf{m}} \Phi_{\mathbf{m}}^{e*}(\mathbf{r}_1)\Phi_{\mathbf{m}}^e(\mathbf{r}_2)e^{-i(t_2-t_1)\omega_{eg}(\mathbf{m},N_0)} .$$

Here,

$$\omega_{eg}(\mathbf{m}, N) = \omega_{eg} + \omega_{\mathbf{m}}^e + E_g(N - 1) - E_g(N) + (N - 1)b_{ge} , \quad (5.15)$$

where the frequency shift of the atomic transition due to inter-atomic interactions appears. Without loss of generality, we can take $E_g(1) = \omega_0^g = 0$ (see eqn. (C.1a)), for the limiting case of $N = 1$, the quantity $\omega_{eg}(\mathbf{m}, 1)$ then recovers the energy-eigenvalue of a single, trapped $|e\rangle$-state atom (see eqn. (C.1b)). In the calculations below, we also explicitly keep the term $\omega_{\mathbf{m}}^e$, which corresponds to the energy in the translational degrees of freedom of the $|e\rangle$-state atom. In agreement with the treatment in the previous sections, we shall see below that the relevant distances $|\mathbf{r}_2 - \mathbf{r}_1|$ in eqn. (5.14) are negligibly small so that eventually the ground-state density $|\Phi_0^g(\mathbf{r}_1)|^2$ determines the atom-surface interaction.

---

[1] Differing from eqn. (2.28), where we introduced the GPE, we do not approximate the term $(N_0 - 1) \approx N_0$ in eqn. (5.12), which allows to perform the limit $N_0 \to 1$ for a cross-check in section 5.3.

Generalized polarizability

With the expression (5.14) for the atomic two-point function, eqn. (5.2) yields for the T-matrix element (after performing the dt_1 and dt_2 integrations and using relation (A.9))

$$
\langle N_0 | T^{(2)} | N_0 \rangle = -\frac{N_0}{(2\pi)^4} \int d^3 r_1 \int d^3 r_2 \, \Phi_0^g(\mathbf{r}_2) \Phi_0^{g*}(\mathbf{r}_1)
$$

$$
\times \int_0^\infty d\xi \, G_{\alpha\beta}(\mathbf{r}_1, \mathbf{r}_2, i\xi) \sum_{\mathbf{m}} a_{\alpha\beta}(\mathbf{m}, \xi) \, \Phi_{\mathbf{m}}^e(\mathbf{r}_1) \Phi_{\mathbf{m}}^{e*}(\mathbf{r}_2) \ .
$$

$$(5.16)$$

The generalized polarizability

$$
a_{\alpha\beta}(\mathbf{m}, \xi) = 2 \mu_\alpha^{ge} \mu_\beta^{eg} \frac{\omega_{eg}(\mathbf{m}, N_0)}{\omega_{eg}^2(\mathbf{m}, N_0) + \xi^2} \ ,
\tag{5.17}
$$

(compare to the single-atom expression $\alpha_{\alpha\beta}^a(i\xi)$ in eqn. (4.15)) contains the interaction- and recoil-shifted resonance frequency $\omega_{eg}(\mathbf{m}, N_0)$ of eqn. (5.15). In eqn. (5.16), we set $T_F = 0$ for simplicity, that is, we neglected the contribution of thermally excited photons.

Recoil shift and (de)localization correction

For simplicity, we now further assume that atoms in the internal state $|e\rangle$ do not experience any trapping potential, that is, we set $V_{trap}^e(\mathbf{r}) \equiv 0$ in eqn. (C.1b). The summation over $\mathbf{m}$ in eqn. (5.16) then becomes an integral over the plane-wave momenta $\mathbf{q}$, and the single-particle energy in eqn. (5.15) takes the value $\omega_{\mathbf{q}}^e = q^2/(2M)$. As an approximate solution for the wave function of the condensate in the potential (5.3), we choose the ansatz of Pérez-García *et al.* (1997): $\Phi_0^g(\mathbf{r})$ is a Gaussian centered at $(0, 0, d)$ with a variational width $\sigma(N_0)$ that depends on the number of condensate particles:[2]

$$
\sigma(N_0) =
\begin{cases}
a_0, & N_0 = 1 \\
a_0 \left(\sqrt{\dfrac{2}{\pi}} \dfrac{N_0 a}{a_0} \right)^{1/5}, & \dfrac{N_0 a}{a_0} \gg 1
\end{cases}
\ .
\tag{5.18}
$$

The result (5.16) for the T-matrix is, however, more generally valid and can be evaluated similarly for other forms of $\Phi_0^g(\mathbf{r})$ and $\Phi_{\mathbf{m}}^e(\mathbf{r})$.

After performing the spatial integrations in eqn. (5.16), we observe that in the polarizability (5.17), the momentum q appears only as a recoil shift of the atomic transition frequency $\omega_{eg}(N_0)$ (5.15). Since the relevant momenta are limited to

---

[2]See the gray dashed-dotted curve in fig. 2.3.

typically $1/\sigma$, the recoil shift is a small correction because $1/(M\sigma^2) = \nu \ll \omega_{eg}$ is usually well satisfied. We therefore expand in powers of q; integrating the first two terms of the series we finally obtain for the atom-surface interaction (see Schiefele and Henkel (2010) for more calculational details)

$$\Delta E_{N_0}(d) = -\frac{N_0}{4\pi\varepsilon_0} \int_0^\infty d\xi \int_0^\infty \frac{k\,dk}{\kappa} \frac{1}{2} e^{-2\kappa d} e^{\kappa^2 \sigma^2} (1 + \mathrm{erf}[\frac{d}{\sigma} - \kappa\sigma]) M_{\alpha\beta}$$
$$\times \left\{ \alpha_{\alpha\beta}(\xi, N_0) + \alpha^{(rc)}_{\alpha\beta}(\xi, N_0, k) \right\}, \tag{5.19}$$

with the matrix $M_{\alpha\beta}$ defined by eqns. (5.7). The polarizability

$$\alpha_{\alpha\beta}(\xi, N_0) = 2\mu_\alpha^{ge} \mu_\beta^{eg} \frac{\omega_{eg}(0, N_0)}{\omega_{eg}(0, N_0)^2 + \xi^2} \tag{5.20}$$

in eqn. (5.19) describes the no-recoil case. The recoil term $\alpha^{(rc)}$ is given by

$$\alpha^{(rc)}_{\alpha\beta}(\xi, N_0, k) = -2\mu_\alpha^{ge} \mu_\beta^{eg} \frac{\omega_{eg}(0, N_0)^2 - \xi^2}{(\omega_{eg}(0, N_0)^2 + \xi^2)^2} \left(\frac{3}{4M(\sigma(N_0))^2} + \frac{k^2}{2M} \right). \tag{5.21}$$

We can attribute this correction to a recoil shift of the effective resonance frequency

$$\omega_{eg} \to \omega_{eg} + \frac{3}{4M(\sigma(N_0))^2} + \frac{k^2}{2M} \tag{5.22}$$

where the two terms describe the kinetic energy from the delocalized condensate wave function and from the absorbed photon momentum in the excited state, respectively.

Expression (5.19) is our main result for the interaction energy of a trapped Bose gas with a plane surface. In the above form, it is clear that it generalizes the result for a stationary single atom in a straightforward manner. Clearly, as we put $N_0 = 1$, we get the single-atom transition frequency $\omega_{eg}(0, 1) = \omega_{eg}$. And with the identity

$$\lim_{\sigma \to 0} \frac{1}{2} e^{-2\kappa d} e^{\kappa^2 \sigma^2} (1 + \mathrm{erf}[\frac{d}{\sigma} - \kappa\sigma]) = e^{-2\kappa d}, \tag{5.23}$$

we get from the no-recoil term of eqn. (5.19)

$$\lim_{\sigma \to 0} \Delta E_1(d) = -\frac{\mu_\alpha^{ge} \mu_\beta^{eg}}{\pi} \int_0^\infty d\xi\, G^R_{\alpha\beta}(\mathbf{r}_A, \mathbf{r}_A, i\xi) \frac{\omega_{eg}}{\omega_{eg}^2 + \xi^2} \tag{5.24}$$

with $\mathbf{r}_A = (0, 0, d)$ the position of the trap center. This is the known result for a perfectly localized single atom as derived by Wylie and Sipe (1985, eqn. (2.28)), or, alternatively, the limit $T_F \to 0$ of eqn. (4.19) derived in the last chapter. The

recoil correction involving $\alpha^{(rc)}$ is discussed in detail in section 5.3. It is usually very small, unless the trap frequency ν is comparable to the atomic resonance ω_{eg}, a case of no practical significance.

For a large atom number N_0, the resonance frequency $\omega_{eg}(0, N_0)$ in eqn. (5.20) incorporates the inter-atomic interactions (see eqn. (5.15)). The overall proportionality factor N_0 of eqn. (5.19) can be understood by recalling that the responsible diagram (5.1) represents a sum of self-energies of N_0 individual ground state atoms.

Single atom revisited: photon recoil corrections

The interaction potential for a single atom can be obtained from eqn. (5.19) by setting $N_0 = 1$. In the dimensionless units of eqn. (5.5), we get

$$
\Delta E_1(x) = -\frac{\omega_{eg}^3}{\pi \varepsilon_0 c^3} \int_0^\infty d\overline{\xi} \int_0^\infty \frac{\overline{k}\, d\overline{k}}{\overline{\kappa}}\, I(\overline{\kappa}, x, \eta)\, M_{\alpha\beta}(\overline{k}, \overline{\xi})
$$
$$
\times\, \omega_{eg} \left\{ \alpha_{\alpha\beta}(\overline{\xi}\omega_{eg}, 1) + \alpha_{\alpha\beta}^{(rc)}(\overline{\xi}\omega_{eg}, 1, \overline{k}\omega_{eg}) \right\}, \qquad (5.25)
$$

where the Lamb-Dicke parameter $\eta = \omega_{eg} a_0 / c$ gives the size of the trap ground state in units of the resonant wavelength, the quantity I was defined in eqn. (5.6), and the matrix $M_{\alpha\beta}$ of eqns. (5.7) depends on the reflection coefficients R^p and R^s and encodes the surface properties. The recoil correction $\alpha^{(rc)}$ is now seen to be proportional to the ratio ν/ω_{eg}:

$$
\omega_{eg}\, \alpha_{\alpha\beta}(\overline{\xi}\omega_{eg}, 1) = 2\mu_\alpha^{ge} \mu_\beta^{eg} (1 + \overline{\xi}^2)^{-1}, \qquad (5.26)
$$

$$
\omega_{eg}\, \alpha_{\alpha\beta}^{(rc)}(\overline{\xi}\omega_{eg}, 1, \overline{k}\omega_{eg}) = -\frac{\nu}{\omega_{eg}}\, 2\mu_\alpha^{ge} \mu_\beta^{eg}\, \frac{1 - \overline{\xi}^2}{(1 + \overline{\xi}^2)^2}\left(\frac{3}{4} + \frac{\overline{k}^2}{2}\eta^2\right) \qquad (5.27)
$$

The trapping frequency $\nu/2\pi$ for a single ground state atom in the potential (5.3) is usually around $10 \ldots 1000$ Hz, much smaller than the frequencies of optical transitions $\omega_{eg}/2\pi \approx 10^{15}$ Hz. This justifies the expansion of the recoil shift for small atom momenta q done in section 5.3. Experimental situations where the recoil correction is enhanced in magnitude could involve tight traps like optical lattices ($\nu/2\pi \sim 100$ kHz) and Rydberg atoms whose transition frequencies can be a factor 10^6 smaller (see Gallagher, 1994).

Expression (5.25) is easily evaluated numerically. Figure 5.2 shows the energy shift of a rubidium atom in the harmonic trapping potential eqn. (5.3) with $\nu/2\pi = 1$ kHz. At this frequency, the oscillator length is $a_0 \approx 340$ nm. The black lines in fig. 5.2 are for the case of a perfectly reflecting surface, with the reflection amplitudes $R^p = 1$ and $R^s = -1$. The red lines involve a frequency-dependent reflection, as appropriate for a gold surface (described by the Drude model, see appendix A.2 for details). The two terms of eqn. (5.25) are shown separately, the
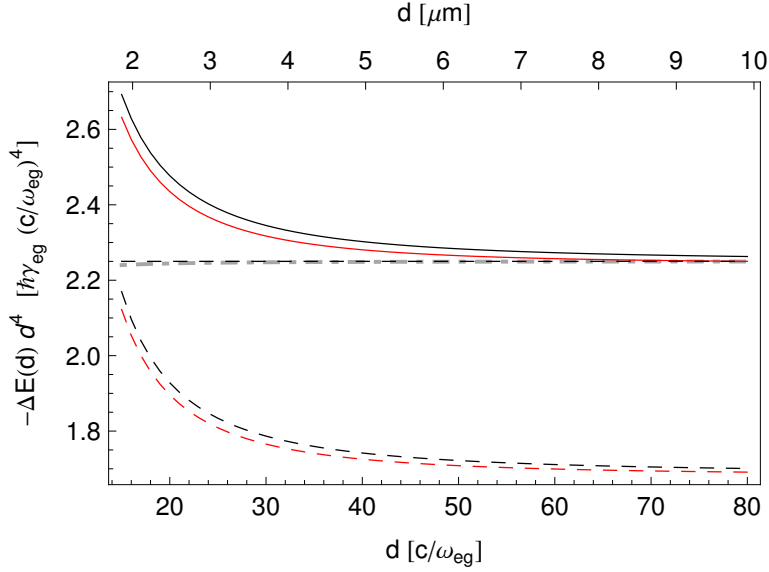
Figure 5.2: Atom-surface interaction energy between a rubidium atom and a perfectly reflecting *(black solid line)* and gold surface *(red solid line)*, field at zero temperature. Distance d in units of the resonance wavelength, energy multiplied by $-d^4$ as in fig. 5.1. *Dashed horizontal line/dot-dashed gray line:* Casimir-Polder asymptote eqn. (4.22) and Casimir-Polder potential eqn. (4.20) for a perfectly localized atom. The atom has isotropic dipole matrix elements and is trapped in a harmonic potential with a trap frequency $\nu/2\pi = 1$ kHz (ground state size $a_0 = 2.8 \, c/\omega_{eg}$). *Lower dashed lines (black/red):* recoil correction multiplied by $-\omega_{eg}/\nu$ [see eqn. (5.25)]. Parameters of the Drude dielectric function for gold, eqn. (A.17): $\omega_p = 5.74 \, \omega_{eg}$ and $\omega_p \tau = 5 \times 10^3$.

recoil correction (dashed lines) is multiplied by a factor of $-\omega_{eg}/\nu$ to fit on the scale. The dashed horizontal line shows the asymptotic expression (4.22) for the Casimir-Polder potential of a pointlike (localized) atom in front of a perfect mirror, which, for an atom with isotropic dipole matrix elements, is usually expressed in terms of the static polarizability $\alpha(0)$ as

$$V_{CP}(d) = -\frac{3}{8\pi} \frac{c \, \alpha(0)}{\epsilon_0 d^4} \ .$$

The gray dashed-dotted curve depicts the exact result (4.20) for the localized atom, which is, at the shown distance range, almost identical to the asymptote $V_{CP}(d)$.

5.4 Summary

The starting point of the calculations in this chapter was a second-quantized Hamiltonian that describes the interaction of a trapped system of N atoms with the elec-

tromagnetic field. We have focused on two simple models for the atomic system: an interacting BEC described by N_0 atoms populating a single condensate wave function and a noninteracting Bose gas at finite temperature, where the N particles populate the various single particle states of the trap . To calculate the interaction energy between the atoms and a plane surface, we made a perturbative expansion of the electromagnetic self-energy and worked out the T-matrix elements to second order in the atom-field coupling. The electric field propagator has been expressed in terms of retarded Green functions that permit to identify easily the contribution brought about by the surface. The characteristics of the surface material then enter through the scattering amplitudes for light, which allows for treating a wide range of materials. For the sake of simplicity, we considered the field to be at zero temperature, but thermal corrections can be included in a straightforward way by considering the temperature dependence in the propagator for the electric field, see eqn. (A.7). Even non-equilibrium situations (bodies at different temperatures) can be covered by combining the techniques of fluctuation electrodynamics (see Rytov *et al.*, 1989) with the Keldysh formalism (see Mkrtchian (2009) for an example).

The expression found in eqn. (5.16) describes the Casimir-Polder like interaction energy of a trapped Bose gas with the surface, for a general condensate wave function $\Phi_0^g(\mathbf{x})$. If the system is reduced to a perfectly localized single atom as treated by Wylie and Sipe (1985), our expression reproduces known results (see eqn. (5.24)). It also highlights that in full generality, the atom-surface interaction does not reduce to an integral over the density distribution of the atoms, due to the (virtual) propagation in the excited state. Although corrections to the results of a simple density averaging (as in eqn. (5.10)) turn out to be small, we think that it is an important (and to the best of our knowledge unique) feature of our calculation that we are able to quantify these deviations, instead of neglecting them right from the start. The Bose gas-surface interaction energy shows an overall scaling with the atom number N_0 (as can be expected at this order of perturbation theory), but even the interaction energy per atom still depends weakly on N_0. We have identified for this dependence the following physical mechanisms. (i) The interaction energy involves a spatial average over the density profile whose width is larger for a repulsive atom-atom interaction. This effect was already taken into account in the pioneering experiments of Harber *et al.* (2005) and Obrecht *et al.* (2007). (ii) The atomic interactions (treated here as a contact potential) shift the optical transition frequency (see for example the experiments of Wynar *et al.* (2000)) and modifies the ground-state polarizability. (iii) The optical spectral line is recoil-broadened due to the kinetic energy of the atoms. This effect is very weak for typical traps and in the fully degenerate limit as the phase gradient of the condensate wave function vanishes.

For the ideal Bose gas (see eqn. (5.5)), the Casimir-Polder interaction per particle does not depend on the atom number. We showed that the influence of a higher

atom temperature on the atom-surface interaction is similar to that of a broadening of the trap potential.

In chapter 6, we will use the formalism developed above to discuss the process of spontaneous emission in a trapped BEC.

CHAPTER **6**

Bosonic enhancement of spontaneous emission near an interface

The material presented in this chapter is based on the paper 'Bosonic enhancement of spontaneous emission near an interface' *by* J. Schiefele and C. Henkel, *Physics Letters A* **375**, 680 (2011).

Spontaneous emission from an excited atom can only take place when a vacuum mode is available to accommodate the emitted photon. This fact is employed in experiments in cavity quantum electrodynamics (cQED) to shift the spontaneous emission rate in small cavities where the structure of the electromagnetic vacuum is modified (see Haroche, 1992; Hinds, 1994; Hulet *et al.*, 1985). In particular, it is known that the lifetime of an excited atom near a plane surface (the simplest 'cavity' system) shows an oscillatory behavior for atom-surface distances comparable to the resonant photon wavelength. Modified spontaneous emission near an interface was first observed by Drexhage (1970), using fatty acid layers to separate dye monolayers from the interface. The effect is not easy to observe with ultra-cold atoms in vacuum since distance control in the sub-micron range is required. A transient signal related to a change in decay rate was observed by Ivanov *et al.* (2004), with cold atoms being probed spectroscopically in the vicinity of a surface using an evanescent light field. Quite analogous to the effect of a cavity on photon modes, the presence of a Bose-Einstein condensate can alter the decay of bosonic atoms, as the macroscopic population of atomic modes stimulates the transition into these (see Hope and Savage, 1996; Javanainen, 1994; Morice *et al.*, 1995). This enhancement is significantly reduced, however, in a uniform system because of momentum conservation. For an excited atom initially at rest, the final state is shifted by the photon recoil momentum, and overlap with the condensate mode

occurs only if repulsive interactions deplete the ground state (as shown by Görlitz *et al.*, 2001), or alternatively, for a confined system where the BEC is spread over a finite width in momentum space.

In the following, we discuss the enhancement of spontaneous emission in a trapped BEC and show in particular that the small oscillations in the decay rate near a surface can be significantly amplified. The trap confinement and the temperature of the BEC are taken into account and provide only a moderate reduction compared to the scaling with the number of atoms in the BEC. We also consider a typical spectroscopy experiment where the enhanced decay rate appears in the absorption spectrum of a weak, near-resonant laser field.

6.1 Decay of an excited wavepacket in a spherical atom cloud

Self energy and transition rate

Consider a factorized initial state $|e, N\rangle$ with one atom in the electronically excited state and N atoms in the (collective) ground state. We apply second-order perturbation theory in the interaction with the em field to get for this state a complex energy shift (self-energy) whose imaginary part gives the Bose-enhanced decay rate. The em self-energy is proportional to the S-matrix element

$$\langle e, N|S^{(2)}|N, e\rangle = \quad \text{} \tag{6.1}$$

$$= -\mu_\alpha \mu_\beta \int d^4x_1 \, d^4x_2 \, \Theta(t_2 - t_1) \langle T\{E_\alpha(x_1)E_\beta(x_2)\} \rangle$$

$$\times \langle e|\Psi_e^\dagger(x_2)\Psi_e(x_1)|e\rangle \langle N|\Psi_g(x_2)\Psi_g^\dagger(x_1)|N\rangle , \tag{6.2}$$

where μ_α ($\alpha = x, y, z$) are the matrix elements of the transition dipole. The Feynman diagram represented above uses bold lines for the many-body system of ground state atoms, dashed lines for individual excited atoms and wavy lines for the photon propagator. The brackets $\langle \dots \rangle$ in the first line of eqn. (6.2) denote an expectation value with respect to an equilibrium state of the em-field, and the symbol $T\{\dots\}$ denotes time-ordering. Ψ_e and Ψ_g are interaction-picture field operators for the atomic levels, with a time dependence governed by the unperturbed atomic Hamiltonian.

In eqn. (6.2), the time dependent phase of the ground state correlation function $\langle N|\Psi_g(x_2) \Psi_g^\dagger(x_1)|N\rangle$ is of the order of typical single particle energies in the trap and thus much smaller than the phase of the term $\langle e|\Psi_e^\dagger(x_2)\Psi_e(x_1)|e\rangle$, which is proportional to $\exp[i\omega_{eg}(t_2 - t_1)]$ where ω_{eg} is the Bohr transition frequency. We will hence neglect the time dependence of the ground state correlation function in eqn. (6.2). (This is equivalent to summing the decay rate over the final ground state modes, see also the remarks below eqn. (4.9).) The time integrations in eqn. (6.2)

can then be performed, yielding for the transition rate ($\hbar = 1$)

$$\gamma_e(N) = 2[1 + N_{\omega_{eg}}]\mu_\alpha\mu_\beta \left[\int d^3r \, |\Phi(\mathbf{r})|^2 \, \mathrm{Im} \, G_{\alpha\beta}(\mathbf{r}, \mathbf{r}, \omega_{eg}) \right. \tag{6.3}$$

$$\left. + \int d^3r_1 \, d^3r_2 \, \Phi(\mathbf{r}_1)\Phi^*(\mathbf{r}_2)\langle N|\Psi_g^\dagger(\mathbf{r}_1)\Psi_g(\mathbf{r}_2)|N\rangle \, \mathrm{Im} \, G_{\alpha\beta}(\mathbf{r}_1, \mathbf{r}_2, \omega_{eg}) \right] ,$$

where the excited state is given by the normalized wave function $\Phi(\mathbf{r})$. We denote $N_{\omega_{eg}}$ the average photon number at frequency ω_{eg} in thermal equilibrium (see eqn. (4.5)). For the sake of simplicity, we restrict ourselves for the rest of the paper to a field at zero temperature where the thermal photon number $N_{\omega_{eg}}$ is negligible. As in the previous chapters, we have expressed the photon propagator through the retarded response (Green) function $G_{\alpha\beta}(\mathbf{r}_1, \mathbf{r}_2, \omega_{eg})$ defined by eqn. (4.12). This quantity is easily calculated in a general environment, for example near a surface (see Wylie and Sipe, 1984), and shows oscillating behavior as a function of the atom-surface separation.

In eqn. (6.3), the decay rate naturally splits into a term $\gamma_e^{(0)}$ that remains in the absence of the atom cloud (first line) and an additional term $\gamma_e^{BEC}(N)$ which describes the bosonic enhancement. The first term has a natural interpretation in terms of an average of the local decay rates (4.17) over the position distribution of the excited state wavepacket. (For a study of the dynamics of the excited state, see Japha *et al.* (1998).) The analysis of the second term is the main focus of this chapter. Note that it depends on the two-point correlation function of the ground state atoms. The bosonic stimulation is thus a probe of the spatial coherence of the Bose gas.

Discussion of Bose enhancement in free space

To illustrate the physics in eqn. (6.3), we will assume that both the ground-state BEC and the excited atom are trapped in overlapping isotropic harmonic potentials, far enough away from any macroscopic body. We use the free-space expression $G_{\alpha\beta}^{(0)}$ of the em Green tensor (see section A.2) which takes the form

$$G_{\alpha\beta}^{(0)}(\mathbf{r}_1, \mathbf{r}_2, \omega_{eg}) = \int \frac{d^3k}{(2\pi)^3} \, G_{\alpha\beta}^{(0)}(k, \omega_{eg}) \, e^{i\mathbf{k}.(\mathbf{r}_1-\mathbf{r}_2)} . \tag{6.4}$$

As is well known, only photons on the light cone contribute to the the imaginary part of this quantity, i.e., $|\mathbf{k}| = \omega_{eg}/c \equiv k_{eg}$. Another relevant length scale is the oscillator length $a_0 = (M\omega_T)^{-1/2}$ of the ground-state trapping potential (M is the atomic mass and ω_T the trap frequency). We assume that the excited-state wave packet $\Phi(\mathbf{r}; \eta)$ is an isotropic Gaussian with a width $\eta \, a_0$. The first term in eqn. (6.3) gives $\gamma_e^{(0)} = \mu^2 k_{eg}^3/(3\pi\varepsilon_0)$, the free space decay rate (see Wylie and Sipe, 1984).

Fig. 6.1 shows how the decay rate $\gamma_e(N)$ varies with the width parameter η, in the presence of a Bose condensate with $N = 10\,000$ Rb atoms (three-dimensional, isotropic trap). We consider both an ideal gas model (solid red lines) and an interacting Bose gas (dash-dotted lines). The upper black curve corresponds to an ideal gas at zero temperature, where all the ground-state atoms populate the trap ground state $\psi_0(\mathbf{r})$, a Gaussian with width a_0. In this case the integrations in eqn. (6.3) can be worked out explicitly. We find analytically that the optimum value of $\gamma_e(N)$ is obtained for

$$\eta_{opt} = \frac{1}{\sqrt{3}} \left(\sqrt{9 + (k_{eg}a_0)^4} - (k_{eg}a_0)^2 \right)^{1/2}, \quad (0 < \eta_{opt} < 1) . \qquad (6.5)$$

This result as well as the typical behavior of $\gamma_e(N)$ is easy to understand by noting that the decay rate for a given photon momentum $\mathbf{k}$ is proportional to the overlap integral

$$\int d^3r \, \Phi(\mathbf{r}, \eta) \, \psi_{\mathbf{n}}^*(\mathbf{r}) \, e^{i\mathbf{k}\cdot\mathbf{r}} , \qquad (6.6)$$

where $\mathbf{n} = \mathbf{0}$ for the BEC ground mode. In the so-called Lamb-Dicke limit $k_{eg}a_0 \ll 1$ (well-localized trap), the exponential in eqn. (6.6) can be approximated by unity, and the overlap is optimal when the two wavepackets are matched in width, $\eta = 1$. The opposite case looks closer to a homogeneous system and is easier to analyze in Fourier space where the photon recoil provides a shift of the momentum distribution. This reduces the overlap and can be compensated for by making an excited-state wave packet wider in momentum space, i.e., $\eta < 1$. At the optimum value, the width is of the order of the photon momentum and the shifted excited-state wave packet still has some overlap with the sharp zero-momentum component of the BEC.

The temperature dependence in Fig. 6.1 closely follows the occupation of the ground-state (condensate) mode. We have used the expression (B.1) by Barnett *et al.* (2000), where the two-point correlation function $\langle N | \Psi_g^\dagger(\mathbf{r}_1) \Psi_g(\mathbf{r}_2) | N \rangle$ for the ideal Bose gas in a 3D trap is given in a simple form, involving only a single summation. This provides the Bose enhancement of $\gamma_e(N)$ in a straightforward manner for atom temperatures T_A below and above the critical temperature T_c (see caption). We see that for any η, the transition rate drops below the zero-temperature value, and for temperatures above T_c, it becomes comparable to $\gamma_e^{(0)}$ (horizontal dashed line). The temperature dependence is shown in fig. 6.2, and compared to the condensate fraction N_0/N (dashed line). The bosonic enhancement closely follows the population of the condensate mode because the excited-state wave packet $\Phi(\mathbf{r})$ has the largest overlap with the trap ground state. The thermal occupation of higher lying trap states hence diminishes the integrals eqn. (6.6). We note that this behavior would change qualitatively in lower-dimensional systems where the Bose gas occupies excited states with a relatively larger weight.
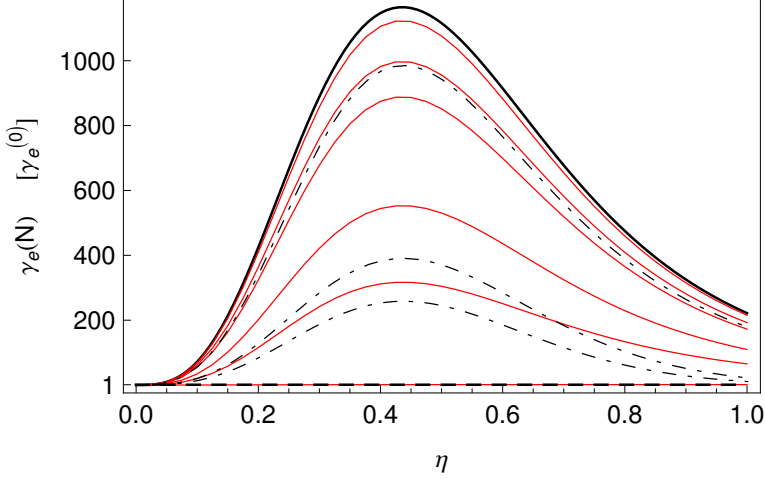
Figure 6.1: Decay rate of an excited wave packet embedded in a Bose conden-
sate with N atoms. The rate $\gamma_e(N)$ [eqn. (6.3)] is normalized to the free-space
value $\gamma_e^{(0)} = \mu^2 k_{eg}^3 / (3\pi\varepsilon_0)$ and plotted as a function of the width $\eta\, a_0$ of the
excited state, scaled to the oscillator length for the BEC trap. The ground-state
cloud consists of $N = 10\,000$ atoms, with trap frequency $\omega_T / 2\pi = 1\,\mathrm{kHz}$ (os-
cillator length $a_0 = 0.34\,\mu\mathrm{m}$), the resonance wavelength is $2\pi / k_{eg} = 780\,\mathrm{nm}$
as for rubidium. The optimal value of η [eqn. (6.5)] is $\eta_{opt} = 0.44$. *Upper
black curve*: ideal Bose gas at zero temperature. *Solid (red) curves*: ideal Bose
gas at temperature $T_A = 0.3, 0.5, 0.6, 0.8, 0.9, 1.2\,T_c$ with critical tempera-
ture $T_c = \omega_T (N/\zeta[3])^{1/3}$ (top to bottom). *Dash-dotted curves*: interacting
Bose gas with mode function eqn. (2.61), for varying s-wave scattering length
$a_s = 1, 5, 10\,\overline{a}_s$ (top to bottom), with $k_{eg}\overline{a}_s = 0.047$ as for rubidium. *Horizon-
tal dashed line*: free-space decay rate $\gamma_e^{(0)}$.

The more realistic case of an interacting Bose gas is also shown in fig. 6.1.
We focus here on repulsive interactions (corresponding to positive s-wave scat-
tering length a_s), and restrict ourselves to temperatures far below T_c, where it is
legitimate to approximate the field operator by the condensate mode only:

$$\langle N | \Psi_g^\dagger(\mathbf{r}_1) \Psi_g(\mathbf{r}_2) | N \rangle \approx N \psi_0^*(\mathbf{r}_1) \psi_0(\mathbf{r}_2) \,. \tag{6.7}$$

Elementary excitations of the condensate can be included within Bogoliubov the-
ory (see Hu *et al.*, 2004; Öhberg *et al.*, 1997; Stringari, 1996). The condensate
wave function $\psi_0(\mathbf{r})$ is a solution of the Gross-Pitaevskii equation. We have used
the approximate variational solution (2.61) originally introduced by Fetter (1997),
that interpolates between a Gaussian and the Thomas-Fermi limit as the parameter
$N_0 a_s / a_0$ is changing from zero to infinity. The result for the decay rate $\gamma_e(N)$
is shown by the dashed-dotted curves in fig. 6.1, as the interaction parameter
$N_0 a_s / a_0$ is increased. Relative to the s-wave scattering length $\overline{a}_s$ of rubidium, we
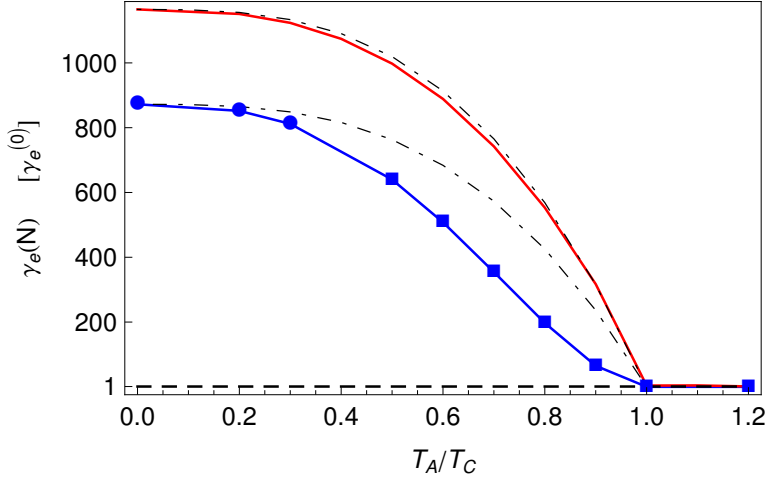
Figure 6.2: Decay rate and absorption line width vs temperature T_A of an (ideal) Bose gas, for an optimized excited state wave packet. The rate $\gamma_e(N)$ is given in units of the free-space value $\gamma_e^{(0)}$. Trap and atom parameters are the same as in fig. 6.1. *Red (upper) curve*: decay rate eqn. (6.3) with $\eta = \eta_{opt} = 0.44$. *Blue (lower) curve*: line width $\gamma_{abs}(N)$ [eqn. (6.15)] of the absorption spectrum. *Dashed-dotted curves*: condensate fraction N_0/N, scaled to the $T = 0$ values. *Horizontal dashed line*: free-space decay rate $\gamma_e^{(0)}$.

took $a_s = 1,\ 5,\ 10\,\overline{a}_s$ (top to bottom) which can be achieved using a Feshbach resonance, for example. The interacting gas shows a flatter density profile in the trap, as is well known; this results in smaller values of the overlap integrals eqn. (6.6).

To summarize the data of fig. 6.1, we find a relatively strong enhancement of the spontaneous decay rate of an excited atom embedded in a Bose condensate. This happens despite the non-perfect overlap that encodes the constraints of momentum conservation and photon recoil. The optimum conditions correspond to a well-localized excited-state wavepacket (on the scale of the transition wavelength) and a strong condensate fraction ($T \leq 0.5\,T_c$).

6.2 Bose enhancement near a surface

In this section, we calculate the transition rate eqn. (6.3) near a surface and demonstrate its enhancement in a Bose condensate of oblate shape. This scenario can be realized with an optical lattice, by retro-reflecting an off-resonant laser beam at the surface (see Spreeuw *et al.*, 1995), or in a bichromatic evanescent wave (see Ovchinnikov *et al.*, 1991). We take the surface in the xy-plane and the trapped atoms centered at a distance d from the surface in the positive z-direction. Concerning the surface material, we use the idealized model of a perfectly reflecting mirror for the sake of simplicity; but with the appropriate choice of (frequency de-
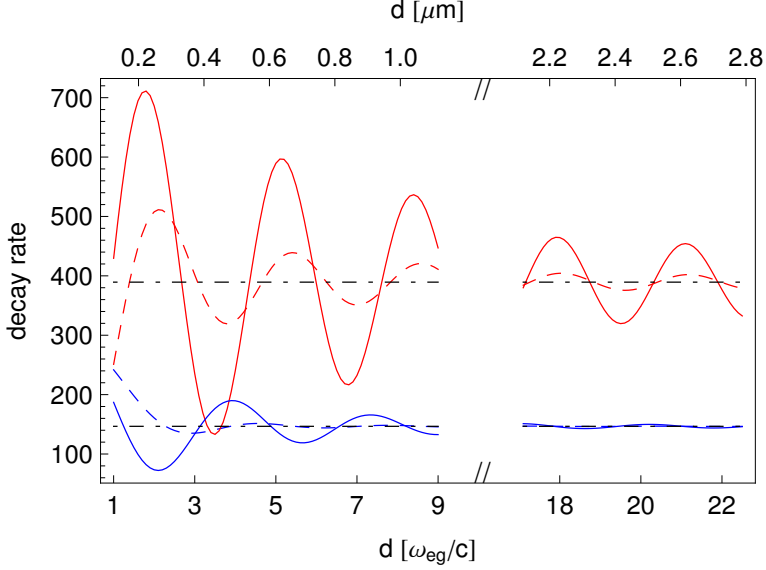
Figure 6.3: Bose-enhanced decay rate $\gamma_e(N)$ near an interface. The BEC contains 10^5 Rb atoms in an oblate wave function at an average distance d from a perfectly reflecting surface. The size parameters are $a_0 = 3.4\,\mu$m parallel and $a_0/\sqrt{\lambda} = 0.01\,a_0$ perpendicular to the surface, corresponding to trapping frequencies of $\omega_\parallel/2\pi = 10$ Hz and $\omega_\perp = 10^4\omega_\parallel$ and a critical temperature $T_c^{(2D)} = 118$ nK. The excited wave packet (resonance frequency as in fig. 6.1) is spatially centered in the BEC, with size parameters $\eta = 0.07$ and $\eta_z = 1$ relative to a_0. *Full red curve*: Bose-enhanced decay rate $\gamma_e^{BEC}(N)$ given by eqn. (6.3), for an excited atom with its dipole moment oriented parallel to the surface. We normalize to the free-space decay rate $\gamma_e^{(0)}(d \to \infty)$. *Full blue curve*: $\gamma_e^{BEC}(N)$ for an excited atom with perpendicular dipole moment. *Horizontal dashed lines*: asymptotic values of $\gamma_e^{BEC}(N, d \to \infty)$ at large separation. *Dashed red (blue) curve*: single-atom decay rate $\gamma_e^{(0)}$ (first line of eqn. (6.3)) for parallel (perpendicular) dipole orientation; these data are multiplied by a factor of 390 and 150, respectively, such that their asymptotic values for large distances d coincide with $\gamma_e^{BEC}(N)$.

pendent) reflection coefficients that appear in the photonic Green function $G_{\alpha\beta}(r_1, r_2, \omega)$, a wide range of surface materials can be treated in the same manner (see Sipe, 1981; Wylie and Sipe, 1984).

As we have measurements in mind where the control over the distance d is essential, we take an oblate Bose condensate and assume for simplicity a single Gaussian mode with widths a_0 (in the xy-plane) and $a_0/\sqrt{\lambda} \ll d$ (along the z-axis). The depletion of the condensate and its broadening due to repulsive interactions could be incorporated as in section 6.1. For the excited state, we adopt again a Gaussian wave packet localized in the cloud center, with widths ηa_0 and $\eta_z a_0/\sqrt{\lambda}$, respectively. The actual values of the trap frequency are given in the caption of fig. 6.3. As the very narrow confinement in the z-direction describes a quasi-2D scenario, the temperature has to be lower than $T_c^{(2D)} = \omega_\parallel (N/\zeta_2)^{1/2}$ to ensure a strong condensate occupation.

Fig. 6.3 illustrates the decay rate $\gamma_e(N)$ obtained from eqn. (6.3) as a function of the distance d. As is well known, the rate depends on the orientation of the dipole moment (parallel or perpendicular to the surface, represented in red and blue, respectively). The full curves show the Bose-enhanced contribution $\gamma_e^{BEC}(N, d)$, while the dashed curves give the single-atom part $\gamma_e^{(0)}(d)$, re-scaled such that the asymptotic value for large distances d coincides with $\gamma_e^{BEC}(N, d \to \infty)$. The numbers given in fig. 6.3 are the result of a compromise between a tight confinement in the vertical (z-) direction and a localized wave packet in the excited state. The atomic wave packets must be confined below the wavelength in the z-direction, otherwise the oscillations in γ_e vs. distance are averaged out. In this limit, the optimal Bose enhancement is found for an excited wave packet that is matched to the condensate ($\eta_z = 1$). For the size parameter in the xy-plane, we find an optimum at $\eta = 0.07$. The asymptotic values $\gamma_e(N, d \to \infty)$ are enhanced by factors of 390 and 150 compared to $\gamma_e^{(0)}(d \to \infty)$ for the parallel and perpendicular dipole, respectively. The difference between these two numbers and the relative phase shift of the oscillation pattern in $\gamma_e^{BEC}(d)$ are due to the radiation pattern of the dipole emission, combined with the shape of the ground state mode that modulates the Bose enhancement in $\mathbf{k}$-space.

Fig. 6.3 thus demonstrates a significant amplification of the decay rate above the surface, with the oscillation amplitude receiving an additional enhancement relative to the asymptotic free-space component. It suggests that even at a distance of a few microns (several transition wavelengths), Bose enhancement can bring the tiny interference structure of the decay rate into an experimentally detectable regime.

6.3 Virtual excited atoms produced by laser absorption

The calculation above assumed the presence of an excited atom prepared in a Gaussian wave packet, and one may ask the question whether this is a realistic description. Indeed, the preparation of such a state would typically proceed by illuminating the system. We therefore describe in this section a calculation of a typical absorption spectrum. We find that the results of the previous section are qualitatively unchanged. The method also illustrates the relevance of two- and four-point correlation functions of the Bose gas. For the sake of simplicity, we restrict this analysis to the ideal Bose gas.

The calculation proceeds by keeping a continuum of modes for the excited state field operator $\Psi_e(x)$ and by identifying the absorption spectrum of a weak laser field with a suitable T-matrix element (self-energy). We take the laser field to be described by a coherent state $|\beta\rangle$ in a given plane-wave mode.

In the leading order of perturbation theory, the absorption by the atom cloud of a photon out of the coherent state $|\beta\rangle$ and re-emitting it into the same state,
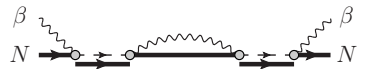
$$\tag{6.8}$$

results in a (complex) energy shift of the laser plus atom system that is described by the T-matrix element

$$\langle N, \beta | T^{(2)} | N, \beta \rangle = \frac{|\beta|^2 \omega_L}{2} \hat{e}_\alpha(\mathbf{k}_L) \hat{e}_\beta(\mathbf{k}_L) \frac{N \mu_\alpha \mu_\beta}{\omega_{eg} - \omega_L - i\epsilon} \ . \tag{6.9}$$

In eqn. (6.9), $|\beta|^2$ is the number of photons in the coherent state, ω_L and $\mathbf{k}_L$ denote the frequency and wave vector of the absorbed photons, the unit vectors $\hat{e}(\mathbf{k}_L)$ denote axes of (linear) photon polarization, and the infinitesimal $\epsilon \searrow 0$ ensures the adiabatic switching-on of the laser field. At this order of perturbation theory, the absorption of photons by the atom cloud is proportional to Im $\langle N, \beta | T^{(2)} | N, \beta \rangle \propto \delta(\omega_{eg} - \omega_L)$.

The next order in perturbation theory brings about the diagram[1]

$$\tag{6.10}$$

---

[1] The relation of this process to the well-kown phenomenon of superradiance is discussed by Schneble *et al.* (2003): The initial state of (6.10), consisting of the condensate and the photon corresponds to the excited electronic state in usual superradiance (see Dicke, 1954). The re-emitted photon accompanied by a recoiling ground-state atom in the virtual state of (6.10) replace the final state of Dicke's superradiance, after spontaneous emission took place.

which gives the following contribution to the T-matrix:

$$\langle N, \beta | T^{(4)} | N, \beta \rangle = -\frac{|\beta|^2 \omega_L}{2} \hat{e}_\alpha(\mathbf{k}_L) \hat{e}_\beta(\mathbf{k}_L) \frac{\mu_\alpha \mu_\beta}{[\omega_{eg} - \omega_L - i\epsilon]^2} \qquad (6.11)$$

$$\times \int d^3 r_1 \int d^3 r_2 \, \langle \Psi_g^\dagger(\mathbf{r}_2) \Psi_g(\mathbf{r}_2) \Psi_g^\dagger(\mathbf{r}_1) \Psi_g(\mathbf{r}_1) \rangle \, \mu_\gamma \mu_\delta G_{\gamma\delta}(\mathbf{r}_1, \mathbf{r}_2, \omega_L)$$

$$\times e^{-i\mathbf{k}_L \cdot (\mathbf{r}_1 - \mathbf{r}_2)} \, .$$

Let us introduce the density correlation function of the Bose gas as

$$C(\mathbf{r}_2, \mathbf{r}_1) = \langle \Psi_g^\dagger(\mathbf{r}_2) \Psi_g(\mathbf{r}_2) \Psi_g^\dagger(\mathbf{r}_1) \Psi_g(\mathbf{r}_1) \rangle - n(\mathbf{r}_2) n(\mathbf{r}_1) \qquad (6.12)$$

where $n(\mathbf{r}) = \langle \Psi_g^\dagger(\mathbf{r}) \Psi_g(\mathbf{r}) \rangle$ is the average density. This splits eqn. (6.11) in two parts: $\langle T^{(4)} \rangle = \langle T_{scat}^{(4)} \rangle + \langle T_{abs}^{(4)} \rangle$. The former contains only densities and can be identified with the elastic scattering of photons off the inhomogeneous density profile of the BEC. This term does not distinguish between a Bose gas and a classical system with the same density. Its imaginary part provides, by the optical theorem, the total scattering cross section of the BEC. The second term $\langle T_{abs}^{(4)} \rangle$, on the contrary, is proportional to density fluctuations, and these are at the origin of bosonic enhancement (see Ketterle and Inouye, 2001; Moore and Meystre, 2001). We therefore identify $\text{Im} \, \langle T_{abs}^{(4)} \rangle$ with the change in the atomic absorption spectrum (line width).

Indeed, if we define the resonant part of the polarizability $\alpha_{\alpha\beta}(\omega)$ of the atom cloud as

$$\alpha_{\alpha\beta}^{res}(\omega) = \frac{N \mu_\alpha \mu_\beta}{\omega_{eg} - \omega - i\epsilon} \, . \qquad (6.13)$$

we see that the process (6.10) can be re-written as a shift of the atomic transition frequency $\omega_{eg} \to \omega_{eg} + \delta\omega_{eg}$ with

$$\langle T^{(2)} \rangle + \langle T_{abs}^{(4)} \rangle = \frac{|\beta|^2 \omega_L}{2} \hat{e}_\alpha(\mathbf{k}_L) \hat{e}_\beta(\mathbf{k}_L) \left[\alpha_{\alpha\beta}^{res}(\omega_L) + \delta\omega_{eg} \frac{\partial \alpha_{\alpha\beta}^{res}(\omega_L)}{\partial \omega_{eg}} \right] \quad (6.14)$$

By identifying eqn. (6.11) and eqn. (6.14), we can read off the frequency shift $\delta\omega_{eg}$ whose imaginary part yields the atomic line width (the inverse lifetime of the virtual state involving an excited atom)

$$\gamma_{abs}(N) = -2 \, \text{Im} \, \delta\omega_{eg} = \frac{2}{N} \mu_\alpha \mu_\beta \left[\int d^3 r \, n(\mathbf{r}) \, \text{Im} \, G_{\alpha\beta}(\mathbf{r}, \mathbf{r}, \omega_L) \right. \qquad (6.15)$$

$$\left. + \int d^3 r_1 \int d^3 r_2 \, C(\mathbf{r}_1, \mathbf{r}_2) \, \text{Im} \, G_{\alpha\beta}(\mathbf{r}_1, \mathbf{r}_2, \omega_L) \, e^{-i\mathbf{k}_L \cdot (\mathbf{r}_1 - \mathbf{r}_2)} \right] \, .$$

This function depends weakly on the laser frequency, and we evaluate it at $\omega_L = \omega_{eg}$ for simplicity. We shall use below Wick's theorem to evaluate the density

correlation function (see Evans and Steer, 1996), as appropriate for the ideal Bose gas:

$$C(\mathbf{r}_1, \mathbf{r}_2) = \left| \langle \Psi_g^\dagger(\mathbf{r}_2) \Psi_g(\mathbf{r}_1) \rangle \right|^2 \tag{6.16}$$

Eqs.(6.15, 6.16) can now be compared to the decay rate $\gamma_e(N)$ of an excited-state wave packet (eqn. (6.3)). The first line in both expressions is very similar, and we see that the laser spectroscopy effectively prepares an excited state density profile matched to the condensate density. The second lines differ because the laser wave-vector appears explicitly. Also the one-body density matrix for the excited state, $\langle e|\Psi_e^\dagger(\mathbf{r}_2)\Psi_e(\mathbf{r}_1)|e\rangle$ in eqn. (6.2), is replaced by its ground-state equivalent $\langle N|\Psi_g^\dagger(\mathbf{r}_2)\Psi_g(\mathbf{r}_1)|N\rangle$ in eqn. (6.15). The prepared wavepacket is hence no longer pure. This makes the temperature dependence of $\gamma_{abs}(N)$ stronger, as can be seen in fig. 6.2 (compare the blue and red curves). The calculation of $\gamma_{abs}(N)$ involves, because of the squared correlation function, a double summation over single-particle trap states (see Barnett *et al.*, 2000) under the integral. At zero temperature, the summations can be done analytically, at the low temperatures $T_A = 0.2, 0.3\, T_c$, the double sum could be evaluated numerically (circles in fig. 6.2), while for $T_A/T_c \geq 0.5$, the summations can be accurately replaced by integrations that evaluate faster (denoted by squares). The size parameter η was set to the optimal value obtained from fig. 6.1. Although the line width $\gamma_{abs}(N)$ is for these parameters around 30% smaller than the optimized decay rate $\gamma_e(N)$, the strong Bose enhancement is still working in a qualitatively similar way for both types of processes. We expect a similar result to hold for an absorption experiment near a surface, using for example evanescent fields as discussed by Aspect *et al.* (1995); Cornelussen *et al.* (2002); Courtois *et al.* (1995).

6.4 Summary

To summarize, the presence of a trapped BEC can significantly enhance the decay of an excited atom by bosonic stimulation. The magnitude of the effect depends on the overlap between the atomic wave functions and the wavevector of the photon involved in the decay. More precisely, our calculations based on a quantum field theory of the atom-photon interaction illustrate the importance of two- and four-point correlation functions of the ground-state field for the Bose enhancement. For an excited atom prepared in a Gaussian wavepacket, the transition rate to the ground state can be increased under optimum conditions by a factor $N/10$ where N is the atom number in the BEC. This effect also amplifies the small oscillations of the decay rate near an interface. We have provided an alternative calculation based on the absorption of a laser beam that qualitatively confirms the simpler wave packet picture. The main difference is that absorption from the laser field prepares a non-pure excited state which matches the one-body density matrix of the Bose gas.

CHAPTER

Self-energy processes in higher orders

In the preceding chapters, we analyzed the self-energy acquired by different atomic systems through their interaction H_{AF} (4.4) with the em-field: single atoms in their internal ground or excited state, Bose-condensates of ground-state atoms, and single excited atoms in the presence of these condensates. Apart from the calculation of the absorption process in section 6.3, where real photons in the initial and final state were involved, we limited ourselves to the leading order of perturbation theory. The purpose of this chapter is to give a brief overview about how the quantities appearing in higher orders can be described with the techniques developed so far.

7.1 Single atom processes

A generic self-energy diagram for a single ground-state atom might be represented by

$$\text{———} = \text{———} + \mathcal{O}(\mu^4) \,. \qquad (7.1)$$

The atom part of the diagrams appearing in the μ^4-term of the series necessarily involves the pattern

$$\text{———} \,, \qquad (7.2)$$

where the presence of (virtual) $|e\rangle$ and $|g\rangle$ atoms is alternating. We already analyzed the first term of the self energy eqn. (7.1) in detail in section 4.3. If we

consider localized pointlike atoms it is of the form

$$\text{—∘- -∿- -∘—} = \int d\omega\, D(\omega)\, \frac{\mu^2}{\omega - \omega_{eg} + i\epsilon} \tag{7.3}$$

(see eqn. (4.10) and the Feynman rules in appendix C). Above, $D(\omega)$ denotes an even, scalar function of the frequency, which is composed of the matrix elements of the Feynman-propagator (4.8).

For an atom close to a surface, we have calculated the atom-surface potential from eqn. (7.3) by inserting an appropriate photon line into the diagram (see section 4.5):

We followed the approach of Agarwal (1975), using the fluctuation-dissipation theorem to link correlations of the electric field to the retarded response functions $G_{\alpha\beta}$ of eqn. (4.12). These in turn can be identified with the known field of a classical dipole oscillating above the surface (see Sipe, 1981).

In the following, by modifying the other elementary building blocks of eqn. (7.3), we can construct the different contributions that appear in higher orders of eqn. (7.1). One possibility to promote diagram (7.3) to a fourth-order process is to include self energy diagrams for the virtual excited atom:

$$\text{—•—•—} = \text{— — — —} + \text{— -∿- —} + \mathcal{O}(\mu^4)\,. \tag{7.4}$$

The above series can be summed formally to yield an integral equation (Dyson's equation, see Dyson (1949a) or Fetter and Walecka (2003, pp. 105)) for the exact Green function of the excited atom. We obtain

$$\underset{x_1 \quad \omega \quad x_2}{\text{—•⇉•—}} = \frac{i\delta(\mathbf{r}_1 - \mathbf{r}_2)}{\omega - \omega_{eg} - \Sigma(\omega)}\,, \tag{7.5}$$

where $\Sigma(\omega)$ is the one-particle irreducible (or proper) self-energy of the $|e\rangle$-state atom. It consists of all self-energy diagrams that cannot be separated in two pieces by cutting a single atom line, and can itself be expanded in orders of μ. We already calculated the first nonvanishing contribution $\Sigma^{(1)}$ (proportional to μ^2) in chapter 4 (see eqn. (4.6b) and eqn. (4.11)). Including the full propagator for the excited atom in eqn. (7.3) thus yields, with the expression (4.11) for $\Sigma^{(1)}$,

$$\text{—∘∿•—•∿∘—} = \text{—∘∿- - -∘—} + \text{—∘∿∿∿∿∘—} + \mathcal{O}(\mu^6) \tag{7.6}$$

$$= \int d\omega\, D(\omega)\left[1 + \Sigma^{(1)}(\omega)\frac{\partial}{\partial\omega_{eg}}\right]\frac{\mu^2}{\omega - \omega_{eg} + i\epsilon} + \mathcal{O}(\mu^6)\,. \tag{7.7}$$

The self-energy $\Sigma^{(1)}$ is proportional to the natural linewidth $\gamma_{eg} \approx \omega_{eg} (\mu\omega_{eg})^2$ (with $\hbar = c = \epsilon_0 = 1$), and eqn. (7.7) shows that the small dimensionless parameter in our perturbation series, playing the role of the fine-structure constant in QED interactions of elementary particles, is actually $(\mu\omega_{eg})^2$.

We encountered an expression similar to eqn. (7.7) in section 6.3 (see eqn. (6.14)), where the frequency was fixed by the incoming laser-photon and we only evaluated the resonant contribution of $\Sigma^{(1)}$. From eqn. (7.5), we see that the substitution (7.4) for the propagation of the virtual state results in a (complex) shift of the atomic frequency ω_{eg}, and the atomic transition acquires a finite line-width. Techniques which make use of resummed expressions like eqn. (7.5) are in the literature often referred to as non-perturbative (see for example Buhmann *et al.* (2004)).

Inclusion of the full propagator (7.5) alone, however, does not yield all higher order terms of the self-energy (7.1). In the same way as discussed above for the frequency-shift, the modification

$$\text{(diagram)} = \text{(diagram)} + \text{(diagram)} + \mathcal{O}(\mu^5) \tag{7.8}$$

results in a shift of the effective atom-light coupling (see Fetter and Walecka, 2003, pp. 402). At the fourth order in eqn. (7.1), the inclusion of the vertex-insertion (7.8) yields a contribution

$$\text{(diagram)} , \tag{7.9}$$

where, in contrast to the μ^4-term of eqn. (7.6), the photons absorbed (emitted) in the virtual state are emitted (absorbed) by the atom in the asymptotic state.

Combining eqn. (7.4) and eqn. (7.8), the one-particle irreducible contributions to eqn. (7.1), which are relevant for the calculation of the energy-shift and lifetime of the asymptotic state, are of the form

$$\text{(diagram)} . \tag{7.10}$$

The self-energy at sixth order in the atom light interaction is thus obtained from (7.10) by inserting vertex parts up to $\mathcal{O}(\mu^3)$ and the green function of the excited atom up to $\mathcal{O}(\mu^4)$. By consistently iterating this procedure, the self energy can be obtained to any desired order in the atom-light interaction.

7.2 Two atom processes

In the following, we want to consider the case of two distinguishable (two-level) atoms (labeled A and B) with no additional interactions between them except

those mediated by photon-exchange, described by H_{AF}. Both atoms are supposed to be in their internal ground-state, but might have different transition frequencies ω_A and ω_B. The atomic wavefunctions are centered at different points $\mathbf{r}_A$ and $\mathbf{r}_B$, separated by a distance $r = |\mathbf{r}_A - \mathbf{r}_B|$ large enough to treat the atoms as pointlike, perfectly localized objects, as discussed in section 4.3. Analogous to eqn. (7.1), we represent the self-energy diagram for the two-atom system as

$$(7.11)$$

Expanding eqn. (7.11) in orders of the interaction, we get disconnected diagrams of second, fourth and higher orders, which describe the single atom processes of the last section for atom A and B without any interaction between them:

$$\mathcal{O}(\mu^6) \ .$$

Apart from these, there are also two fourth order diagrams with photon lines that connect atom A with atom B:

$$(7.12)$$

If the two atoms are described as pointlike, localized objects, a straightforward calculation using the Feynman rules given in appendix C shows that the sum of the two diagrams in eqn. (7.12) leads (with the field at zero temperature), to a purely real T-matrix element, which yields the interatomic potential[1]

$$V(\mathbf{r}_A, \mathbf{r}_B) = \int_0^\infty \frac{d\xi}{2\pi} G_{\alpha\beta}(\mathbf{r}_A, \mathbf{r}_B, i\xi) G_{\delta\gamma}(\mathbf{r}_B, \mathbf{r}_A, i\xi) \alpha_{\gamma\alpha}^{A\,g}(i\xi) \alpha_{\beta\delta}^{B\,g}(i\xi) \ . \quad (7.13)$$

Above, $G_{\alpha\beta}$ denotes the Green-function of the electric field eqn. (4.12), and $\alpha_{\alpha\beta}^{A,B\,g}$ the atomic polarizabilities (4.15) for atom A and B, respectively. For two atoms in free space, the potential (7.13) yields the result of Casimir and Polder (1948): the attractive interaction potential between the two atoms behaves as r^{-6} for interatomic distances smaller than typical atomic transition wavelengths from the ground state and as r^{-7} for larger distances, thus showing a similar retardation effect as the atom-surface potential calculated in section 4.5. In (Craig and Thirunamachandran, 1998, chap. 7), the potential (7.13) is derived by means of conventional fourth-order perturbation theory. The relevant terms are then depicted by

---

[1]For a generalization to finite field temperature and resonant interactions between $|g\rangle$- and $|e\rangle$-state atoms, see Haakh *et al.* (2012).

twelve different time-ordered graphs, which are compactly represented in eqn. (7.12). As discussed in section 4.4, the Green-functions $G_{\alpha\beta}$ can can also incorporate additional boundary conditions from nearby surfaces. A calculation of the processes in eqn. (7.12) near a perfectly conducting surface was first done by Power and Thirunamachandran (1982). Passante and Spagnolo (2007) generalize the calculation of Power and Thirunamachandran by including the effects of thermal photons which are present at finite field temperature. The thermal occupation of the excited atomic degree of freedom can usually be neglected.

The two diagrams of eqn. (7.12) can also be constructed from the leading order self-energy (7.3) of a single atom by including the presence of an additional atom into the propagation of the virtual photon. Pictographically, this 'dressing' of the virtual photon amounts to the substitution
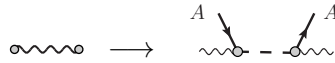
in eqn. (7.3). A similar approach is applied by Novotny and Henkel (2008) and by Messina *et al.* (2008), where the Casimir-Polder potential between two atoms is derived as the interaction energy of one atom interacting with the photon cloud dressing the other atom.

7.3 Generalization to many-body systems

In chapter 5, we already treated self-energies of atomic systems that consist of a large number N of $|g\rangle$-state atoms. In second order in the perturbation H_{AF}, these involved a mixed (that is, containing Ψ_g and Ψ_e operators) correlation function $\langle \Psi_g^\dagger(x_2)\Psi_e(x_2)\Psi_e^\dagger(x_1)\Psi_g(x_1)\rangle$ as in eqn. (5.2). At the next order, the corresponding expressions

$$\text{} \quad \text{and} \quad \text{} \tag{7.14}$$

appear. The first of the above diagrams contains repeated subprocesses where a single atom is excited and decays again, as it is the case for the single atom processes in eqn. (7.6) and (7.9). The second diagram differs by the simultaneous presence of two excited atoms, as in the expressions (7.12) for the interatomic potential. If we focus on the case where the atomic Hamiltonian H_A contains only interaction terms between the $|g\rangle$-state atoms, thus neglecting the interaction between the two species and amongst the few excited atoms, the mixed correlation functions in (7.14) factor into a correlation function for ground-state and one for excited-state operators, each.

Under the assumption that the field correlation functions vary only slightly on the scale of the single particle energies of the $|e\rangle$-state atoms, we can approximate,

in the same manner as in eqn. (4.9),

$$\langle \Psi_e^\dagger(x_4)\Psi_e(x_3)\Psi_e^\dagger(x_2)\Psi_e(x_1)\rangle \approx \delta(\mathbf{r}_4 - \mathbf{r}_3)\delta(\mathbf{r}_2 - \mathbf{r}_1) \ .$$

The atom-light interaction can then, similar to the Fermi-theory for weak interactions, be visualized by an effective vertex

which does not resolve the spatial propagation of the excited atom in the virtual state. (We quantified the error resulting from this approximation in section 5.3, and found that it scales with the small ratio between trap frequency and the optical transition frequency.) In this way, the fourth order diagrams (7.14) are simplified to structures as in eqn. (6.11), which involves the atomic correlation function at only two different coordinates, $\langle \Psi_g^\dagger(\mathbf{r}_2)\Psi_g(\mathbf{r}_2)\Psi_g^\dagger(\mathbf{r}_1)\Psi_g(\mathbf{r}_1)\rangle$.

The correlation functions of the field interacting with the atoms can now either be local or connect two different coordinates. We can depict these two possibilities as

$$(7.15)$$

which involves integration over $D_{\alpha\beta}^F(\mathbf{r}_1, \mathbf{r}_1, \omega)D_{\gamma\delta}^F(\mathbf{r}_2, \mathbf{r}_2, \omega')$, and

$$(7.16)$$

with an integrand proportional to $D_{\alpha\beta}^F(\mathbf{r}_1, \mathbf{r}_2, \omega)D_{\gamma\delta}^F(\mathbf{r}_1, \mathbf{r}_2, \omega')$. The processes contained in diagram (7.16) cannot be described by averaging a local operator –as for example the Casimir-Polder potential– over a density distribution.

For temperatures below T_c, the atomic part of diagrams (7.15) and (7.16) is typically nonzero over distances $r = |\mathbf{r}_1 - \mathbf{r}_2|$ which are comparable to the size of the condensate wavefunction (compare fig. 2.2). Our analysis for the ideal Bose-gas in section 6.3 showed that this long-range order is responsible for the enhancement of spontaneous emission processes discussed in chapter 6. It breaks down at temperatures higher than T_c (see the blue line in fig. 6.2). By the same mechanism, any fourth order process described by the above diagrams gets enhanced whenever one of the modes into which the virtual excited atoms can decay is macroscopically populated with a large number N_0 of ground state atoms. This bosonic enhancement changes the dimensionless parameter in the fourth order of

the perturbation series from $(\mu\omega_{eg})^2$ to $N_0(\mu\omega_{eg})^2$. We found in chapter 6 that the actual numerical factor which scales the relative magnitude between leading and next-to-leading order processes depends on the spatial coherence properties of the Bose gas: the relevant quantity for the enhancement is the number of ground state atoms inhabiting a volume characterized by the coherence length.

7.4 Perspectives for future work

In the previous chapters, we were evaluating self-energy processes for atomic systems interacting with light. Our results of section 6.3, where photons from a laser beam interact with the Bose gas, can also be rephrased by putting the emphasis on photon propagation: the photon propagator is dressed by the atomic system, and the refractive index of the BEC depends on its density correlation function (see Fleischhauer, 1999; Morice *et al.*, 1995).

Also, we only considered condensate distributions which were fixed relative to the surface. Moving condensate clouds could be interesting for investigating the phenomenon of quantum friction.[2] Friction as the exchange of momentum between two surfaces can be described as an exchange of particles. In the classic case of friction with wear, atoms are exchanged between the surfaces. Momentum exchange can also occur via the exchange of (thermal or virtual) photons between the surfaces, which create excitations of equal and opposite momentum on each of them. This quantum friction due to virtual photon exchange puts a theoretical limit on the reduction of friction (see DelRio *et al.*, 2005). Effects of quantum friction should also occur for a condensate cloud moving above a surface or between two counter-rotating condensates in toroidal traps.

The attractive potential between two BECs trapped in a double-well potential can be calculated analogous to the van der Waals interaction between two point-like atoms mentioned in section 7.2. This additional potential modifies the potential barrier between the two condensate clouds (see Haakh *et al.* (2012) for more details). A deformation of the potential barrier can be detected in a change of the atomic tunneling current between the two wells. Such double-well setups have been used to study a bosonic analogue to the Josephson-junction.[3]

Finally, in the evaluation of energy shifts and decay rates, we used so far only two simple models for the atomic system, namely an ideal Bose gas and a pure interacting condensate. A straightforward task for future investigations is the effect of thermal excitations in an interacting gas on the CP-interaction and on decay processes of excited atomic states. We obtained preliminary results repeating the decay rate calculation of chapter 6 for a one-dimensional, interacting Bose gas

---

[2]On quantum friction, see for example Mkrtchian (1995); Pendry (1997); Volokitin and Persson (1999).

[3]See Smerzi *et al.* (1997); Sols (1999) and the experiments by Albiez *et al.* (2005) and Schumm *et al.* (2005).

(see Mazáč, 2010). The bosonic enhancement shows a different temperature dependence compared to the three-dimensional case.

Summary

The phenomena belonging to the context of cavity QED and the broader class of Casimir effects have in common that fluctuations of fields are subject to boundary conditions. In this work, we discussed several of these effects involving atomic Bose-Einstein condensates.

In the description of interacting BECs, we focused on the low-temperature behavior, where one single-particle state is macroscopically occupied by a large number of atoms. Following Bogoliubov, the fluctuations of this matter wave field can be treated as non-interacting bosonic quasiparticles. In spatially homogeneous systems, the energy spectrum can be solved analytically, and behaves linear for small momenta. We showed that, similar to the zero-point fluctuations of the electromagnetic field, the quantum fluctuations of the quasiparticles give rise to a phononic Casimir energy when the atomic system is subject to external boundary conditions. The qualitative behavior of the Casimir energy depends on the dispersion relation. In particular, for the ideal Bose gas at zero temperature, there is no such effect.

While the phononic Casimir effect arises when external boundary conditions are imposed on the atom field, cavity QED describes phenomena where the electromagnetic field is spatially confined. Recently, Bose-Einstein condensates (BECs) of ultracold atoms have been used to test the predictions of cavity QED. In order to merge single-atom cavity QED with the many-body theory needed to describe trapped atomic BECs, we used a quantum field theory of atoms and light that treats atom and photon field on the same footing. We identified the Casimir-Polder energy of BECs near surfaces with the real part of electromagnetic self-energy processes, the imaginary part describing decay processes.

The self-energy is expressed in terms of correlation functions for the electromagnetic and the atom field. The electromagnetic correlations (photon prop-

agator) have been expressed in terms of retarded Green functions that permit to identify easily the contribution brought about by the surface, and to remove the divergent free-space Lamb shift. The characteristics of the surface material then enter through the scattering amplitudes for light, which allows for treating a wide range of materials.

By performing a perturbative expansion of the Dyson series in terms of Feynman diagrams, we are able to reproduce standard results of cavity QED, like the van der Waals-London interaction between two atoms in the fourth order of atom-field interaction, in a transparent and economic fashion.

For a BEC trapped near a surface, we showed that, in full generality, the atom-surface interaction does not reduce to an integral over the density distribution of the atoms, due to the (virtual) propagation in the excited state. The interaction energy between Bose gas and surface shows an overall scaling with the atom number. But, for an interacting gas, the interaction energy per atom still depends weakly on the atom number.

The spontaneous emission rate of atoms in an internal excited state can be significantly enhanced if the atom is embedded in a trapped Bose-Einstein condensate of ground-state atoms. This effect amplifies the small oscillations of the decay rate near an interface. The stimulation depends on the overlap of the excited matter wave packet with the macroscopically occupied condensate wave function, and provides a probe of the spatial coherence of the Bose gas.

Our calculations illustrate the importance of two- and four-point correlation functions of the ground-state field for the Bose enhancement. We pointed out in a qualitative manner processes of higher orders in the atom-light interaction, like vertex renormalization and resummation techniques. As the details of the atomic system and the surface enter the calculation via separate correlation functions, our approach provides a consistent modular concept to describe different effects associated with atomic systems near interfaces.

Appendices

Correlation functions for the electric field

The time-ordered (or Feynman-) propagator for the electric field is defined as

$$D_{\alpha\beta}^F(x_1; x_2) = \langle T\{E_\alpha(x_1)E_\beta(x_2)\}\rangle \tag{A.1}$$

$$= \int \frac{d\omega}{2\pi} e^{i\omega(t_1-t_2)} D_{\alpha\beta}^F(\mathbf{r}_1, \mathbf{r}_2; \omega), \tag{A.2}$$

where the brackets $\langle\ldots\rangle$ in eqn. (A.1) denote an expectation value with respect to an equilibrium state of the field at temperature T_F, and the symbol $T\{\ldots\}$ denotes time-ordering. The retarded propagator (or Green-function) for the electric field is defined as

$$G_{\alpha\beta}(x_1, x_2) = i\langle[E_\alpha(x_1), E_\beta(x_2)]\rangle\Theta(t_1 - t_2) \tag{A.3}$$

$$= \int \frac{d\omega}{2\pi} e^{i\omega(t_1-t_2)} G_{\alpha\beta}(\mathbf{r}_1, \mathbf{r}_2, \omega), \tag{A.4}$$

where Θ denotes the Heaviside step function. If the field is in equilibrium, $D_{\alpha\beta}^F(\omega)$ and $G_{\alpha\beta}(\omega)$ are related via

$$iD_{\alpha\beta}^F(\mathbf{r}_1, \mathbf{r}_2, \omega) = \text{Re}\,[G_{\alpha\beta}(\mathbf{r}_1, \mathbf{r}_2, \omega)] + i\,\coth[\omega/(2T_F)]\,\text{Im}\,[G_{\alpha\beta}(\mathbf{r}_1, \mathbf{r}_2, \omega)] \tag{A.5}$$

(see Fetter and Walecka, 2003, sec. 31).

A.1 Integral identities in the complex frequency plane

Using the fact that $\text{Re}\,[G_{\alpha\beta}(\omega)]$ is an even function of ω while $\text{Im}\,[G_{\alpha\beta}(\omega)]$ is odd (see Scheel and Buhmann, 2008, App. A) together with relation (A.5), we can
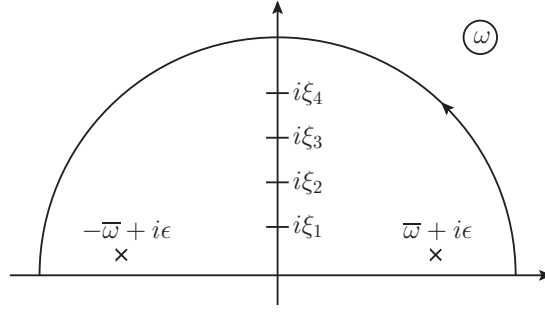
Figure A.1: Contour of integration for eqn. (A.6).

express the integrals appearing in eqn. (4.11) as

$$\int \frac{d\omega}{2\pi} \frac{D(\omega)}{\overline{\omega} \pm i\epsilon - \omega} = \int \frac{d\omega}{2\pi i} \frac{\overline{\omega} \pm i\epsilon}{(\overline{\omega} \pm i\epsilon)^2 - \omega^2} G(\omega) \left(1 + \coth[\omega/(2T_F)]\right) .$$
(A.6)

As $G_{\alpha\beta}(\omega)$ has poles only in the lower halfplane and falls of at least as fast as $|\omega|^{-2}$ for large $|\omega|$ in the upper halfplane, we can integrate along the contour in fig. A.1 and obtain

$$\int \frac{d\omega}{2\pi} \frac{D(\omega)}{\overline{\omega} \pm i\epsilon - \omega} = G(\pm\overline{\omega}) \frac{1}{2} \left(1 \pm \coth[\overline{\omega}/(2T_F)]\right) + 2T_F \sum_n{}' \frac{\overline{\omega}}{\overline{\omega}^2 + \xi_n^2} G(i\xi_n) ,$$
(A.7)

where the primed summation denotes that the $n = 0$ term is multiplied with a factor $\frac{1}{2}$, and

$$\xi_n = 2\pi n T_F, \quad n = 0, 1, 2, \dots .$$
(A.8)

With $d\zeta = \zeta_{n+1} - \zeta_n = 2\pi T_F$, the sum can be approximated by an integral if T_F is sufficiently low such that $k_B T_F$ is small compared to the frequency scale ω_{eg} on which the functions under the sum vary. In the limit of low temperatures, we obtain

$$\lim_{T_F \to 0} \int \frac{d\omega}{2\pi} \frac{D(\omega)}{\overline{\omega} \pm i\epsilon - \omega} = \theta(\pm\overline{\omega}) G(\pm\overline{\omega}) + \frac{1}{\pi} \int_0^\infty d\xi \frac{\overline{\omega}}{\overline{\omega}^2 + \xi_n^2} G(i\xi) . \quad (A.9)$$

A.2 Explicit expressions for $G_{\alpha\beta}$

The Green function in the presence of an interface can be split into a free space and a reflected part:

$$G_{\alpha\beta} = G_{\alpha\beta}^{(0)} + G_{\alpha\beta}^R .$$
(A.10)

$G_{\alpha\beta}^{(0)}$ in free space

The retarded Green function in free space depends only on the coordinate difference $\mathbf{r} = \mathbf{r}_1 - \mathbf{r}_2$:

$$G_{\alpha\beta}^{(0)}(\mathbf{r},\omega) = \frac{4\pi}{3}\delta(\mathbf{r})\,\mathbb{1} + e^{ikr}k^2\left[\frac{1}{r}(\mathbb{1} - \hat{r}_\alpha\hat{r}_\beta) + \left(\frac{i}{kr^2} - \frac{1}{k^2r^3}\right)(\mathbb{1} - 3\hat{r}_\alpha\hat{r}_\beta)\right]$$

(A.11)

(see for example Scheel and Buhmann, 2008, App. A). In the limit $r \to 0$, the real part of (A.11) diverges, but the imaginary part stays finite:

$$\mathrm{Im}\left[G_{\alpha\beta}^{(0)}(\mathbf{r} = 0, \omega)\right] = \mathbb{1}\frac{2}{3}\omega^3 + \mathcal{O}(r^2) \ .$$

The spatial Fourier transform of eqn. (A.11) reads

$$G_{\alpha\beta}^{(0)}(\mathbf{r},\omega) = \int \frac{d^3k}{(2\pi)^3}\,G_{\alpha\beta}(\mathbf{k},\omega)\,e^{i\mathbf{k}\cdot\mathbf{r}} \ ,$$

(A.12)

$$G_{\alpha\beta}^{(0)}(\mathbf{k},\omega) = 4\pi\left(\frac{\mathbf{k}\mathbf{k} - \omega^2\mathbb{1}}{(\omega + i\epsilon)^2 - k^2} + \mathbb{1}\right) \ .$$

(A.13)

$G_{\alpha\beta}^{R}$ in the presence of an interface

The reflected part of the retarded Green function in the presence of an interface (as presented by Wylie and Sipe (1984, eqn. (3.4)), see also Panasyuk *et al.* (2009, sec. 2) for an overview) reads

$$G_{\alpha\beta}^{R}(\mathbf{r}_1, \mathbf{r}_2, \omega) = -\frac{i\omega^2}{2\pi\varepsilon_0 c^2}\int \frac{d^2k}{k_z}\,R_{\alpha\beta}(\mathbf{k},\omega)\,e^{ik_z(z_1+z_2)+i\mathbf{k}\cdot(\mathbf{x}_1-\mathbf{x}_2)} \ , \quad \text{(A.14)}$$

with $k_z = \sqrt{\omega^2/c^2 - k^2}$. Here, the two-dimensional vectors $\mathbf{x}$ and $\mathbf{k}$ denote the position and momentum vectors parallel to the surface, respectively. The matrix $R_{\alpha\beta}(\mathbf{k},\omega)$ is defined as

$$R_{\alpha\beta}(\mathbf{k},\omega) = (\hat{s}\hat{s})_{\alpha\beta}\,R^s + (\hat{p}_{0+}\hat{p}_{0-})_{\alpha\beta}\,R^p$$

(A.15)

The functions R^s and R^p in eqn. (A.15) are the Fresnel reflection coefficients for s- and p-polarized light, which can be modeled to realize different surface materials. For the case of a perfectly reflecting surface, $R^s = -1$ and $R^p = 1$, while in general the reflection coefficients are frequency dependent (see Sipe, 1981; Wylie and Sipe, 1984, 1985): Considering an interface between vacuum ($\epsilon_0 = 1$) and a material with a local and isotropic dielectric function $\epsilon(\omega)$, R^s and R^p are given

by

$$R^s = \frac{k_z - (\omega^2 \, \epsilon(\omega) - k^2)^{1/2}}{k_z + (\omega^2 \, \epsilon(\omega) - k^2)^{1/2}} , \tag{A.16a}$$

$$R^p = \frac{\epsilon \, k_z - (\omega^2 \, \epsilon(\omega) - k^2)^{1/2}}{\epsilon \, k_z + (\omega^2 \, \epsilon(\omega) - k^2)^{1/2}} . \tag{A.16b}$$

In section 5.3, we use the Drude model for a metal surface, with

$$\epsilon(\omega) = 1 - \frac{\omega_p^2}{\omega(\omega + i/\tau)} , \tag{A.17}$$

where ω_p is the plasma frequency and τ the collision time. Finally, the dyadic elements $(\hat{s}\hat{s})_{\alpha\beta}$ and $(\hat{p}_{0+}\hat{p}_{0-})_{\alpha\beta}$ in eqn. (A.15) involve the normalized polarization vectors

$$\hat{\mathbf{s}} = \hat{\mathbf{k}} \times \hat{\mathbf{z}} \tag{A.18}$$

$$\hat{\mathbf{p}}_{0\pm} = \frac{k\,\hat{\mathbf{z}} \mp k_z \hat{\mathbf{k}}}{\omega} . \tag{A.19}$$

For the idealized case of a perfectly reflecting surface, the reflected part of the Green function assumes the simple form (see Wylie and Sipe, 1984, eqn. (3.12))

$$G_{xx}^R(\mathbf{r}_d, \mathbf{r}_d, i\xi) = G_{yy}^R(\mathbf{r}_d, \mathbf{r}_d, i\xi) = \frac{1 + \sigma + \sigma^2}{8d^3} e^{-\sigma} , \tag{A.20}$$

$$G_{zz}^R(\mathbf{r}_d, \mathbf{r}_d, i\xi) = \frac{1 + \sigma}{4d^3} e^{-\sigma} , \tag{A.21}$$

where $\mathbf{r}_d$ denotes the vector $(0, 0, d)$ and $\sigma = 2\xi d/c$.

Mathematical details

B.1 One-body correlation function for an ideal BEC in a harmonic trap

Using the analytical properties of the single-particle wave functions, the one body correlation function (2.2) for the ideal Bose gas can be constructed from the mode expansion of the field operator $\hat{\Psi}$. A useful form, found by Barnett *et al.* (2000), that combines the summations over the multiple index j of eqn. (2.7) into a single sum reads

$$n^{(1)}(\mathbf{r}_1, \mathbf{r}_2) = \frac{1}{\pi^{3/2} a_\perp^2 a_z} \sum_{j=1}^{\infty} \left\{ \frac{e^{j\beta\mu}}{\left(1 - e^{-2j\beta\omega_\perp}\right)\left(1 - e^{-2j\beta\omega_z}\right)^{1/2}} \right. \tag{B.1}$$

$$\times \exp\left[-\frac{(\mathbf{r}_{\perp 2} + \mathbf{r}_{\perp 1})^2 \tanh[\frac{1}{2}j\beta\hbar\omega_\perp] + (\mathbf{r}_{\perp 2} - \mathbf{r}_{\perp 1})^2 \coth[\frac{1}{2}j\beta\hbar\omega_\perp]}{4a_\perp^2} \right]$$

$$\left. \times \exp\left[-\frac{(z_2 + z_1)^2 \tanh[\frac{1}{2}j\beta\hbar\omega_z] + (z_2 - z_1)^2 \coth[\frac{1}{2}j\beta\hbar\omega_z]}{4a_z^2} \right] \right\}.$$

Here, $a_\perp$ and a_z denote the oscillator-lengths eqns. (2.55) of the axisymmetrical potential (2.52). We adopt the convention of setting the eigenenergy of the ground state to zero, the chemical potential μ is then negative-valued.

B.2 Approximating the error function integral

In the integrands of eqn. (5.5) and eqn. (5.25), we encounter the expression

$$I(\overline{\kappa}, x, \eta) = \frac{1}{2} \exp[-2\overline{\kappa}x + \overline{\kappa}^2\eta^2]\left(1 + \mathrm{erf}[\frac{x}{\eta} - \overline{\kappa}\eta]\right) \tag{B.2}$$

where $\overline{\kappa}$ is integrated from zero to infinity, $\eta = \omega_{eg} a_0/c$ is fixed by the atomic transition frequency and mass and the positive distance x varies such that $x > \eta^2$ is always fulfilled.

Noting that the argument of the error function changes sign at $\overline{\kappa} = x/\eta$, we can approximate the error function for large values of $\overline{\kappa}$ (see Gradshteyn and Ryzhik, 1980, eqn. (8.254)) to obtain

$$I(\overline{\kappa}, x, \eta) \;\approx\; \frac{\exp[-x^2/\eta^2]}{2\sqrt{\pi}\,(\overline{\kappa}\eta - x/\eta)} \;, \quad \text{for } \overline{\kappa} \gg \frac{x}{\eta^2} \;, \tag{B.3}$$

which is exponentially small in the quantity $(x/\eta)^2$. In numerical integrations, we will thus cut off the $d\overline{\kappa}$-integration at $\overline{\kappa} = x/\eta^2$, omitting terms of order $\mathcal{O}\big(\exp[-(x/\eta)^2]\big)$ in the integrand. The neglected quantities are small: for a rubidium atom at $T = 0$ trapped in a $\nu/2\pi = 1$ kHz trap at an atom-surface distance $d \approx 2\,\mu\text{m}$ ($x = \omega_{eg}d/c \approx 15$), we have $(x/\eta)^2 \approx 30$. Technically speaking, the high momentum cut-off is necessary as the atomic probability density $|\phi_0(\mathbf{r})|^2$ we adopt here is not zero at the surface, but only exponentially small, namely of the same order as the terms neglected in eqn. (B.3).

Feynman rules for pointlike atoms

We assume that both internal states of the atom experience a trapping potential which localizes the atoms in space. In general, atoms in excited electronic states move in a potential $V_{trap}^e(\mathbf{r})$ which differs from the potential $V_{trap}^g(\mathbf{r})$ characterizing the ground state, because the magnetic moments of the two species differ. The single-particle eigenfunctions $\Phi_{\mathbf{n}}^g(\mathbf{r})$ and $\Phi_{\mathbf{m}}^e(\mathbf{r})$ of $|g\rangle$- and $|e\rangle$ state atoms are defined by

$$[-\frac{\overrightarrow{\bigtriangledown}^2}{2m} + V_{trap}^g(\mathbf{r})]\,\Phi_{\mathbf{n}}^g(\mathbf{r}) = \omega_{\mathbf{n}}^g\,\Phi_{\mathbf{n}}^g(\mathbf{r})\ , \tag{C.1a}$$

$$[-\frac{\overrightarrow{\bigtriangledown}^2}{2m} + \omega_{eg} + V_{trap}^e(\mathbf{r})]\,\Phi_{\mathbf{m}}^e(\mathbf{r}) = (\omega_{eg} + \omega_{\mathbf{m}}^e)\,\Phi_{\mathbf{m}}^e(\mathbf{r})\ , \tag{C.1b}$$

where the collective labels $\mathbf{n}$ and $\mathbf{m}$ denote the spatial degrees of freedom. The atomic field operators can be expanded as

$$\Psi_g(\mathbf{r}) = \sum_{\mathbf{n}} \Phi_{\mathbf{n}}^g(\mathbf{r})\hat{g}_{\mathbf{n}}\ , \tag{C.2a}$$

$$\Psi_e(\mathbf{r}) = \sum_{\mathbf{m}} \Phi_{\mathbf{m}}^e(\mathbf{r})\hat{e}_{\mathbf{m}}\ , \tag{C.2b}$$

and the unperturbed atomic Hamiltonian in this occupation-number basis reads

$$H_A = \sum_{\mathbf{n}} \omega_{\mathbf{n}}^g g_{\mathbf{n}}^\dagger g_{\mathbf{n}} + \sum_{\mathbf{m}} (\omega_{eg} + \omega_{\mathbf{m}}^e)e_{\mathbf{m}}^\dagger e_{\mathbf{m}}\ . \tag{C.3}$$

From eqns. (C.2) and eqn. (C.3), the Wick-contractions of atom operators read

$$\overline{\Psi_e^\dagger(x_1)\Psi_e}(x_2) = i \int \frac{d\omega}{2\pi} e^{-i\omega(t_2-t_1)} \sum_{\mathbf{m}} \frac{\Phi_{\mathbf{m}}^e(\mathbf{r}_2)\Phi_{\mathbf{m}}^{e*}(\mathbf{r}_1)}{\omega - \omega_{eg} - \omega_{\mathbf{m}}^e + i\epsilon} \qquad \text{(C.4a)}$$

$$\overline{\Psi_g^\dagger(x_1)\Psi_g}(x_2) = i \int \frac{d\omega}{2\pi} e^{-i\omega(t_2-t_1)} \sum_{\mathbf{n}} \frac{\Phi_{\mathbf{n}}^g(\mathbf{r}_2)\Phi_{\mathbf{n}}^{g*}(\mathbf{r}_1)}{\omega - \omega_{\mathbf{n}}^g + i\epsilon} \qquad \text{(C.4b)}$$

For calculations of the Casimir-Polder interaction between a single atom and a surface or the dispersion interaction between two atoms, the individual atoms can usually be treated as perfectly localized, pointlike objects. This description is obtained from eqns. (C.4) by considering a very tightly confining trap potential such that the atoms can occupy only the lowest trap-state (with $\omega_0^{g,e} = 0$) and the product of wavefunctions in the numerators of eqns. (C.4) approaches a spatial δ-function. For distinguishable atoms (labeled $A, B, \ldots$ as in section 7.2), we then arrive at the following Feynman-rules in frequency-space:

- Atom propagators:

$$\underset{A}{\overset{x_1 \quad \omega \quad x_2}{\circ\!\!-\!\!\!\longrightarrow\!\!\!-\!\!\circ}} = \frac{i\,\delta(\mathbf{r}_1 - \mathbf{r}_2)}{\omega + i\epsilon}\,, \qquad \underset{A}{\overset{x_1 \quad \omega \quad x_2}{\circ\!\!-\!\!\!\dashrightarrow\!\!\!-\!\!\circ}} = \frac{i\,\delta(\mathbf{r}_1 - \mathbf{r}_2)}{\omega - \omega_{eg}^A + i\epsilon}\,.$$

- Field propagator:

$$\overset{x_1, \alpha \quad \omega \quad x_2, \beta}{\circ\!\!\!\sim\!\!\!\sim\!\!\!\sim\!\!\!\circ} = D_{\alpha\beta}^F(\mathbf{r}_1, \mathbf{r}_2, \omega)\,.$$

(The explicit form of $D_{\alpha\beta}^F(\mathbf{r}_1, \mathbf{r}_2, \omega)$ might depend on the boundary conditions set by the presence of a surface.)

- Vertex factors:

$$\underset{A}{\overset{\alpha}{}}\!\!-\!\!\!\overset{\alpha}{\circ}\!\!-\! A = -i\mu_\alpha^{A\,eg}\,, \qquad A -\!\!-\!\!\overset{\alpha}{\circ}\!\!-\!\!- A = -i\mu_\alpha^{A\,ge}\,.$$

- Atoms in asymptotic states (located at position $\mathbf{r}_A$):

$$A \overset{x}{\longrightarrow\!\circ} = \sqrt{\delta(\mathbf{r} - \mathbf{r}_A)}\,, \qquad \overset{x}{\circ\!\longrightarrow} A = \sqrt{\delta(\mathbf{r} - \mathbf{r}_A)}\,.$$

$$A -\!\!\underset{\omega_{eg}^A}{\dashrightarrow}\overset{x}{\circ} = \sqrt{\delta(\mathbf{r} - \mathbf{r}_A)}\,, \qquad \overset{x}{\circ}\underset{\omega_{eg}^A}{\dashrightarrow}\!\!- A = \sqrt{\delta(\mathbf{r} - \mathbf{r}_A)}\,.$$

Arrows in the various elements indicate the energy-flow, a label x denotes the spacetime-point $(t, \mathbf{r})$. As we set the internal energy of the state $|g\rangle$ to zero, incoming (outgoing) ground-state atoms do not contribute to the energy sum at a vertex. To calculate a T-matrix element, impose energy conservation on each vertex. Then integrate over all independent loop-energies and over the spatial coordinates $\mathbf{r}_i$. Afterwards divide by a factor of $(-2\pi i)$.

Bibliography

Agarwal, G. S., 1975, Phys. Rev. A **11**, 230.

Albiez, M., R. Gati, J. Fölling, S. Hunsmann, M. Cristiani, and M. K. Oberthaler, 2005, Phys. Rev. Lett. **95**, 010402.

Andersen, J. O., 2004, Rev. Mod. Phys. **76**, 599.

Anderson, M. H., J. R. Ensher, M. R. Matthews, C. E. Wieman, and E. A. Cornell, 1995, Science **269**, 198.

Andrews, M. R., C. G. Townsend, H.-J. Miesner, D. S. Durfee, D. M. Kurn, and W. Ketterle, 1997, Science **275**, 637.

Antezza, M., L. P. Pitaevskii, and S. Stringari, 2004, Phys. Rev. A **70**, 053619.

Aspect, A., R. Kaiser, N. Vansteenkiste, P. Vignolo, and C. I. Westbrook, 1995, Phys. Rev. A **52**, 4704.

Bachmann, S., and A. Kempf, 2008, J. Phys. A **41**, 164021.

Bagnato, V., D. E. Pritchard, and D. Kleppner, 1987, Phys. Rev. A **35**, 4354.

Barnett, S. M., S. Franke-Arnold, A. S. Arnold, and C. Baxter, 2000, J. Phys. B **33**, 4177.

Barton, G., and N. S. J. Fawcett, 1988, Phys. Rep. **170**, 1.

Baym, G., and C. J. Pethick, 1996, Phys. Rev. Lett. **76**, 6.

Bender, H., P. W. Courteille, C. Marzok, C. Zimmermann, and S. Slama, 2010, Phys. Rev. Lett. **104**, 083201.

Bernard, C. W., 1974, Phys. Rev. D **9**, 3312.

Bethe, H. A., 1947, Phys. Rev. **72**, 339.

Biswas, S., 2007, J. Phys. A **40**, 9969.

Bloch, I., T. W. Hänsch, and T. Esslinger, 2000, Nature **403**, 166.

Boesten, H. M. J. M., C. C. Tsai, J. R. Gardner, D. J. Heinzen, and B. J. Verhaar, 1997, Phys. Rev. A **55**, 636.

Bogoliubov, N. N., 1947, J. Phys. USSR **11**, 23, reprinted in (Pines, 1997, p. 292).

Bordag, M., U. Mohideen, and V. M. Mostepanenko, 2001, Physics Reports **353**, 1.

Bradley, C. C., C. A. Sackett, and R. G. Hulet, 1997, Phys. Rev. Lett. **78**, 985.

Bradley, C. C., C. A. Sackett, J. J. Tollett, and R. G. Hulet, 1995, Phys. Rev. Lett. **75**, 1687.

Buhmann, S. Y., L. Knöll, D.-G. Welsch, and H. T. Dung, 2004, Phys. Rev. A **70**, 052117.

Buks, E., and M. L. Roukes, 2001, Phys. Rev. B **63**, 033402.

Carnaglia, C. K., and L. Mandel, 1971, Phys. Rev. D **3**, 280.

Casimir, H. B. G., 1948, Proc. Kon. Nederl. Akad. Wetensch. **51**, 793.

Casimir, H. B. G., and D. Polder, 1948, Phys. Rev. **73**, 360.

Castin, Y., 2001, in *Coherent atomic matter waves*, edited by R. Kaiser, C. Westbrook, and F. David (Springer, Berlin/Heidelberg), volume 72 of *Les Houches*, pp. 1–136.

Cohen-Tannoudji, C., and C. Robilliard, 2001, Comptes Rendus de l'académie des sciences - physique **2**, 445.

Cornelussen, R. A., A. H. van Amerongen, B. T. Wolschrijn, R. J. C. Spreeuw, and H. B. van Linden van den Heuvell, 2002, Eur. Phys. J. D **21**, 347.

Courtois, J.-Y., J.-M. Courty, and S. Reynaud, 1995, Phys. Rev. A **52**, 1507.

Craig, D. P., and T. Thirunamachandran, 1998, *Molecular Quantum Electrodynamics* (Dover Publications).

Dalvit, D. A. R., P. A. M. Neto, A. Lambrecht, and S. Reynaud, 2008, Phys. Rev. Lett. **100**, 040405.

Davis, K. B., M.-O. Mewes, M. R. Andrews, N. J. van Druten, D. S. Durfee, D. M. Kurn, and W. Ketterle, 1995, Phys. Rev. Lett. **75**, 3969.

Decca, R. S., E. Fischbach, G. L. Klimchitskaya, D. E. Krause, D. López, and V. M. Mostepanenko, 2003, Phys. Rev. D **68**, 116003.

DelRio, F. W., M. P. de Boer, J. A. Knapp, E. David Reedy, P. J. Clews, and M. L. Dunn, 2005, Nature Materials **4**, 629.

Dicke, R. H., 1954, Phys. Rev. **93**, 99.

Dobson, J. F., 1994, Phys. Rev. Lett. **73**, 2244.

Drexhage, K. H., 1970, Journal of Luminescence **1-2**, 693.

Dyson, F. J., 1949a, Phys. Rev. **75**, 486.

Dyson, F. J., 1949b, Phys. Rev. **75**, 1736.

Eberlein, C., and D. Robaschik, 2006, Phys. Rev. D **73**, 025009.

Edery, A., 2006a, Journal of Statistical Mechanics: Theory and Experiment **2006**, P06007.

Edery, A., 2006b, J. Phys. A **39**, 685.

Eisenschitz, R., and F. London, 1930, Zeitschrift für Physik **60**, 491.

Evans, T. S., and D. A. Steer, 1996, Nuclear Physics B **474**, 481.

Fetter, A., 1997, Journal of Low Temperature Physics **106**, 643.

Fetter, A. L., 1972, Annals of Physics (NY) **70**, 67.

Fetter, A. L., 1999, in *Bose-Einstein condensation in Atomic Gases (Proceedings of the International School of Physics «Enrico Fermi», Course CXL)*, edited by M. Inguscio, S. Stringari, and C. E. Wieman (IOS Press, Amsterdam), pp. 201–263.

Fetter, A. L., and D. Rokhsar, 1998, Phys. Rev. A **57**, 1191.

Fetter, A. L., and J. D. Walecka, 2003, *Quantum Theory of Many Particle Systems* (Dover Publications).

Fleischhauer, M., 1999, Phys. Rev. A **60**, 2534.

Gallagher, T. F., 1994, *Rydberg atoms* (Cambridge University Press).

Gambassi, A., C. Hertlein, L. Helden, S. Dietrich, and C. Bechinger, 2009, Europhysics News **40**, 18.

Gaul, C., and C. A. Müller, 2008, Europhysics Letters **83**, 10006.

Gies, H., 2008, J. Phys. A **41**, 164039.

Görlitz, A., A. P. Chikkatur, and W. Ketterle, 2001, Phys. Rev. A **63**, 041601.

Gorza, M. P., and M. Ducloy, 2006, European Physical Journal D **40**, 343.

Gradshteyn, I. S., and I. M. Ryzhik, 1980, *Table of Integrals, Series, and Products*, volume 2 (Academic, New York).

Gross, E. P., 1961, Nuovo Cimento **20**, 454.

Haakh, H. R., J. Schiefele, and C. Henkel, 2012, in preparation – to appear in Int. J. Mod. Phys. A., proceedings of the QFEXT 2011 conference.

Harber, D. M., J. M. Obrecht, J. M. McGuirk, and E. A. Cornell, 2005, Phys. Rev. A **72**, 033610.

Haroche, S., 1992, in *Fundamental Systems in Quantum Optics (Les Houches, Session LIII)*, edited by J. Dalibard, J.-M. Raimond, and J. Zinn-Justin (North-Holland, Amsterdam), p. 767.

Hawking, S. W., 1977, Comm. Math. Phys. **55**, 133.

Healy, W. P., 1982, *Non-relativistic quantum electrodynamics* (Academic, New York).

Henkel, C., K. Joulain, J.-P. Mulet, and J.-J. Greffet, 2002, J. Opt. A: Pure Appl. Opt. **4**, S109.

Hinds, E. A., 1994, in *Cavity Quantum Electrodynamics*, edited by P. R. Berman (Academic, New York), Adv. At. Mol. Opt. Phys., p. 30, suppl. 2.

Hinds, E. A., and V. Sandoghdar, 1991, Phys. Rev. A **43**, 398.

Hohenberg, P. C., and P. C. Martin, 1965, Annals of Physics (NY) **34**, 291.

Hope, J. J., and C. M. Savage, 1996, Phys. Rev. A **54**, 3177.

Hu, B., G. Huang, and Y.-L. Ma, 2004, Phys. Rev. A **69**, 063608.

Hugenholtz, N. M., and D. Pines, 1959, Phys. Rev. **116**, 489.

Hulet, R. G., E. S. Hilfer, and D. Kleppner, 1985, Phys. Rev. Lett. **55**, 2137.

Huse, D. A., and E. D. Siggia, 1982, Journal of Low Temperature Physics **46**, 137.

Ivanov, V. V., R. A. Cornelussen, H. B. van Linden van den Heuvell, and R. J. C. Spreeuw, 2004, J. Opt. B: Quantum Semiclass. Opt. **6**, 454.

Japha, Y., V. M. Akulin, and G. Kurizki, 1998, Phys. Rev. Lett. **80**, 3739.

Japha, Y., and Y. B. Band, 2002, Journal of Physics B **35**, 2383.

Javanainen, J., 1994, Phys. Rev. Lett. **72**, 2375.

Kapusta, J. I., and C. Gale, 2006, *Finite-Temperature Field Theory*, Cambridge Monographs on Mathematical Physics (Cambridge University Press), second edition.

Ketterle, W., and S. Inouye, 2001, Phys. Rev. Lett. **86**, 4203.

Klein, A., and M. Fleischhauer, 2005, Phys. Rev. A **71**, 033605.

Kohn, W., 1961, Phys. Rev. **123**, 1242.

Lamoreaux, S. K., 1997, Phys. Rev. Lett. **78**, 5.

Lamoreaux, S. K., 2005, Reports on Progress in Physics **68**, 201.

Landragin, A., J.-Y. Courtois, G. Labeyrie, N. Vansteenkiste, C. I. Westbrook, and A. Aspect, 1996, Phys. Rev. Lett. **77**, 1464.

Lee, T. D., K. Huang, and C. N. Yang, 1957, Phys. Rev. **106**, 1135.

Leggett, A. J., and F. Sols, 1991, Foundations of Physics **21**, 353.

Lennard-Jones, J. E., 1932, Trans. Faraday Soc. **28**, 333.

Lewenstein, M., L. You, J. Cooper, and K. Burnett, 1994, Phys. Rev. A **50**, 2207.

London, F., 1930, Zeitschrift für Physik **63**, 245.

Martin, P. A., and V. A. Zagrebnov, 2006, Europhys. Lett. **73**, 15.

Maxwell, J. C., 1874, Nature **10**, 477.

Mazáč, D., 2010, Enhancement of decay rates in quasi-1D interacting BEC, internship-report (unpublished).

Mehra, J., 1967, Physica **37**, 145.

Messina, R., R. Passante, L. Rizzuto, S. Spagnolo, and R. Vasile, 2008, J. Phys. A **41**, 164031.

Milonni, P. W., 1993, *The Quantum Vacuum: An Introduction to Quantum Electrodynamics* (Academic, New York).

Milton, K. A., 2001, *The Casimir Effect: Physical Manifestations of Zero - Point Energy* (World Scientific, Singapore).

Mkrtchian, V. E., 1995, Physics Letters A **207**, 299.

Mkrtchian, V. E., 2009, Armen. J. Phys. **1**, 229.

Moore, M. G., and P. Meystre, 2001, Phys. Rev. Lett. **86**, 4199.

Moreno, G. A., D. A. R. Dalvit, and E. Calzetta, 2010, New J. Phys. **12**, 033009.

Morice, O., Y. Castin, and J. Dalibard, 1995, Phys. Rev. A **51**, 3896.

Mostepanenko, V. M., R. S. Decca, E. Fischbach, G. L. Klimchitskaya, D. E. Krause, and D. López, 2008, J. Phys. A **41**, 164054.

Mostepanenko, V. M., and N. N. Trunov, 1997, *The Casimir Effect and its Applications* (Clarendon Press, Oxford).

Novotny, L., and C. Henkel, 2008, Opt. Lett. **33**, 1029.

Obrecht, J. M., R. J. Wild, M. Antezza, L. P. Pitaevskii, S. Stringari, and E. A. Cornell, 2007, Phys. Rev. Lett. **98**, 063201.

Öhberg, P., E. L. Surkov, I. Tittonen, S. Stenholm, M. Wilkens, and G. V. Shlyapnikov, 1997, Phys. Rev. A **56**, R3346.

Ovchinnikov, Y. B., S. V. Shul'ga, and V. I. Balykin, 1991, J. Phys. B **24**, 3173.

Panasyuk, G. Y., J. C. Schotland, and V. A. Markel, 2009, J. Phys. A **42**, 275203.

Parsegian, V. A., 2005, *Van der Waals forces: A Handbook for Biologists, Chemists, Engineers, and Physicists* (Cambridge University Press, Cambridge).

Passante, R., and S. Spagnolo, 2007, Phys. Rev. A **76**, 042112.

Pendry, J. B., 1997, Journal of Physics: Condensed Matter **9**, 10301.

Penrose, O., and L. Onsager, 1956, Phys. Rev. **104**, 576.

Pérez-García, V. M., H. Michinel, J. I. Cirac, M. Lewenstein, and P. Zoller, 1997, Phys. Rev. A **56**, 1424.

Pethick, C., and H. Smith, 2002, *Bose-Einstein Condensation in Dilute Gases* (Cambridge University Press).

Pines, D., 1997, *The many-body problem* (Addison-Wesley).

Pitaevskii, L., 1961, Sov. Phys. JETP **13**, 451.

Pitaevskii, L., and S. Stringari, 2003, *Bose - Einstein Condensation*, International Series of Monographs on Physics, 116 (Clarendon Press, Oxford).

Posazhennikova, A., 2006, Rev. Mod. Phys. **78**, 1111.

Power, E. A., and T. Thirunamachandran, 1982, Phys. Rev. A **25**, 2473.

Power, E. A., and S. Zienau, 1959, Philos. Trans. R. Soc. London A **251**, 427.

Proukakis, N. P., and B. Jackson, 2008, J. Phys. B **41**, 203002.

Recati, A., J. N. Fuchs, C. S. Peca, and W. Zwerger, 2005, Phys. Rev. A **72**, 023616.

Reichel, J., and V. Vuletic (eds.), 2011, *Atom Chips* (Wiley-VCH), first edition.

Roberts, D. C., and Y. Pomeau, 2005, Casimir Friction II: Casimir effect and drag in zero temperature superfluids, to appear in: I. Aref'eva, D. Sternheimer (editors), *Modern Encyclopedia of Mathematical Physics* (Springer), `arXiv: cond-mat/0503757`.

Rodberg, L. S., 1958, Phys. Rev. **110**, 277.

Rytov, S. M., Y. A. Kravtsov, and V. I. Tatarskii, 1989, *Elements of Random Fields*, volume 3 of *Principles of Statistical Radiophysics* (Springer, Berlin).

Saharian, A. A., 2008, hep-th 0708.1187 .

Scheel, S., and S. Y. Buhmann, 2008, Acta Physica Slovaca **58**, 675.

Schiefele, J., and C. Henkel, 2009, J. Phys. A **42**, 045401.

Schiefele, J., and C. Henkel, 2010, Phys. Rev. A **82**, 023605.

Schiefele, J., and C. Henkel, 2011, Physics Letters A **375**, 680.

Schneble, D., Y. Torii, M. Boyd, E. W. Streed, D. E. Pritchard, and W. Ketterle, 2003, Science **300**, 475.

Schumm, T., S. Hofferberth, L. M. Andersson, S. Wildermuth, S. Groth, I. Bar Joseph, J. Schmiedmayer, and P. Kruger, 2005, Nature Physics **1**, 57.

Sipe, J. E., 1981, Surf. Sci. **105**, 489.

Smerzi, A., S. Fantoni, S. Giovanazzi, and S. R. Shenoy, 1997, Phys. Rev. Lett.

79, 4950.

Sols, F., 1999, in *Bose-Einstein condensation in Atomic Gases (Proceedings of the International School of Physics ≪Enrico Fermi≫, Course CXL)*, edited by M. Inguscio, S. Stringari, and C. E. Wieman (IOS Press, Amsterdam), pp. 453–468.

Sparnaay, M., 1958, Physica **24**, 751 .

Spreeuw, R. J. C., T. Pfau, U. Janicke, and M. Wilkens, 1995, Europhys. Lett. **32**, 469.

Stipe, B. C., H. J. Mamin, T. D. Stowe, T. W. Kenny, and D. Rugar, 2001, Phys. Rev. Lett. **87**, 096801.

Stringari, S., 1996, Phys. Rev. Lett. **77**, 2360.

Sukenik, C. I., M. G. Boshier, D. Cho, V. Sandoghdar, and E. A. Hinds, 1993, Phys. Rev. Lett. **70**, 560.

Sushkov, A. O., W. J. Kim, D. A. R. Dalvit, and S. K. Lamoreaux, 2011, Nature Physics **7**, 230.

Svaiter, N. F., and B. F. Svaiter, 1991, Journal of Mathematical Physics **32**, 175.

Toms, D. J., 1980, Phys. Rev. D **21**, 928.

Volokitin, A. I., and B. N. J. Persson, 1999, Journal of Physics: Condensed Matter **11**, 345.

Weinberg, S., 2005, *The Quantum Theory of Fields*, volume I - Foundations (Cambridge University Press).

Wylie, J. M., and J. E. Sipe, 1984, Phys. Rev. A **30**, 1185.

Wylie, J. M., and J. E. Sipe, 1985, Phys. Rev. A **32**, 2030.

Wynar, R., R. S. Freeland, D. J. Han, C. Ryu, and D. J. Heinzen, 2000, Science **287**, 1016.

Zhang, W., and D. F. Walls, 1994, Phys. Rev. A **49**, 3799.

Ziman, J. M., 1969, *Elements of Advanced Quantum Theory* (Cambridge University Press).